Biologically Inspired Wing Planform Optimization

by

Sarah Elizabeth Taylor

A Thesis

Submitted to the Faculty

of the

WORCESTER POLYTECHNIC INSTITUTE

in partial fulfillment of the requirements for the

Degree of Master of Science

in

Mechanical Engineering

by

____

May 2009

APPROVED:

____

Professor David J. Olinger

____

Professor Islam Hussein

____

Professor John Blandino

____

Professor Yiming Rong

Abstract

The goal of this project is to use inspiration acquired from bird flight to optimize the wing planform of micro-air vehicle wings. Micro-air vehicles are used by the military for surveillance and for search and rescue missions by civilian first-responders. These vehicles fly in the same low Reynolds number regime as birds, and have low aspect ratios similar to the pheasants and grouse of the order Galliformes. Conventional analysis is difficult for low Reynolds numbers, prompting use of biologically inspired methods of optimization. Genetic algorithms, which mimic the process of evolution in nature, were used to define wing shapes that were tested in wind tunnel experiments. In these experiments, lift-drag ratios at various angles of attack were measured on scale model micro-air vehicle wings (with variable length feathers) similar in shape to a bird wing. The planform shape of the scale model wing evolved in the wind tunnel flow over successive generations to ultimately produce superior wings with higher lift-drag ratios. The low angle of attack wings were easily optimized into a wing shape different from and potentially more efficient than the oft-used Zimmerman planform. The process was repeated for a higher angle of attack, near stall conditions, which yielded a different wing planform shape. Chord distributions of the optimized low angle of attack wings were found to closely match the same distributions of birds from the order Galliformes. Results from flow visualization studies meant to illuminate possible physics responsible for the higher lift-drag ratios were also investigated.

Acknowledgements

Without the contributions of the following groups and people, this project would not have been possible. Firstly, I would like to thank Professor Olinger. The original idea of using genetic algorithms to study micro-air vehicle wing planforms was Professor Olinger's, and his guidance and knowledge were central to the project.

I would also like to thank Andrew Day, who established the process in which to use the genetic algorithm, laying the foundation for future work such as mine.

Neil Whitehouse's knowledge of construction was essential to creating the flat plate wings. His time and help are greatly appreciated.

Professor Jim Hermanson and Jack Ross of the University of Washington kindly volunteered expert information on the creation and use of oil film flow visualization.

The beautiful pictures of bird wings found throughout this project is the work of the Slater Museum of the University of Puget Sound, who thoughtfully gave me permission to use them.

Finally, I would like to thank my family for their support, and especially my sister Rebecca Taylor for her photographic expertise.

Table of Contents

List of Figures

Nomenclature

A	= wing area (m^2)
α	= angle of attack (degrees)
AoA	= angle of attack (degrees)
AR	= aspect ratio
b	= wing span (cm)
β	= slope of calibration string with wind tunnel wall (degrees)
c	= chord (cm)
D	= drag (gram-force)
D_1	= horizontal component of drag (gram-force)
E	= endurance (time)
F_A	= axial force (gram-force)
L	= lift (gram-force)
L_L	= change in weight measured by left scale (gram-force)
L_R	= change in weight measured by right scale (gram-force)
MAV	= micro-air vehicle
N	= normal force (gram-force)
R	= range (distance)
Re	= Reynolds number
ρ	= density (kg/m^3)
S_1	= slope of drag calibration line (gram-force/voltage)
S_2	= slope of wing trailing edge
θ_1	= left slope of calibration string (degrees)
θ_2	= right slope of calibration string (degrees)
μ	= viscosity ($N\ s/m^2$)
V	= voltage during test (V)
V_0	= voltage before test (V)
V_∞	= freestream airspeed (m/s)
W	= weight (g)
W_i	= takeoff weight
W_f	= final weight
$X_{1\ldots n}$	= X coordinate of points on wing outline
$Y_{1\ldots n}$	= Y coordinate of points on wing outline
Z	= horizontal distance from wing root

1. Background Information

1.1 Introduction

Micro-air Vehicles (hereafter also referred to as MAV's) less than 15 cm in size are being developed for use in military and civilian applications such as surveillance and search and rescue. MAV's operate in a low Reynolds number (also referred to as Re) flight regime of approximately 10^5 to $5x10^5$. In this low Re regime, an open question is: what is the wing planform shape that maximizes the lift-drag (L/D) ratio for the aircraft? Increasing the L/D ratio would increase MAV range. Conventional analysis using theory or computer simulations is difficult in the Re range of MAV's leaving experimental study a desirable approach.

Gliding birds fly in a similar Re range raising the question of whether biologically inspired methods, such as genetic algorithms (GA), can be used to optimize wing planform shape. Genetic algorithms mimic the biological process of natural selection and mutation through successive generations to optimize designs. Previous work by Day[1] has shown that genetic algorithms, combined with wind tunnel testing of candidate wing shapes to measure lift-drag ratios, can yield improved designs with higher aerodynamic efficiency. The present study extends the work of Day[1] in the following ways;

1. Certain detailed aspects of the work of Day[1] are studied and verified including confirming that the optimized wing shapes are independent of the

initial wing population. Modifications to the genetic algorithm to reduce human influence were also made.

2. Genetic algorithms are applied to develop improved wing shapes at high angles of attack near stall for the first time.

3. Chord distributions of optimized wing shapes are found and compared to the chord distributions measured on order Galliformes bird wings (pheasants, etc.) with low aspect ratios and high wing loadings.

4. Flow visualization, with tuft studies and oil film techniques, is performed on the optimized wing designs to gain physical insight into why these planforms yield higher lift-drag ratios.

This thesis is organized as follows.

- Chapter one provides literature review and background information on MAV's, low Re air flow, genetic algorithms, and flow visualization.
- Chapter two details the project objectives.
- Chapter three includes the methodology and equipment used to perform the studies.
- Chapter four contains the results and analysis of the results.
- Chapter five summarizes the conclusions
- Chapter six provides examples of future work to extend and improve this project.

1.2 Micro-Air Vehicles

Recent advances in battery and electric motor technology have enabled the production of small (on the order of 15cm) flying vehicles known as micro-air vehicles. The small size of these vehicles opens up many new applications impossible for larger aircraft. Uses for MAV's include: military surveillance, search and rescue, mapping, and even exploration on other planets[2]. MAV's have a variety of flight methods, such as rotary wings (helicopters), flapping wings (ornithopters), and fixed wings. In this work the focus is on fixed wing MAV's such as in Figure 1.

Figure 1 WPI 2007 Micro Air Vehicle, Approx. 15cm wide[3]

Due to their small size, micro-air vehicles fly in a different Re regime than larger aircraft, and therefore require a new method of study. Since birds, bats, and insects already operate in similar airflows, studying them may yield useful information about how to improve MAV's.

MAV’s that fly in cluttered environments, such as urban or forested areas, require short wings. Longer wings are delicate and likely to hit obstacles, and are also harder to store. Historically, broad winged MAV’s are usually equipped with the Zimmerman wing planform, seen in Figure 2. This planform is created by joining two ellipses and has been extensively studied at low speeds[4].

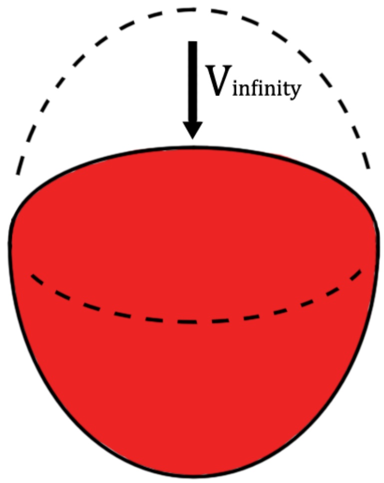

Figure 2 Zimmerman Planform

Because MAV’s are instruments of data gathering, having high endurance and range are very important, both of which are proportional to lift divided by drag. MAV’s with increased L/D values will perform better than those with lower values as seen in Equations 1 and 2.

$$R = \frac{L}{D}\frac{V_\infty}{c}\ln\left(\frac{W_i}{W_f}\right) \tag{1}$$

$$E = \frac{L}{D}\frac{1}{c}\ln\left(\frac{W_i}{W_f}\right) \tag{2}$$

In Equations 1 and 2, R is range, E is endurance, L is lift, D is drag, W_i is takeoff weight, W_f is final weight, V_∞ is the freestream velocity, and c is chord length. The higher the L/D value, the higher the range and endurance[5].

Previous investigations have studied the effect of wing planform on L/D. Mueller and Torres[6] studied various wing planforms, including the Zimmerman planform, and their effects on L/D. Day[1] created a genetic algorithm to find wing planforms with high L/D values.

1.3 Aerodynamics

Production of Lift and Drag

Before investigating specific aspects of flight and aerodynamics it is important to reiterate some of the fundamentals. This project primarily concerns lift and drag. Lift is a force directed perpendicular to the freestream fluid velocity. Airfoils and other shapes can produce lift when they move through a fluid. There are three main mechanisms involved in the production of the lift force on MAV's. Some lift is generated as the wing produces an area of low pressure above the wing. The curvature of the wing forces the air to accelerate over the upper surface of the wing (the Bernoulli Effect) creating an area of lower pressure compared to the lower surface of the wing. Lift is also generated by the angle of attack (AoA); the angle of the wing deflects air downwards to produce a counterforce, which also pushes the wing up. In low aspect ratio wings wingtip vortices also create lift by forming low-pressure areas on the upper surface of the wing[7].

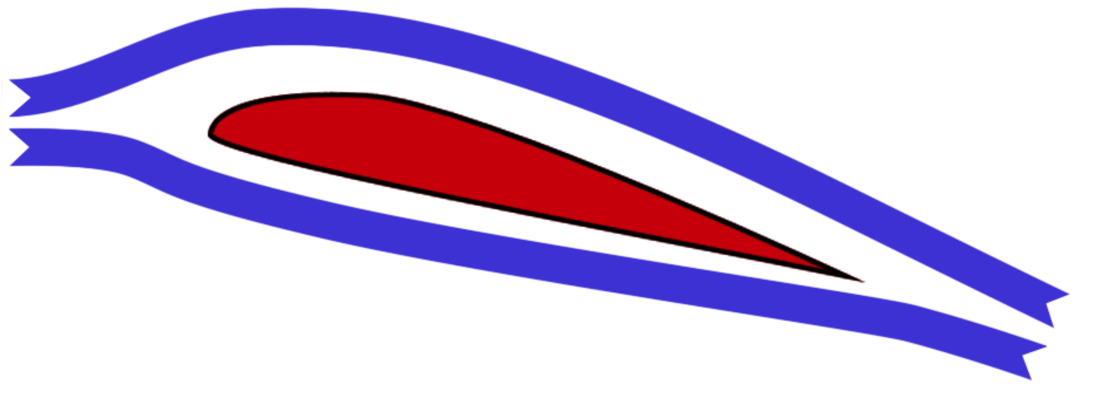

Figure 3 Path of Streamlines (Blue) Around an Airfoil

The plastic feathered wing in the wind tunnel tests in this study is essentially a flat plate airfoil. As a result the angle of attack and tip vortices are the primary means of lift production.

Measuring lift and drag is just one way of characterizing the forces on a wing. Normal and axial forces are usually easier to measure. Lift and drag can be easily calculated from the normal and axial forces, and vice versa. The directions of the forces and the equations used to convert them are shown below. The normal force is perpendicular to the wing chord, while the axial force is parallel to the chord. Lift is perpendicular to the direction of the oncoming airflow, and drag is parallel to the oncoming airflow. Equations 3 and 4 can be used to convert normal and axial forces to lift and drag[8].

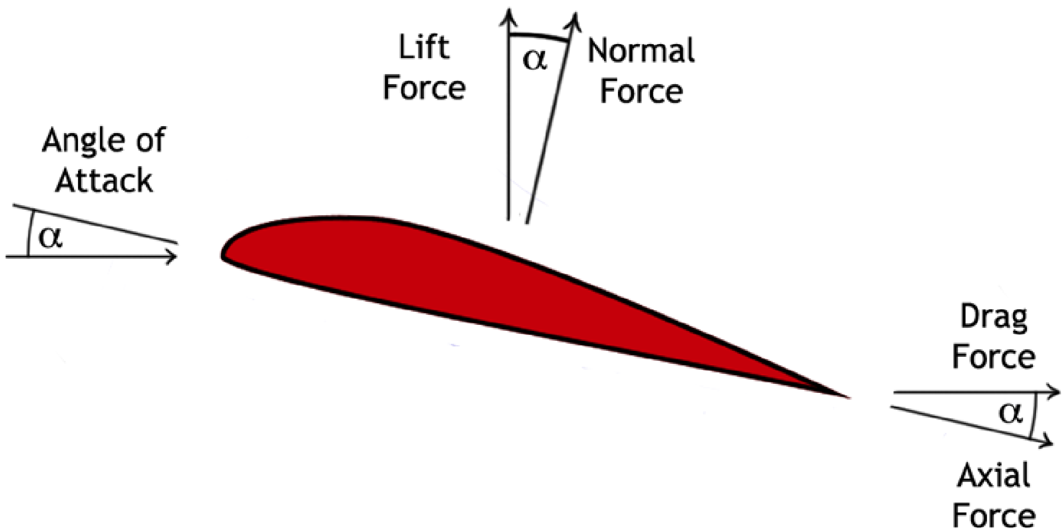

Figure 4 Various Forces on an Airfoil

$$L = N\cos(\alpha) - F_A\sin(\alpha) \quad (3)$$

$$D = N\sin(\alpha) + F_A\cos(\alpha) \quad (4)$$

In Equations 3 and 4, L is lift, N is the normal force, α is the angle of attack, F_A is the axial force, and D is the drag.

It is difficult to determine the angle of attack for flapping birds because the airflow around the wing is the sum of both the wing's flapping movement and the forward motion of the bird. However, it is easier to determine the angle of attack of MAV's, many of which have fixed wings. A common angle of attack for a cruising MAV is around four degrees.

Flight Regime

The Reynolds number characterizes the ratio of inertial forces to viscous forces. The Re determines the flow regime, as turbulent, laminar, or transitional. Similar shapes in different regimes will behave differently, and a proper analysis demands understanding the Reynolds number of the flow, given by Equation 5

$$Re = \frac{\rho V_\infty c}{\mu} \tag{5}$$

Here, ρ is the density of the fluid, c is the characteristic length (usually the chord), V_∞ is the freestream velocity of the fluid, and μ is the viscosity of the fluid.

Laminar flows tend to follow the contours of objects and have predictable streamlines. Laminar flow around an airfoil is usually considered to have Reynolds numbers of less than 500,000, though near 500,000 the flow can be transitional and have properties of laminar and turbulent flow.

Turbulent flow occurs for higher Reynolds numbers, greater than 500,000. Turbulent flows contain many eddies and vortices and are unpredictable and chaotic.

Boundary layers are layers of air surrounding solid surfaces in a fluid flow where both viscous and inertial effects are important. Due to the no slip condition flow velocity must go to zero at a surface, above the surface the velocity increases to the freestream velocity. The boundary layer is generally considered to end when the velocity reaches 99% of the freestream velocity[9].

Separated flow occurs when flow moves upstream, against the free stream velocity. This is caused by an adverse pressure gradient, where pressure increases in the downstream direction and opposes the motion of the flow. Even in otherwise laminar conditions, once a flow becomes separated is usually also becomes turbulent and chaotic. Separated flows cause severe drag and are generally undesirable on airfoils. Figure 5 shows the velocity profile of a separated flow. The dotted line indicates the edge of the boundary layer[8].

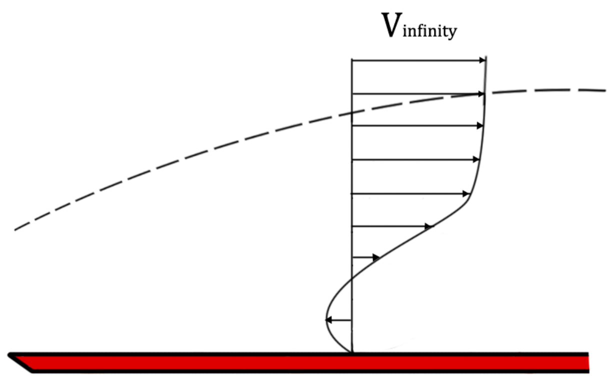

Figure 5 Separated Flow in a Boundary Layer

Laminar boundary layers are susceptible to flow separation, while turbulent boundary layers go from the no slip condition to higher velocities in a relatively shorter distance, as seen in Figures 6 and 7[9], giving them higher momentum and allowing them to resist flow separation more than laminar flows. However, as long as the flow is attached laminar boundary layers impart less drag on a surface than turbulent boundary layers do, because of their gradual velocity change[8].

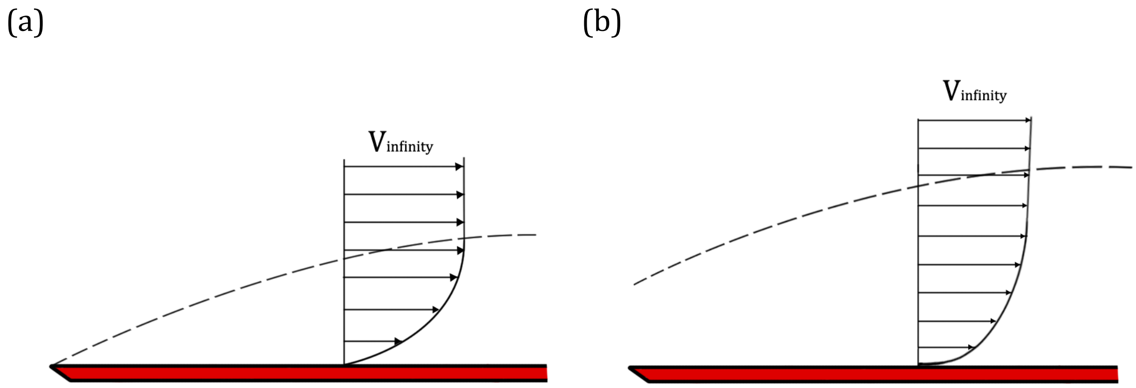

Figure 6 Laminar (a) and Turbulent (b) Boundary Layers

The plastic feathered wings in this study have Reynolds numbers of approximately $1.8 \cdot 10^5$, similar to the Reynolds numbers of medium sized birds and MAV's. For a wing with a Reynolds number of $1.8 \cdot 10^5$, the leading edge flow is likely laminar, then possibly becoming transitional and turbulent as it travels toward the trailing edge, depending on disturbances in the flow. These transition points are hard to predict, although flow visualization, which is conducted in this study can help determine these points.

Separation bubbles occur in transitional flow. A separation bubble occurs when laminar air separates from the wing; at very low Reynolds numbers the flow will then become completely separated. If the flow then becomes turbulent enough (that is, has enough momentum in the boundary layer) it can reattach to the wing, creating a vortex obstructing the surface airflow and drastically increasing drag, as seen in Figure 7[10]. When the adverse pressure gradient is too great the bubble can burst again, causing the flow to become completely separated and increasing drag. In previous studies by Bannasch[11] flow visualization with smoke revealed that separated flow over low Reynolds number wings often consists of an attached separation vortex preceding the separated airflow, shown in Figure 8.

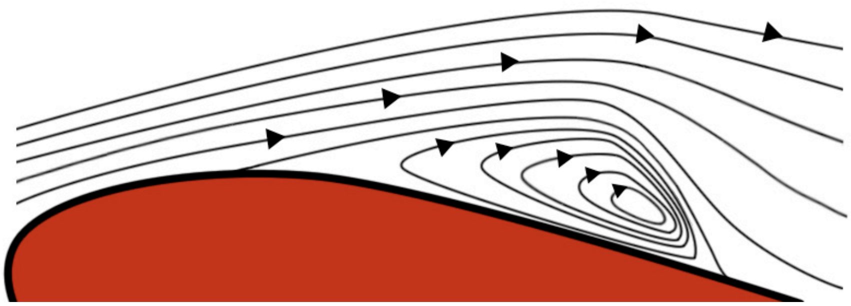

Figure 7 Attached Laminar Separation Bubble on Airfoil

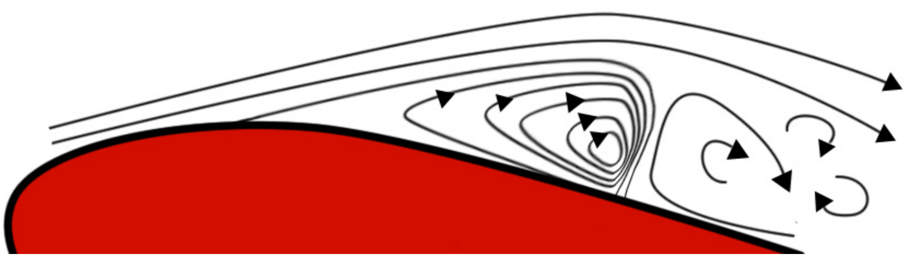

Figure 8 Separated Flow Following Attached Separation Bubble

Wingtip vortices can energize the flow over the wing, causing the flow to remain attached near the wingtips[12]. For this reason separation bubbles tend to occur near the wing root and not the wing tips.

Three Dimensional Effects

The wing aspect ratio is defined as the ratio of the wingspan to the chord length. Most MAV's have low aspect ratios, less than two, while gliders can have aspect ratios of nearly 20. In non-rectangular wings the aspect ratio is found with Equation 6

$$AR = \frac{b^2}{A} \tag{6}$$

In Equation 6, AR is the aspect ratio, b is wingspan and A is total wing area.

Given the low aspect ratio of the wings; three-dimensional effects will play a strong role in the airflow about the wing, with the most prominent effect being wing tip vortices. Wing tip vortices are formed by high-pressure air from the lower wing surface moving into the low-pressure area on the upper surface of the wing, creating a long cylindrical vortex trailing behind each wing tip. As seen in Figure 9, the vortices accelerate the air around the wingtips downwards. Since the local airflow is moving downwards, the effective angle of attack is less than the actual angle of attack. Since lift is perpendicular to the local airflow, it re-orients the direction of lift in the aft direction, creating induced drag[8].

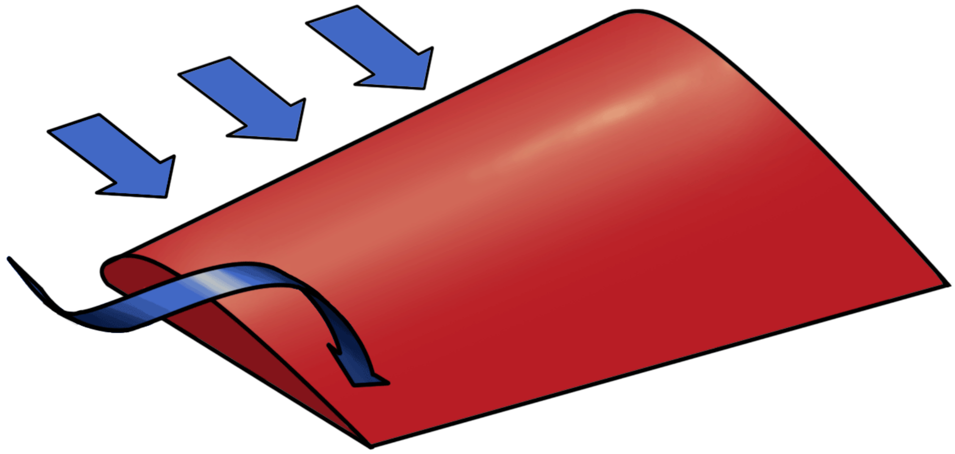

Figure 9 Wingtip Vortex

However, this can be advantageous. The fast rotation of the vortices gives them a lower pressure, and as they travel over the wing's upper surface they produce lift near the wingtips, this is most prominent at moderate to high angles of attack[12]. Wingtip vortices also increase the angle a wing can fly at before stalling. Since they decrease the angle of attack experienced by the wingtip it can fly at higher angles before the airflow separates.

Biologically inspired methods for reducing induced drag have been investigated by Tucker[13], where the slotted wingtips of a Harris' hawk were found to decrease induced drag by spreading out the wing tip vortices.

1.6 Flow Visualization

Visualizing the flow of air around an object is essential to understanding it. Therefore, many forms of flow visualization depend on showing the effects of airflow with fluids, strings, or other light materials. One potential problem with these techniques is that if the airflow is affecting a material in addition to the wing, the extra material is in turn affecting the airflow. This modified airflow is not necessarily the same airflow as before, and must be monitored to make sure it is not changing too much.

Tuft Flow Visualization

Small strings on the surface of a wing will orient themselves in the direction of the local airflow. Rows of strings (tufts) can be used to show the airflow over the surface of an object. This type of flow visualization has been used to great effect, though the tufts can interfere with the airflow[14].

Oil Film Visualization

Another method of flow visualization is with oil film technique. Oil or some low viscosity liquid with low surface tension is mixed with a pigment and painted on the surface of the object to be studied. As the air flows over the base fluid, it naturally forms streaks that follow the local air velocity. The higher the air velocity at the height of the oil film, as in turbulent flow, the greater the effect on the film. The pigment makes these streaks visible and they can be used to qualitatively study the flow field on the surface of the object. Oil film techniques are used for determining areas of flow separation, laminar to turbulent transition, and the locations of vortices. Provided the fluid is much thinner than the boundary layer, it produces negligible effects on the air flow, so it can be assumed the flow field around the model painted with fluid is very similar to the flow field around the bare model[15].

Oil films are usually made of a medium, solid pigment, and/or a dye. Mediums should have low surface tension and dry quickly. The lower the freestream velocity, the less viscous the medium should be. Kerosene is a commonly used medium, but alcohol can be used for slower velocities. To make the pigment visible it should be in high contrast to the color of the model. For instance, white kaolin pigment on a black model, or lampblack pigment on a white model will show up well. In very low speed flows dyes should be used instead of pigments.

There are several disadvantages to oil film techniques that must be acknowledged. One is that the model cannot change positions, another is that the fully developed flow must be assumed to be similar to the transient flow at the beginning, or that the transient flow does not last long enough to significantly move the pigment. Once the test is complete the model should be photographed to record the final patterns. Afterwards, if the pigment is not permanent the model can be washed off and repainted again[15].

If the flow becomes separated, the pressure change can create a suction that collects the fluid. The fluid will form a ridge that can affect the air flow around it[15].

Gravity can also affect the pigment if it is placed on vertical or inclined surface. The effect of gravity also depends on the viscosity of the pigment medium and the inclination of the surface. Observing whether or not the pigment moves without any airflow can indicate whether or not there is a problem. If the pigment flows quickly in still air, it will interfere with the data[16].

It is important to remember, when analyzing the resulting data, that the pigment only records the flow on the surface of the object, within the boundary layer. Here the flow can be very different from what is happening outside the boundary layer. Still, the pigments can reveal very important phenomena, such as areas of flow separation and local streamlines.

1.4 Bird Wings

Classification of life forms is central to the study of biology. The modern classification system was developed by Carolus Linneaus and uses physical attributes to distinguish different groups.

Animals are organized into the following ranks, from largest and least specific to smallest and more specific: kingdom, phylum, class, subclass, superorder, order, suborder, family, genus, and species.

Animalia is the kingdom consisting of animals. Chordata is the phylum that contains vertebrate animals, or at least animals with notochords. Aves is the class that distinguishes birds. Neornithes is the subclass of modern toothless birds. Neognathae is the superorder that contains most modern birds, distinguished by their jaw anatomy. Galliformes is the order that is of the most relevance to this investigation[17].

Order Galliformes includes turkey, grouse, quail, and pheasant, as well as other land fowl. Most galliforms live in heavily forested areas. These birds commonly have heavy round bodies that require high wing loadings, short wings with low aspect ratios to navigate between closely packed trees, and well developed legs. Having evolved to carry heavy masses with short wings makes these birds of particular relevance to MAV's, which also have high wing loadings. The wing loading can be found by Equation 7

$$Wing\ Loading = \frac{W}{A} \tag{7}$$

In Equation 7, W is the weight and A is the wing area.

If galliform birds have been evolving for millions of years to optimize low aspect ratio wings with high wing loadings, it is likely that we can learn from them.

The wings of galliform birds often display a particular shape not commonly seen in other birds. They have a curved leading edge, and a rounded trailing edge with a conspicuous indentation or notch, as shown in Figures 10 through 13. Trailing edge notches have been previously investigated and found to decrease drag for low aspect ratio galliform wings by Drovetski[18]. However, triangular notches on MAV wings were found to produce little beneficial effect by Cubin[3]. Figures 10 through 13 show several galliform wings with the notch indicated by a red arrow. The pictures were generously provided by the Slater Museum[19] and will be useful in analyzing the wing chord distribution as a function of the distance along the wing span in Section 4.3.

Mountain Quail, Mar, adult, male

Figure 10 Mountain Quail Oreortyx pictus

Chukar, Mar, adult, male

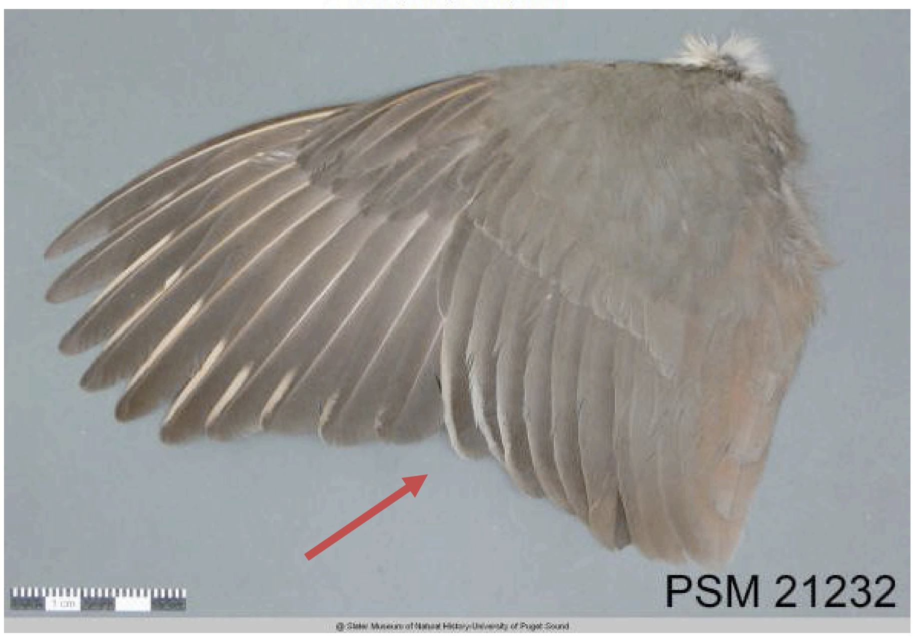

Figure 11 Chukar Alectoris chukar

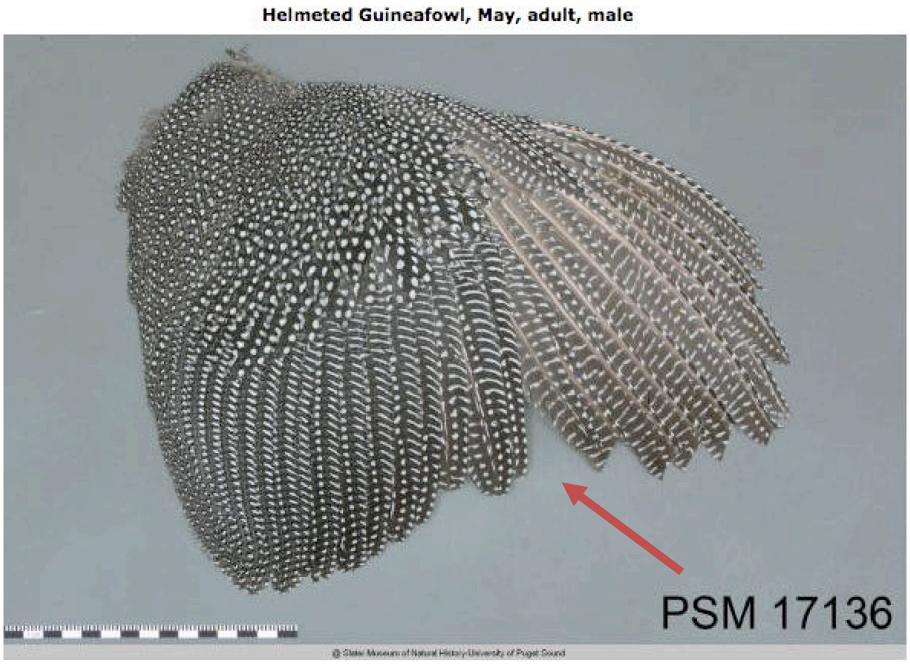

Figure 12 Helmeted Guineafowl Numida meleagris

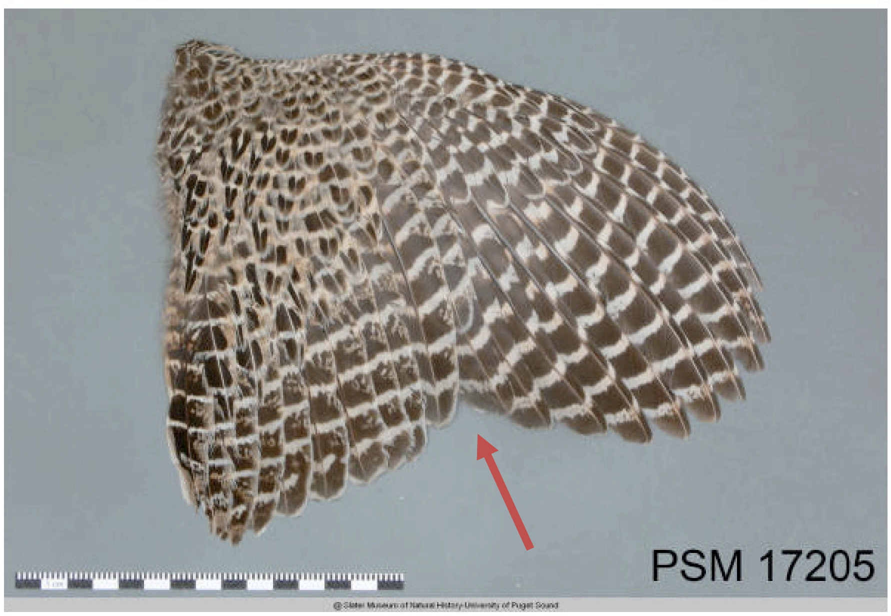

Figure 13 Ring Necked Pheasant Phasianus colchius

In contrast to the shorter, notched galliform wings, the wings of other birds tend to have higher aspect ratios and more tapered wings. Figures 14 through 16 show typical bird wings apart from galliforms.

Large birds that soar on thermals, such as hawks and eagles, have larger and longer wings in comparison to their body size. Their wings have a nearly elliptical planform, as seen in Figure 14.

Figure 14 Bald Eagle Haliaeetus leucocephalus

Soaring birds that cannot rely on thermals have even longer and thinner wings, shown in Figure 15. The albatross and sea gull are examples of long ultra-efficient wings.

Figure 15 Black Footed Albatross Phoebastria nigripes

Small seed and insect eating birds, such as the goldfinch in Figure 16, have short elliptical wings.

Figure 16 American Goldfinch Carduelis tristis

There are some cases where non-galliforms show a small galliform-like notch in their wings. Small indentations can be seen in Figures 17 and 18. Not surprisingly this occurs in owls and woodpeckers, both forest birds with short wings, lending credence to the possibility that this is convergent evolution, where different species evolve similar traits. However, neither wing shows the size notch that galliform wings do.

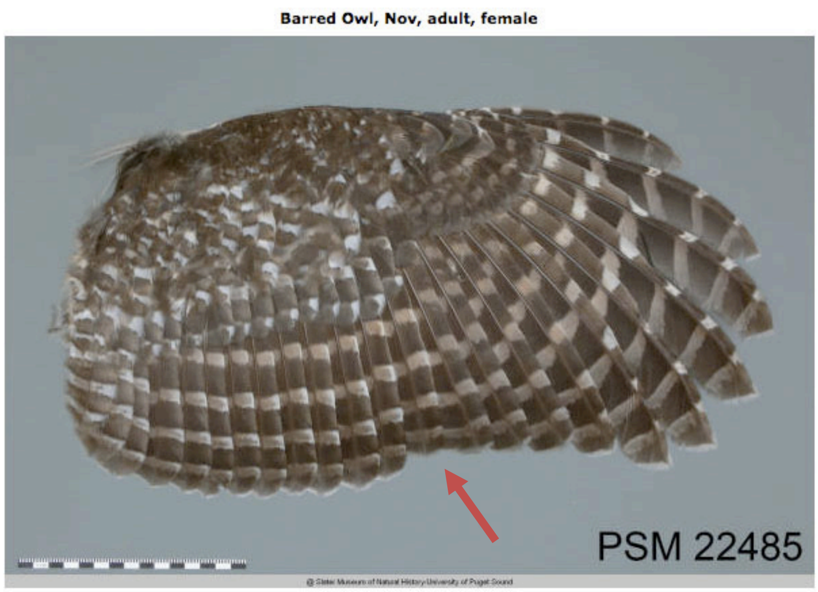

Figure 17 Barred Owl Strix varia

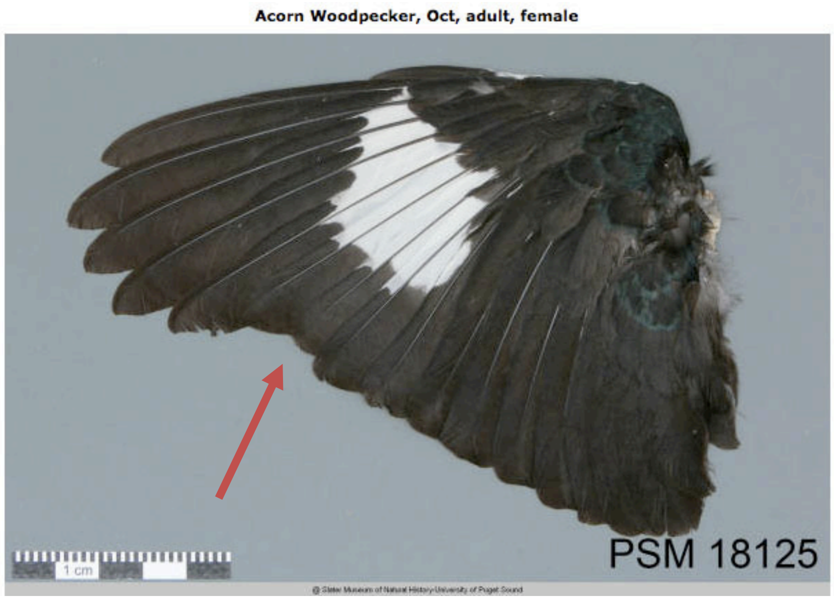

Figure 18 Acorn Woodpecker Melanerpes formicivorus

1.5 Genetic Algorithms

Natural selection is the process behind evolution. Due to mutation, no two individuals have the same genes, the units of information that determine physical characteristics. Individuals with beneficial genes for their environment are more likely to survive and pass on these genes to their descendents. Detrimental genes will be disadvantageous and are less likely to be passed on. Over time the population of individuals will generally have the beneficial genes, while the detrimental genes will become less likely and may eventually disappear[20].

Genetic algorithms are an artificial process designed to mimic natural selection. A generation of random chromosomes (sets of genes) is generated. The genes and their position in the chromosome determine the characteristics of the candidate solutions. These solutions are then tested against each other. The solutions judged superior will be more likely to pass their genes onto a new generation, where they will again be judged on fitness. This process repeats each generation. Every generation should be better than the last in terms of fitness, and if done correctly the later generations will converge to an optimal solution[21]. In this study individuals are judged superior or inferior based on their L/D values. High L/D values are desired while low L/D values are judged inferior. Figure 19 shows an outline of the process.

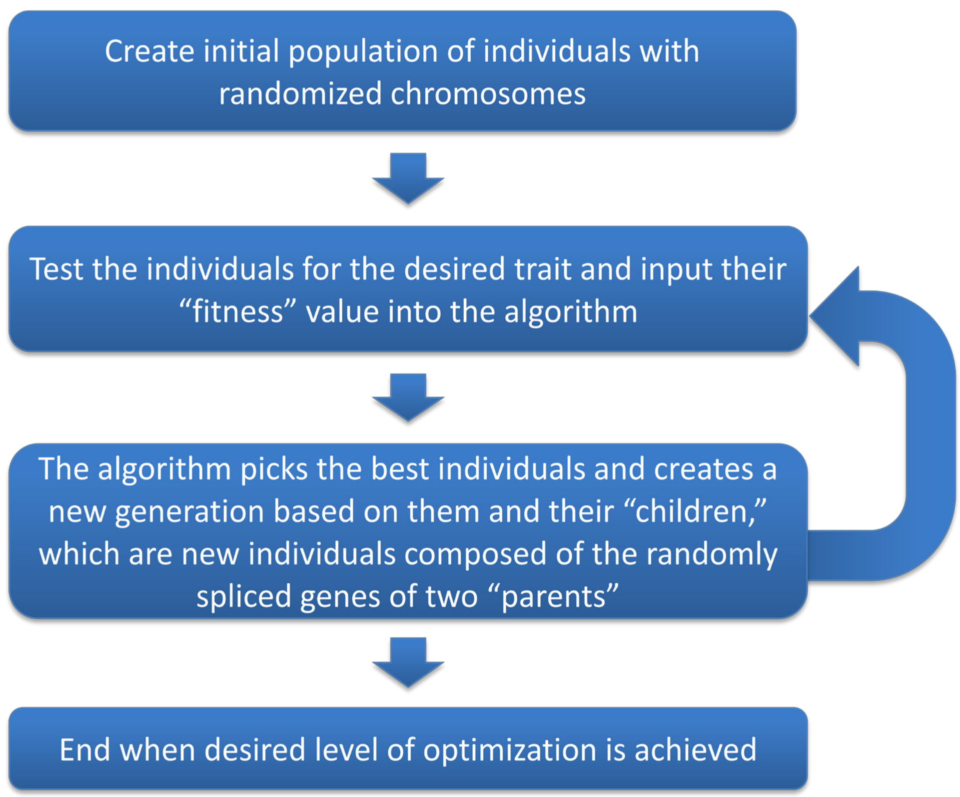

Figure 19 Genetic Algorithm Process

There are many different ways chromosomes can be selected for later generations. The genetic algorithm in this experiment employed a fitness function paired with roulette selection. The fitness function is a method of transforming the value of the desired trait into a number suitable to use in selecting the chromosomes. In this case the fitness function took the L/D value of each tested wing and subtracted from it the lowest L/D value from the same generation. This increases the proportional difference between the fitness of each wing and ensures to worst wing is never selected (as its fitness function is zero). To select the wings for the next generation a selection roulette is employed. The roulette method assigns different selection probabilities to each wing based on the fitness function. Wings with higher fitness functions are more likely to be selected, while wings with lower fitness functions are less likely. This ensures that even poorly performing wings can still be selected for the next generation, giving more variety to the gene pool and helping to avoid convergence at only a local optimum[21].

The techniques used to create gene variety in this experiment included sexual reproduction (also known as crossover) and mutation. Twelve wings were selected by the roulette for each new generation. The other twelve wings were created from the parent's genes by crossover and mutation. Crossover involves two of the selected individuals swapping their genes to create a 'child' with genes that come from both parents. In this case the genes of the child were picked randomly from either parent, shown in Figure 20, as opposed to neatly splitting the parent chromosomes in half and joining them[21].

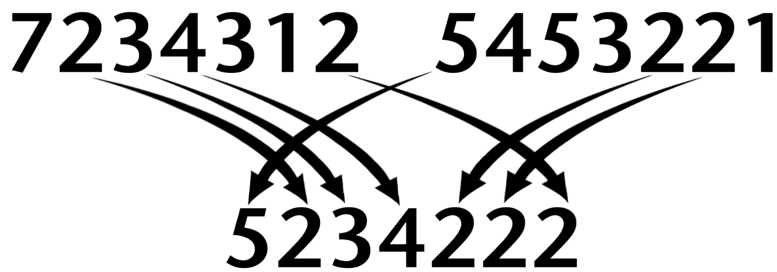

Figure 20 Parent Chromosomes Splicing Genes to Create New Chromosome

Mutation is the random alteration of a gene. This algorithm had few mutations, but their existence allowed for more variety than otherwise could have been[22].

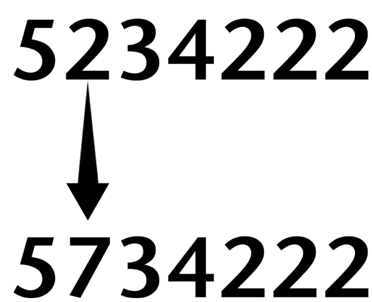

Figure 21 Random Mutation

It is interesting to note that while mutation always exists in natural selection, simply due to the imperfections of reproduction, sexual reproduction does not always occur. Most single celled organisms and some lizards reproduce via cloning. In fact, there is some evidence that sexual reproduction is optimal for promoting flexible genes that work well with others, instead of finding an optimized chromosome[23]. In genetic algorithms crossover has been compared to macro-mutations, and the mixing it provides may not be necessary[22].

Termination of the genetic algorithm often occurs when the population consists of one type of chromosome (mutation will always ensure that the population is never entirely uniform) and an optimum is reached. Genetic algorithms can also be terminated due to time constraints. Generally the experimenter must make the decision of when to terminate while trying to balance issues of time and success at optimization.

Genetic Algorithms are exceptionally good at finding solutions in large solution spaces when no immediate intuitive solution exists. For this reason they are often used in aeronautical design, where there are many possible solutions. Mueller and Torres created a genetic algorithm to optimize the stability, range/endurance, and payload of a MAV, altering aspect ratio, wing planform, and tail placement[6]. Obayashi, Oyama, and Nakamura studied the use of Adaptive Range Genetic Algorithms (ARGAs) to optimize transonic wings for high L/D values[24]. Quagliarella and Cioppa applied genetic algorithms to the optimization of transonic airfoils[25]. Jones, Crossley, and Lyrintzis used a genetic algorithm to optimize rotorcraft airfoils for low drag and low noise within certain constraints[26].

As a note on the language used in this report, it is important to remember that genetic algorithms are not intelligent. The computer is not exercising any creativity or decision-making prowess. A simple code is producing the results. Despite this, the results and process can often appear creative or intelligent, and due to the limitations of English, which tends to anthropomorphize things, the words used may sometimes make it appear as though the code is acting intelligently. This will be avoided when possible, but may still occur.

1.7 First Genetic Algorithm Low Angle of Attack Test

A goal of this project is to confirm the 2007 work of Andrew Day, for that reason his genetic algorithm methodology is repeated, with a few differences. Chromosomes that are similar (having more than four identical genes) to the original best chromosome are removed from the initial generation. If the process is repeated and still produces similar results, it will strengthen the original conclusions and show the optimized wing is independent of the initial population.

In Day[1], each generation in the first use of the genetic algorithm showed a general progression from lower L/D values to higher values and a final wing was produced with an L/D value of about 3.3, as shown in Figure 22[1].

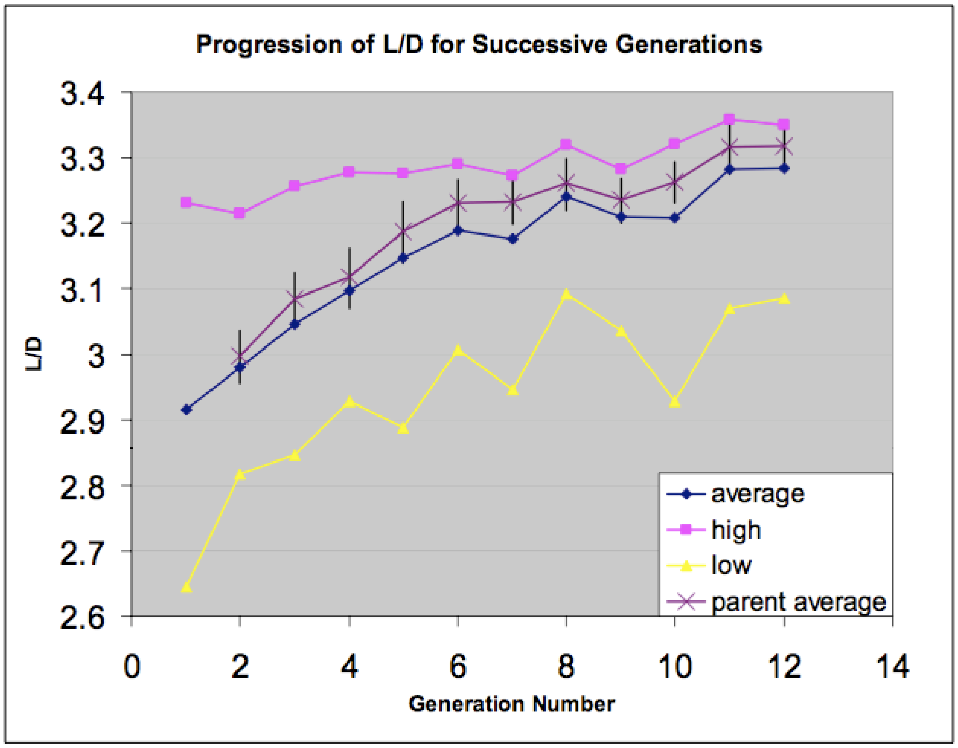

Figure 22 First GA Application L/D Values[1]

The final, best performing wing had chromosome 7732100 seen in Figure 23. The optimized wing planform sports a notch in the trailing edge, also seen in the wings of galliforms and the low aspect ratio wings with the highest L/D values found by Drovetski[18].

Figure 23 First Iteration Low AoA Optimized Wing

2. Project Objectives

The overarching goal of this thesis is to perform wing planform optimization using biologically inspired methods such as genetic algorithms, and conducted with low aspect ratio bird wings in mind. Flow visualization will then be used to study the airflow of particularly interesting wings. The following bullets list the specific objectives.

- Verify the results of Day's 2007 genetic algorithm to optimize the low angle of attack wing planform by performing a second application of the genetic algorithm under the same conditions. This study will confirm that the final optimized wing shape is independent of the chosen initial population.

- Apply the genetic algorithm with the wing at a higher angle of attack, to obtain optimized planforms with maximum lift-drag ratios for wing conditions near stall. High angle of attack flight is also important to MAV design and allows for low speed flight.

- Analyze and compare the wing chord versus span distribution for the best wings from the genetic algorithm with order Galliformes bird wings characterized by low aspect ratio and high wing loadings.

- Perform flow visualization using various methods, including tuft studies and oil film techniques, to observe and record flow. The flow visualization should give insight on why some wing planforms yield higher lift to drag ratios by detailing flow separation, and laminar to turbulent transition.

3. Equipment and Methods

3.1 Wind Tunnel

The WPI recirculating wind tunnel was used to obtain the data for this experiment. The wind tunnel has a test section with a width and height of .61 meters and a length of 2.4 meters in the flow direction with transparent walls and a variety of ports to insert equipment. Upstream of the test section a wind tunnel contraction with a contraction ratio of 6:1 accelerates the flow. The air flows through turbulence suppression screens, reducing large scale eddies. All tests were conducted at a freestream tunnel velocity of 18 m/s. At these speeds the air has a freestream turbulence level of less than .73%[27].

3.2 Feathered Wing

The present study uses the same experimental apparatus as Day[1], a flat wing with variable length feathers, shown in Figure 24 and 25. With the feathers fully extended, the test wing is shaped like the Zimmerman planform. The length of the seven feathers can be changed to alter the shape of the wing. Each wing shape is identified by a chromosome, which consists of seven numbers. The chromosome of the Zimmerman approximation is 7766543, each number referring to the amount of visible lines shown on each feather, marking distances of about 1 cm as shown in Figure 24. The wing can take on nearly 400,000 different combinations of feather lengths.

Figure 24 Wing with Feathers Fully Extended

Figure 25 Wing with Feathers Retracted

The leading edge of the wing is rounded and the sides of the feathers are tapered to a point to reduce flow disturbances since the feathers overlap. Eight equally spaced .5 cm diameter holes with screws fasten the wing securely to the wing base. The wing span from the center of the holes (wing root) to wing tip is 14.2 cm. The maximum chord length is 15.5 cm with the feathers fully extended. The wing root has a length of 10.4 cm. When inserted into the wind tunnel, all feathers must be entirely visible. To allow the wing to fit into the wind tunnel, the trailing edge of the wing lacks a feather near the wing root, as a result it is not a perfect Zimmerman planform.

With a chord length of .155 m, a freestream velocity of 18 m/s, air density of 1.21 kg/m^3, and air viscosity of 1.81 x 10^{-5} Ns/m^2 the Reynolds number for the feathered wing at test conditions is 186,513[9].

3.3 Force Balance and Calibration

The feathered wing (see Figure 26) is mounted on an aluminum frame designed and constructed by a team of WPI students[28]. The frame consists of two parts, an immobile base and a floating island that holds the wing. The island was designed to preclude vertical movement, while still being flexible in the axial direction. Two thin aluminum strips allow the wing to move back and forth when different axial forces are applied.

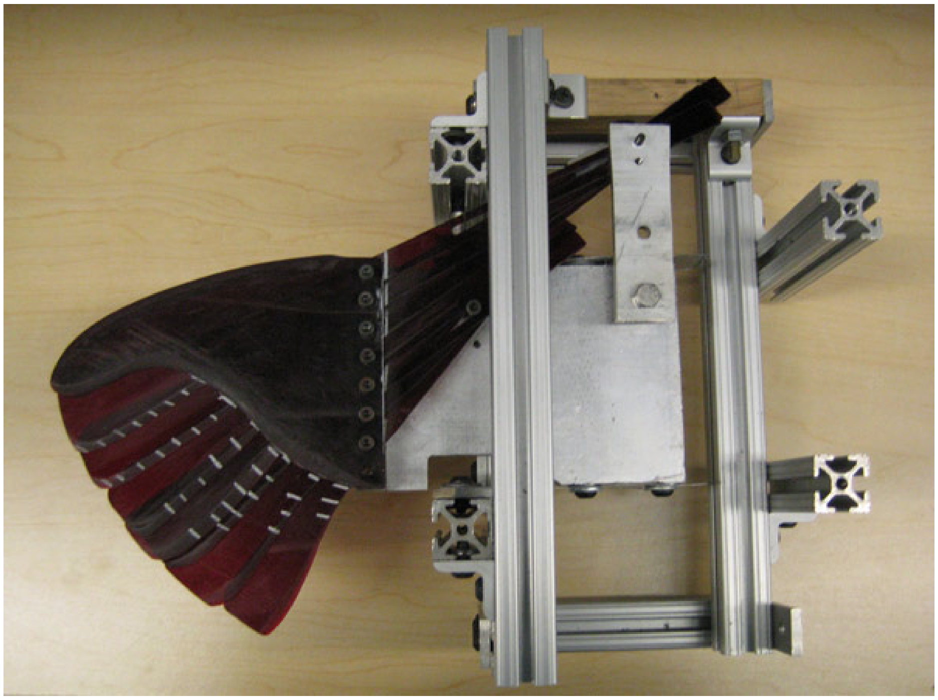

Figure 26 Feathered Test Wing and Frame

3.4 Drag Measurement

An Indikon AP-1297 proximity probe (Figure 27) mounted at the front of the base generates a magnetic flux field that varies with the distance between the proximeter and steel plate attached to the island. As the wing moves in the axial direction, the plate moves with it.

Figure 27 Indikon AP-1297 Proximeter

The proximeter converts the change in the magnetic field into a voltage that varies linearly with the distance to the plate. The voltage is then displayed by a multimeter with a precision of one millivolt. The voltage readout can then be used to measure the movement of the wing in the axial direction. The drag force can then be determined after the setup is calibrated. Calibrating is done by attaching weighted strings to the wing and wind tunnel, as shown in Figure 28, and then using simple trigonometry to determine the drag force applied to the wing. The horizontal force applied to the wing by the weights is determined by Equation 8.

$$D = \frac{M}{\cos(\alpha)}(\tan(\theta_1) + \tan(\theta_2))\cos(\beta) \tag{8}$$

In Equation 8, θ_1 and θ_2 are the angles of the string, α is the angle of attack, β is the angle the string makes with the wind tunnel wall as seen from above, and M is the mass in grams. All forces in this test are measured in gram-weights, the force one gram produces with an acceleration of $9.8 m/s^2$.

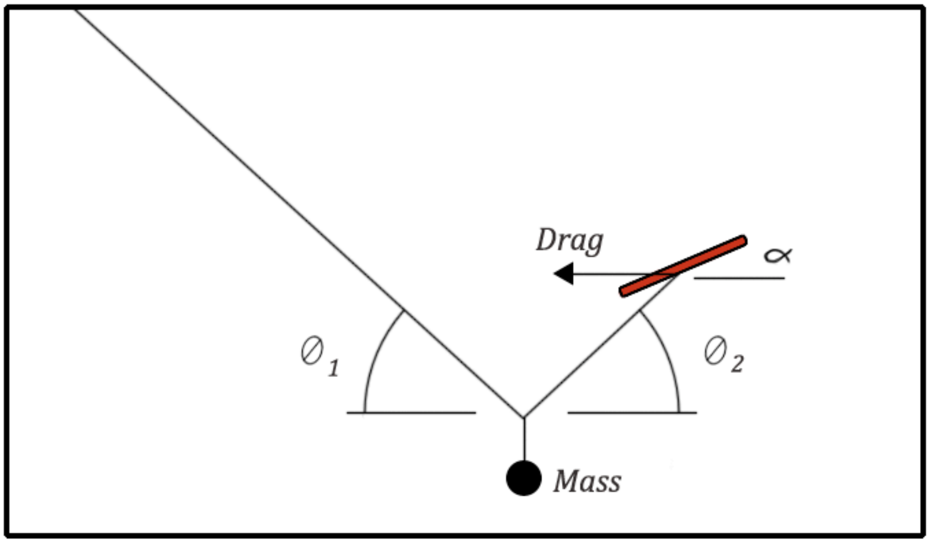

Figure 28 Calibration Setup

At least four weights were used (from zero to thirty grams) in the calibration process. A least squares fit line was applied to the drag and voltage data, the slope yields the mV to grams conversion. To ensure accuracy, R^2 values of more than .995 were desired, if the R^2 value was less the setup was checked and the calibration was repeated.

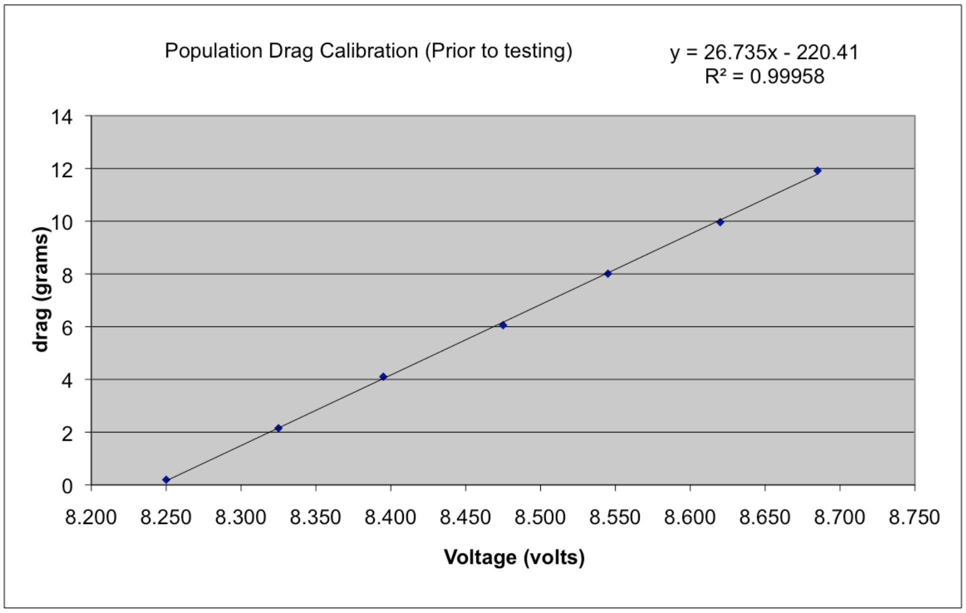

Figure 29 Sample Calibration Graph

The horizontal component of the axial force can then be found by Equation 9,

$$D_1 = S_1(V - V_0) \tag{9}$$

In Equation 9, D_1 is the horizontal component of the axial force, S_1 is the slope of the calibration line, V_0 is the voltage with no applied force, and V is the voltage during the test.

The calibration only determines the horizontal component of the axial force; however the lift also exerts a force in the axial direction, counter to the axial force. Therefore the drag equation must include this effect in Equation 10[1].

$$D = D_1 + L\sin(\alpha) \tag{10}$$

If the normal force is measured instead of the lift, the horizontal component of the normal force must be included in the drag. The normal force is perpendicular to the axial direction and cannot be measured by the proximeter, so its contribution to drag must be included in the drag equation.

$$D = D_1 + N\sin(\alpha) \tag{11}$$

The frame and equipment were placed outside of the wind tunnel so as not to interfere with the airflow, while the wing fit through a small hole in the test section wall seen in Figure 30. A sheet of clear transparency plastic was used to limit any airflow through the open area of the hole. The sheet still needed to allow the wing and island to move freely to take accurate measurements, so there were gaps around the transparency that allowed some air to pass through. This was unfortunate as it produced flow different from what a real MAV wing would experience, but was necessary to record accurate data.

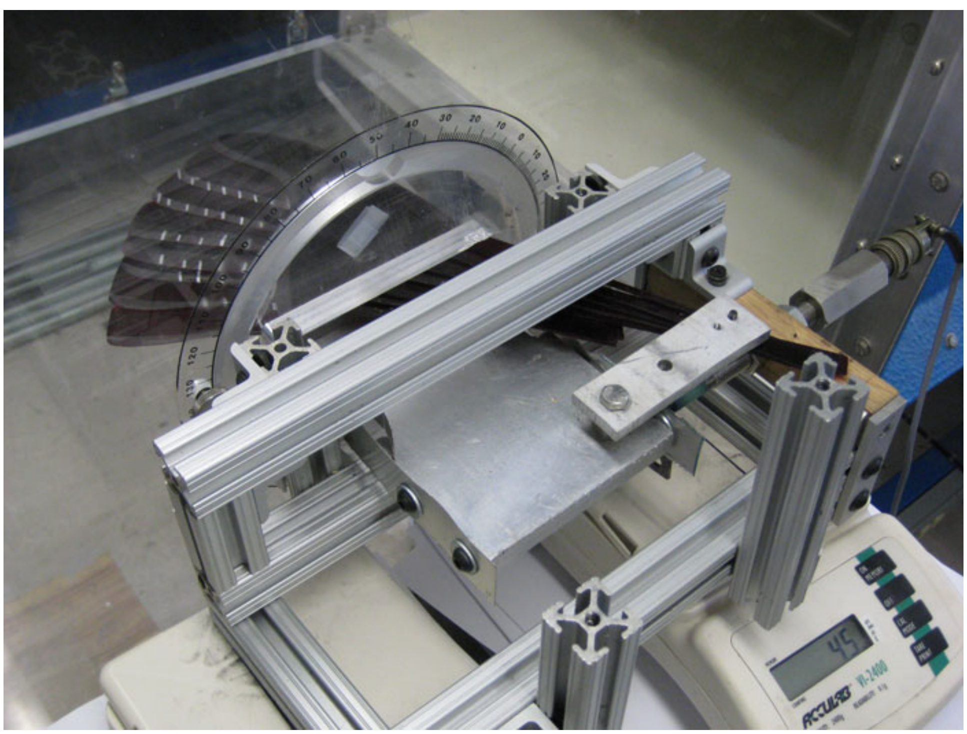

Figure 30 Close-up of Wing and Wind Tunnel Setup

3.5 Lift Measurement

Depending on the setup of the wing apparatus, either the normal force or the lift force is measured. Both are measured with two Acculab VI-2400 digital scales, each with an precision of ±0.1 grams. Before each test the scales are set to zero. As the lift reduces the weight of the wing on the scales they display a negative weight. The sum of the negative weight measured by the two scales is the lift or normal force, depending on the orientation of the scales.

The lift force is measured when the scales are horizontal and the wing is placed on them at an angle, and the normal force is measured when the scales and wing are at the same angle. Figure 31 shows the general setup for a lift reading. The stacks of paper allow for quick adjustments of the height and angle of the wing.

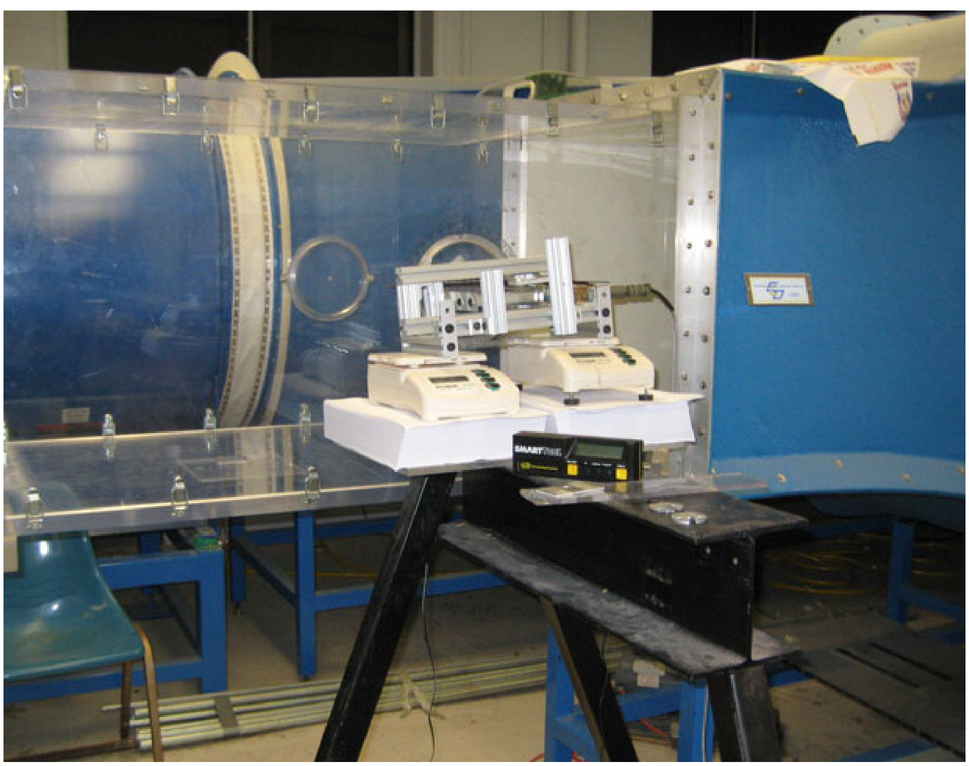

Figure 31 Equipment Setup for Lift Measurements

Figure 32 shows a setup that measures the normal force. The lift can be found from the normal and axial forces. Where F_A is the axial force, D_1 (also called Drag 1 in the appendices) is the horizontal component of the axial force, L_L is the weight measured by the left scale, and L_R is the weight measured by the right scale. The weights are initially displayed as negative values, though they indicate positive lift.

$$F_A = \frac{D_1}{\sin(\alpha)} \tag{12}$$

$$L = N\cos(\alpha) - F_A\sin(\alpha) \tag{13}$$

Figure 32 Equipment Setup for Normal Force Measurements

3.5 Testing Process

Once the wing was inserted and set to the desired shape, the wing was checked for any interference with the wind tunnel wall. This was done by pushing the wing island and checking that it moved freely and oscillated without quickly damping out. The scales were set to zero and the voltage readout from the proximeter was recorded as V_0. Then, the wind tunnel was set to the 18 m/s. After the air reached full speed, which took approximately three minutes, the voltage was again recorded, along with both of the weights from the scales.

These values were input into an Excel spreadsheet that applied the appropriate equations, depending on whether or not the scales were set to measure the normal or lift force. The spreadsheet then returned the L/D values. See Appendix A for spreadsheet examples.

Whenever a wing was repeated, either by chance or because it was reproduced in a later generation, it was retested completely. It would be easy to simply rewrite the data, but that would potentially allow errors to occur more than once. Therefore each test was performed anew.

3.6 Genetic Algorithm Process

The calculations for the genetic algorithm were done using Matlab codes. The first generation needed a large set of randomly generated wing planform shapes, 72 for this experiment, to provide good coverage of the solution space. The chromosomes were produced by the Initial Population Matlab code, seen in Appendix B. The code produces an Excel spreadsheet with the name of populations.xls that contains the chromosomes. These chromosomes were then tested, and the spreadsheet returned the L/D and fitness function values from the test data.

Each generation is contained on a new sheet in the populations.xls spreadsheet. The first generation's sheet is named '1,' the second '2,' and so on.

The Genetic Algorithm Matlab code asks the user to input the number of the last completed generation, and then uses the L/D values in the populations.xls spreadsheet to select and produce the next generation on a new sheet in the same spreadsheet, calling up the selection roulette routine in the process. The selection roulette made it more likely for the better performing wings to be picked for the new generation. All generations after the first had 24 chromosomes, the first twelve were taken directly from the previous generations and the last twelve were created by crossover and mutation from two 'parents' in the first twelve chromosomes.

This process repeats each successive generation until the user is satisfied with the optimized wing, or otherwise decides to end the process. Between each generation wind tunnel testing is conducted to measure the L/D values for the wing shapes for the previously created generation.

The genetic algorithm is detailed in Day[1]. The codes used in this study were very similar, with a few small changes for the sake of efficiency. The new Matlab code was altered to automatically produce 'random' numbers seeded from the clock time, using the twister algorithm provided by Matlab. Random numbers determine which wings are picked for each generation (however the likelihood of each wing being chosen depends on the fitness function), where crossover occurs in the chromosome, and when mutation occurs. This meant that a human was no longer required to roll dice as in the first experiment.

In keeping with the desire to remove human interference from the algorithm, the fitness function was changed for the high AoA tests. In Day[1] and the low AoA genetic algorithm of the present study the fitness function was chosen by the operator, it was a number always slightly higher or equal to the lowest L/D value of an individual in that generation. In the high AoA genetic algorithm the lowest L/D value of the generation was subtracted from all L/D values from the same generation. This increased their relative differences and makes the selection routine more likely to pick superior chromosomes.

3.7 Low Angle of Attack Genetic Algorithm Tests

The results of Day[1] needed to be verified before any further work was done. Only one run of the genetic algorithm was completed in the original work. To substantiate the results, a similar experiment was run, repeating the genetic algorithm at the same angle of attack. A different initial population was used in the present study to confirm that the resulting optimized wings are independent of the initial population.

The genetic algorithm was modified to remove certain chromosomes from the initial population. An issue with genetic algorithms is that a particularly high performing individual in an early generation can force the later generations to adopt their genes, not allowing different chromosomes to be explored. Since the previous work already proved the 7732100 chromosome effective at producing a high L/D, individuals with similar chromosomes were removed in generation one. If indeed 7732100 is the optimized chromosome, then random mutation and interbreeding should produce it again, otherwise different options will be explored by the algorithm. Chromosomes with more than four genes with the same values and position as 7732100 were considered similar enough to be removed.

The wing was held at 4.6 degrees angle of attack for this study.

3.8 High Angle of Attack Genetic Algorithm Tests

Flight at high angles of attack are useful for MAV's flying at slow speeds, furthermore high angles of attack generally yield flow visualizations with more distinct flow phenomena, such as boundary layer separation. To optimize for this flight condition another genetic algorithm study was conducted at an angle near stall.

Setup and data recording were very similar to the low angle tests, though normal force measurements instead of lift were taken. Because of this, Equations 13 and 10 were used to find lift and drag, respectively.

3.9 Flow Visualization

In order to gain insight into possible reasons that the higher performing wings yielded high L/D values, flow visualization studies (tufts and oil films) were conducted in order to observe and characterize flow phenomena on various wings.

Flat Plate Wings

Tuft studies were initially conducted on the original feathered wings, but due to their overlapping feathers the wings have ridges and gaps that would not necessarily appear on an MAV wing. Furthermore, the focus of this thesis is wing planforms, and not modifications to the wing airfoil or surface. Flat aluminum wings were created to test the wing planforms without any surface or curvature effects.

Three wing planforms were chosen for the flat plate tests. These were an approximate Zimmerman planform based on the fully extended feathered wing, the best high angle of attack planform, and a ring necked pheasant planform. The Zimmerman planform is a standard wing for MAV's. The best high angle of attack wing was selected to investigate why it yields high L/D values. The pheasant wing was selected as a representative galliform wing. The low angle of attack planform was not selected to be made into an aluminum wing because of uncertainty about whether or not interesting flow patterns would be visible at such a low angle of attack, as few phenomena of interest had appeared on the low angle tuft studies.

Photos of the feathered wing set to the Zimmerman approximation (Figure 24) and best performing high AoA shapes were taken with a digital camera and used to create three-dimensional models in Solidworks 2008. A photograph of a ring necked pheasant provided by the Slater museum was also used (Figure 13). These models were the same size as the original feathered wings and had the same eight holes to attach them to the frame. The Solidworks models were then turned into a set of drilling instructions for a CNC mill using GibbsCAM. Using the program, the three wings were then machined out of 1/8th inch aluminum plate as seen in Figure 33. See Appendix C for the Solidworks drawings of all three wings.

Figure 33 Machining the Wings in a CNC Mill

To create a high contrast surface for flow visualization, the wing surfaces were spray-painted matte black. Spray paint was used because it has a smoother finish than brushed paint.

Figure 34 Flat Plate Aluminum Wings

Tuft Studies

To find why the various chromosomes of the original feathered wing produced differing L/D values flow visualization was needed. To this end a tuft study was completed.

Polyester strings were taped to the wing with their free ends able to move. The strings were 1.5 cm in length with approximately .2 cm under the tape, giving 1.3 cm of free string. The strings were spaced 1.3 cm apart in both the direction of the flow and perpendicular to the flow, to avoid them getting tangled with each other (see Figure 35). Neon yellow strings were used so they would show up well against the dark maroon of the wing[14].

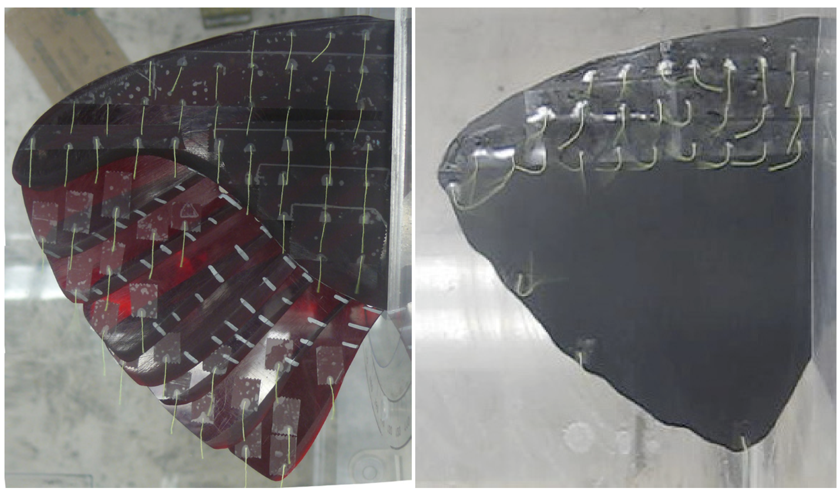

Figure 35 Tuft Placement for Feathered (Left) and Aluminum (Right) Wings

For the feathered wings, with mobile overlapping feathers, the trailing end of the wing could not have as consistent placement of the tufts as the leading edge. They were still placed as consistently as possible however.

A Panasonic camera was used to take 8-megabyte pictures of the wing. Videos of the wings in the wind tunnel were also created, each one lasting at least twelve seconds.

Lift and drag measurements from the tuft studies of the feathered scale model wings revealed that they had much less lift and drag than wings without tufts.

This raised concerns about the tufts affecting the airflow. To mitigate this for the aluminum wing tuft studies only three rows of tufts were added to the leading edge and four tufts were added to the trailing edge, as shown in Figure 35.

Oil Film Techniques

An oil film technique commonly known as china clay technique was used in the present study. China clay (also known as kaolin) is mixed with a liquid medium and painted on the wing in a thin film. When air flows over the wing, the flow produces patterns in the film that reveals aspects of the surface flow. Kaolin is a common ingredient in stomach medications and makeup, and poses little threat of combustion. It also is relatively inexpensive.

Kerosene is commonly used as the medium, and is readily available. Important requirements for any base fluid are transparency, low surface tension, and rapid vaporization.

Kaolin and kerosene were mixed in a 1:6 ratio, other pigments could be added but were never necessary for this experiment. When mixing, the kaolin generally settles at the bottom of the container. Before the mixture is applied to the wing, it must be mixed first, and then applied to the wing.

When mixed with kerosene, the kaolin is nearly clear and slightly brown. It will change to white when it dries in the airflow. The mixture was brushed onto the wing surface lightly and perpendicular to the airflow so any streaks from brushing are obviously not produced by the flow. Only a very light coat is required.

The flat plate wings were placed in the wind tunnel at an 11.8^0 and 4.6^0 angle of attack. To test whether or not gravity would affect the flow, the wings were painted with the kaolin mixture and allowed to dry in still air at the two angles of attack. It was confirmed that gravity had no effect on the flow visualization results by painting the wings and letting them dry in still air. They were then painted with the kaolin and kerosene paint. As soon as the wings were painted the wind tunnel was sealed and set to 18 m/s.

There is the possibility that during wind tunnel startup, the changing airflow is affecting the paint and rendering an inaccurate pattern. Since the paint was observed to dry only after the full speed was reached this seems unlikely. If higher airspeeds were tested it would take longer to reach the final speed and drying would be more likely, however it was not an issue for this experiment.

As the paint dries the kaolin becomes highly visible. Where the paint dries first is an early indicator of the flow, the rate of drying is directly related to the amount of convection to remove the kerosene. Therefore, the areas that dry first are probably experiencing the fastest airflow near the wing surface, while the areas that dry last have the slowest airflow. Video of the drying paint can also be a form of flow visualization.

After the paint has dried, a white pattern appeared and the kaolin will only be dislodged by contact, not low velocity airflow, so the airflow was halted and the wing was photographed.

3.10 Effect of Flow Visualization Tests

The types of flow visualization used in this study have the potential to affect the airflow. To check that this is not the case, lift and drag of the flat plates with and without flow visualization were measured and compared to each other. Five tests of each flat plate wing were conducted, with tufts, with oil film, and with no flow visualization at all. If the results are similar the flow visualization could be considered to have negligible effect on the airflow. The L/D values of the flat plate wings at 11.8^0 AoA were also compared to the L/D values of the feathered wings at 11.8^0 AoA.

3.11 Chord Distribution Study

To compare the shape of the best wings from the genetic algorithms to bird wings of order Galliformes, the chord distribution along the wing span was measured. X and Y coordinates of approximately fifty points following the outline of the wing were recorded. A Matlab code then organized the points and estimated the chord length throughout the entire span of the wing. Given a set of coordinates the program first normalizes them, which resizes the wings shapes to allow for direct comparison between them. Then, the program locates the leading and trailing edges and finds two trailing edge points directly behind each leading edge point. The program interpolates the space between trailing edge points as a line, and the slope of the line connecting them is the found by Equation 14. The location of the interpolated point is found by Equation 15, and the chord length is found with Equation 16.

$$S_2 = \frac{Y_3 - Y_2}{X_3 - X_2} \tag{14}$$

$$Y_i = (X_2 - X_1)S_2 + Y_2 \tag{15}$$

$$C = Y_1 - Y_i \tag{16}$$

In Equations 14 through 16, X_2, Y_2 and X_3, Y_3 are two trailing edge points behind the leading edge point, X_i, Y_i is the location of the interpolated point, and X_1, Y_1 is the position of the leading edge point.

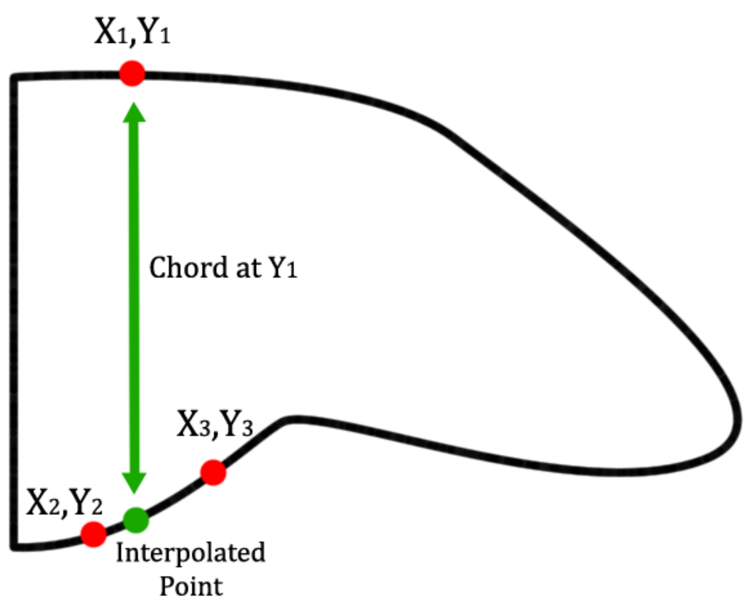

Figure 36 Finding the Chord Length

The program doesn't necessarily find the points to the left and right of the leading edge point, so it is capable of properly locating the interpolated point based on the two closest trailing edge points even when both are to the left or right of the leading edge point.

A detailed account of the process can be found in Appendix D.

3.12 Null Hypothesis

It has been assumed that the genetic algorithm will eventually reach a steady state where a locally or globally optimal chromosome takes up most, and eventually all, of the population. To prove this, the inverse must also be tested. If the results from a test with severe noise and no actual data are similar to the actual results, then the tests are flawed. The process and results are located in Appendix E.

4. Results

4.1 Low Angle of Attack Genetic Algorithm

As discussed in Section 2, a genetic algorithm study was undertaken to confirm the results of Day[1] at low AoA. A different initial population was used in order to verify that the resulting best wing is independent of the initial population in the first generation.

The initial generation, created by the twister algorithm and input to an excel spreadsheet by Matlab consisted of 72 individuals of a wide variety of shapes. Two of the generated chromosomes were very similar to the 7732100 chromosome, so they were removed and substituted with two chromosomes from a second spreadsheet created in the same way as the first.

All other variables were kept as similar as possible to the process as Day[1]. This included a 4.6^0 angle of attack. However, the lift at the same recorded angle of attack was consistently higher than the lift recorded by Day[1] by approximately 10%. This is believed to be due to variations in the orientation and placement of the floating island in the force balance structure.

Results of Low Angle of Attack Tests

Figure 37 shows the variation of the average, minimum, and maximum L/D values as the genetic algorithm proceeds.

The L/D values generally increased as the generation number increased. The first generation had an average below 3.3 while the final generations rose to an average of around 3.6.

The error bars on the average L/D ratios indicate repeatability errors. These were found by taking the standard deviation of the wing shape with the most separate tests, the 6611110 shape. The standard deviation for the low AoA genetic algorithm was .07808.

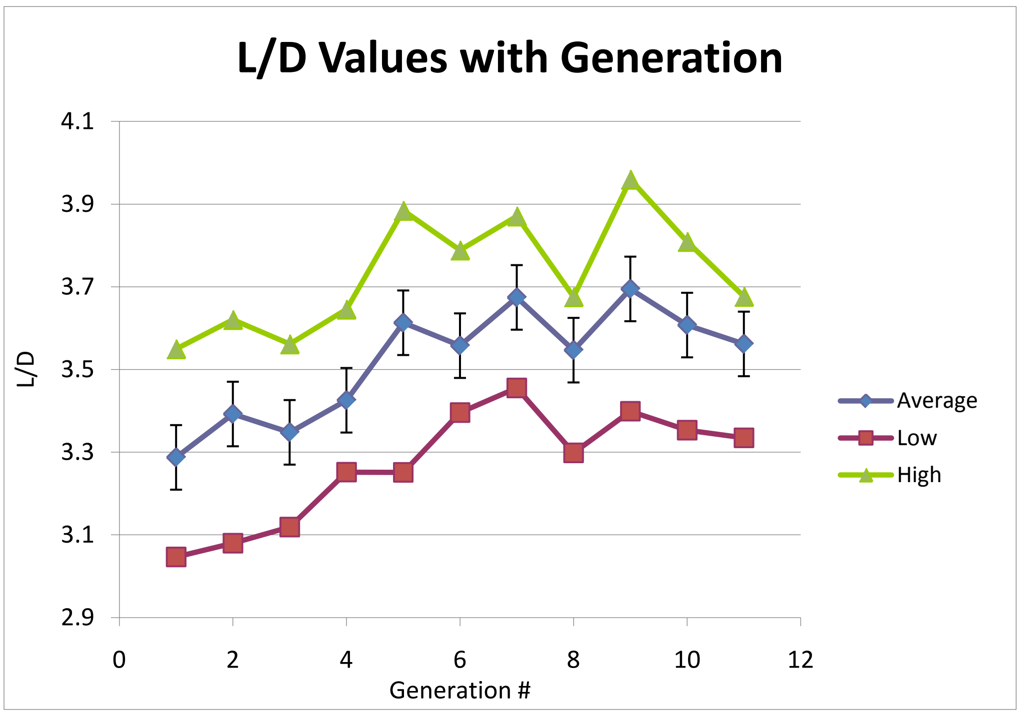

Figure 37 Low AoA Genetic Algorithm L/D Values, Present Study

Some of the generations had lower average L/D values than the previous generations. Because genetic algorithms are based on random numbers this can happen, however the general trend is upwards.

Due to its consistent high L/D values and ubiquity in the final generations, the wing shape defined by chromosome 6611110 is considered the 'best' wing from the present study.

Figure 38 Low AoA Best Wing, Present Study

When comparing the shape of chromosome 6611110 from the present study to the shape of chromosome 7732100 from Day[1] in Figure 39, some interesting similarities emerge.

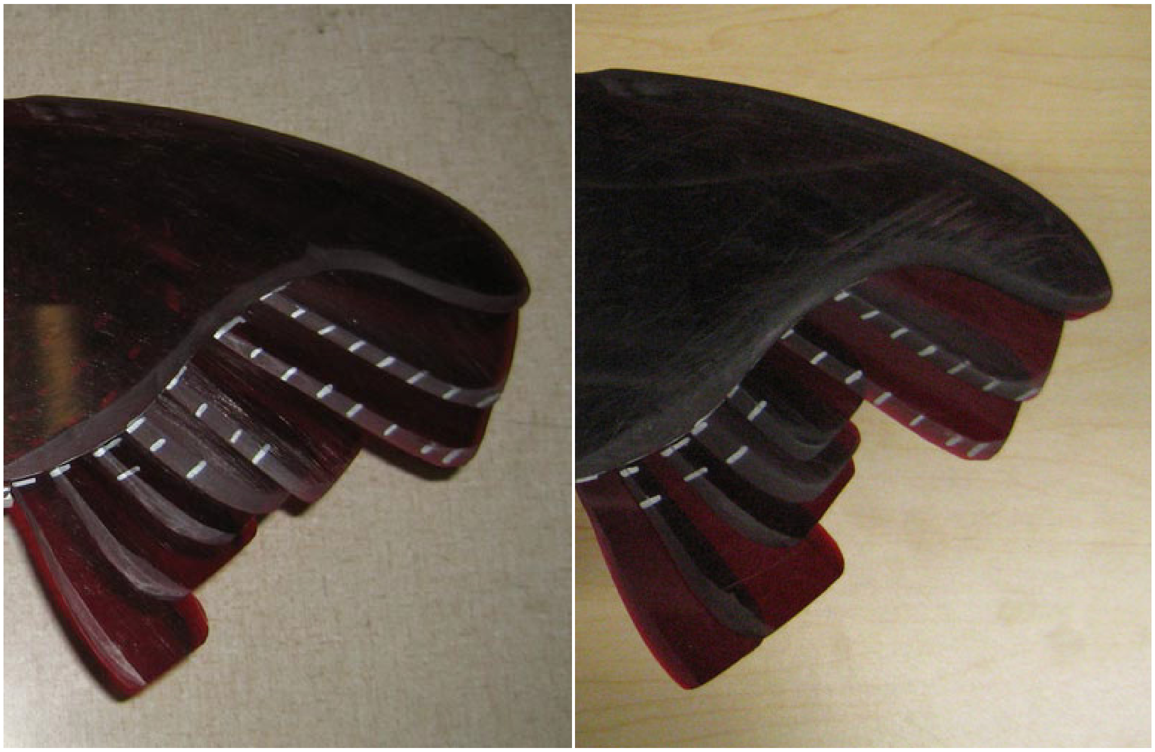

Figure 39 Wing 7732100 from Day[1] (Left) Versus Wing 6611110 from Present Study (Right)

Both wings have the first two feathers extended to close to the wing tip, while the middle feathers are much shorter and the final feather completely retracted to near the wing root. Similar to galliform wings, there is a notch located at the center of the span, where the chord suddenly shortens. This wing notch is more prominent in wing 6611110.

To further compare the shapes of wing 7732100 and 6611110 the chord distribution versus wing span location is presented in Figure 40. The most visible difference between the wings is the where the chord remains at a constant length near the middle of the span for wing 6611110, the 7732100 wing has a much smaller area of constant chord.

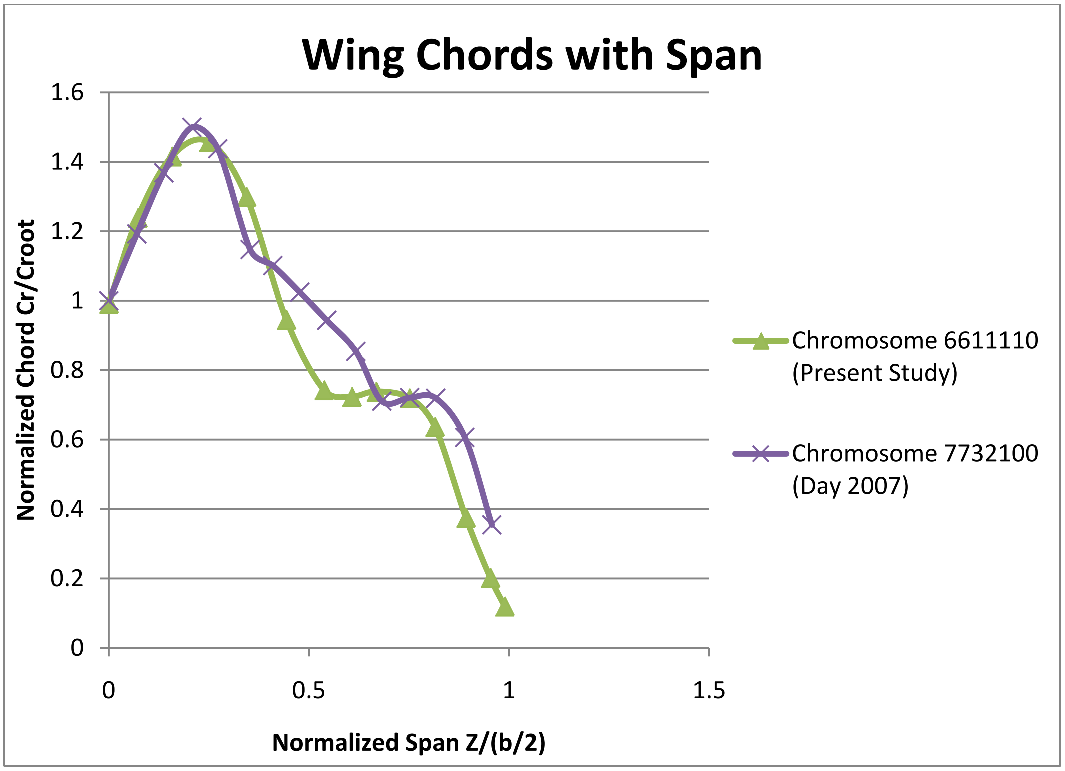

Figure 40 Wing Chords Versus Span Location for Best Low AoA Wings

These wings were then tested in the wind tunnel at a variety of angles of attack, shown in Figure 41. Except for very high angles of attack both 'best' wings had higher L/D values than the Zimmerman approximation wing. The Zimmerman approximation had particularly low L/D values at 4^0 degrees angle of attack. Chromosome 6611110 of the present study performed slightly better than chromosome 7732100 of Day[1]. The original data can be found in Appendix F.

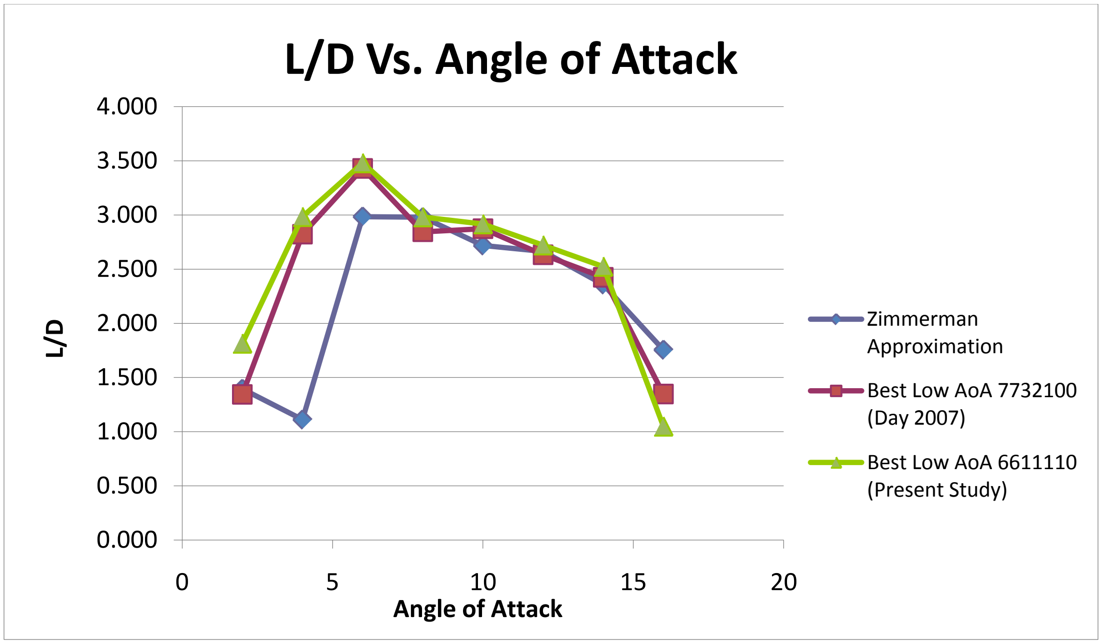

Figure 41 L/D Versus AoA for 'Best' Low AoA and Zimmerman Approximation Wings

The following section details the evolution of the wing shapes throughout the generations. The raw data from the low AoA genetic algorithm is located in Appendix G.

Generation One

The first generation had a wide range of performance. Of all the wings the highest L/D values belonged to individuals 7620111 and 2711102, with values of 3.5 and 3.6 respectively. Figure 42 shows the highest performing wing of generation one.

Figure 42 Wing 2711102 of Generation One

Generation Two

The 7620111 chromosome was reproduced for generation two, but 2711102 was not. Chromosome 6631321, a decent performer was also selected for generation two, and many of its offspring, also with good but not exceptional L/D values, were carried over into the next couple of generations. 7620111 performed well in generation two but was outperformed by one of the new offspring chromosomes 4633121 with the highest L/D of 3.6. Figure 43 shows the highest performing wing of generation two.

Figure 43 Wing 4633121 of Generation Two

Generation Three

Chromosome 7620111 was then selected for generation three, as well as 4633121. In generation three 7620111 was again the best performer, with an L/D of 3.6, while 4633121 followed closely with and L/D of 3.5. Figure 44 shows the highest performing wing of generation three.

Figure 44 Wing 7620111 of Generation Three

Generation Four

Chromosome 7620111 was selected for generation four by the genetic algorithm, while 4633121 was not. Chromosome 7620111 performed well, but proved inferior to the offspring individual 6610120 with an L/D value of 3.6. Figure 45 shows the highest performing wing of generation four.

Figure 45 Wing 6610120 of Generation Four

Generation Five

The 6610120 chromosome and its siblings became dominant, having a slightly higher L/D value than chromosome 7620111 and its offspring. However, the highest L/D value for generation five belonged to individual 2311220, with a very high L/D value of 3.9. Considering that that later testing never reproduced this very high value for chromosome 2311220, it is likely that was an error not recognized at the time. Aside from that, the best two L/D's for generation five were 7611222 and 6611220 with values of 3.7 and 3.7 respectively. Figure 46 shows the highest performing wing of generation five.

Figure 46 Wing 6611220 of Generation Five

Generation Six

When chromosome 2311220 was retested it failed to reproduce its previous high result, with the highest value instead belonging to individual 7612210 with a value of 3.8. Figure 47 shows the highest performing wing of generation six.

Figure 47 Wing 7612210 of Generation Six

Generation Seven

The best performing individual in generation seven was 7611110 with an L/D of 3.9, an offspring chromosome from generation six. Individual 7612210 performed second best, with a value of 3.8. Figure 48 shows the highest performing wing of generation seven.

Figure 48 Wing 7611110

Generation Eight

Individual 6611110 performed best, with an L/D of 3.7. Individual 7611110 performed second best, with an L/D value of 3.7. At this point the generation is almost completely composed of chromosomes similar to 7611110 and 6611110. Figure 49 shows the highest performing wing of generation eight.

Figure 49 Wing 6611110 of Generation Eight

Generation Nine

Individual 7611110 turned out to have the highest L/D value ever of every tested shape of 4.0. The second best performance belonged to the similar wing

6611110, with an L/D value of 3.8. Figure 50 shows the highest performing wing of generation nine.

Figure 50 Wing 7611110 of Generation Nine

Generation Ten

The highest L/D of 4.0 was never again reproduced by chromosome 7611110, though it still performed well. This time the two best performing wings both had the 6611110 chromosome. The best performing wing had an L/D of 3.8 and the second best had an L/D of 3.8. Figure 51 shows the highest performing wing of generation ten.

Figure 51 Wing 6611110 of Generation Ten

Generation Eleven

The highest L/D of 3.7 belonged to individual 6611110. The second best L/D was 6.7; which was achieved by two wings, individual 6611110 and individual 6611101. Figure 52 shows the highest performing wing of generation eleven.

Figure 52 Wing 6611110 of Generation Eleven

The results of the present low AoA genetic algorithm study show that the resultant 'best' wings are largely independent of the initial population in the first generation. However, the differences between the wings suggest that the 'best' wing from Day1 is not a global optimum.

4.2 High Angle of Attack Genetic Algorithm

Controlled landings, loitering, and low speed flight are all important to potential MAV missions. As discussed in Section 2, another genetic algorithm was conducted to find wings with higher L/D values at high angles of attack.

To determine the stall angle the best low AoA wings and Zimmerman wings were tested at angles of attack from 0^0 to 16^0 as seen in Figure 53. The stall angle is difficult to determine, not unexpected given that low aspect ratio wings delay stall to high AoA, but analysis of drag and lift measurements place it after 14^0 and before 16^0. As a result the high angle tests were conducted at an angle of attack of 11.8^0. The original data can be found in Appendix F.

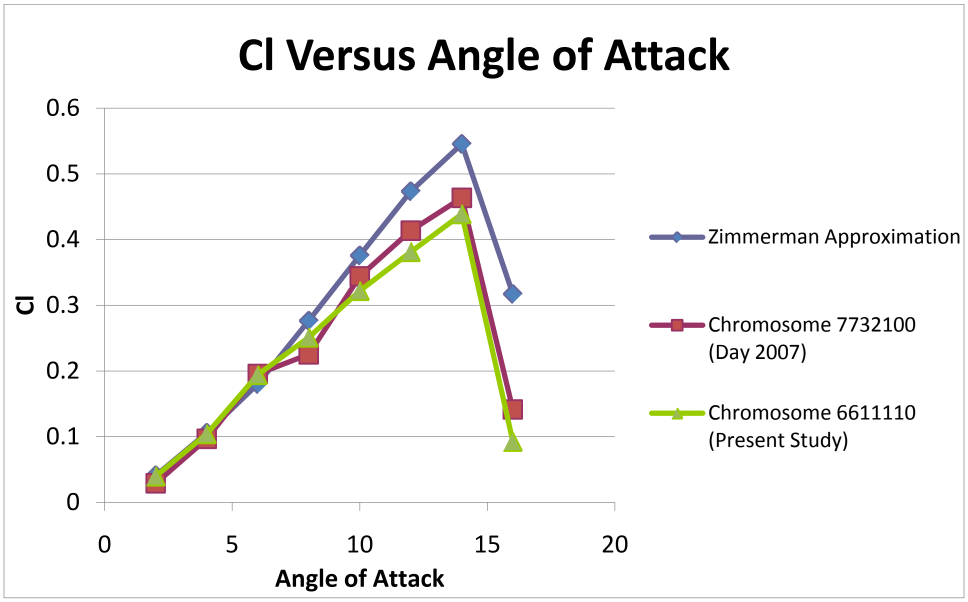

Figure 53 Coefficient of Lift Versus AoA for Best Low AoA and Zimmerman Approximation Wings

The same process as the low AoA tests was used; however no chromosomes were removed from the first generation.

Results of High Angle of Attack Genetic Algorithm

Generally, the wings had lower L/D values at the higher angle of attack. This was not very surprising considering that drag drastically increases at higher angles. Figure 54 shows an upwards trend of the L/D values as the generations increase, though it is less visible than the trend for the low angle of attack tests. Two generations showed severe decreases in average L/D from the generation before, again due to the actions of random chance that genetic algorithms require.

The error bars on the average L/D ratios indicate repeatability errors. These were found by taking the standard deviation of the wing shape with the most separate tests, the 4143120 shape. The error for the high AoA genetic algorithm tests was .07022. This was slightly smaller than the error in the low AoA tests; however the differences in the L/D ratios of the high AoA tests were much smaller, making the error much larger in comparison.

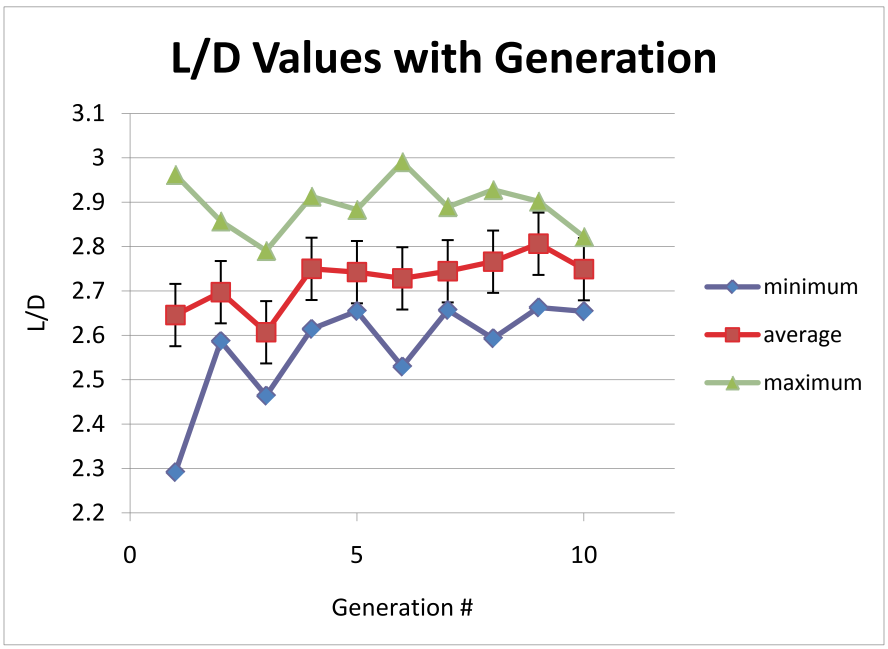

Figure 54 High AoA Genetic Algorithm L/D Values

Despite the error, chromosome 4143120 was common in later generations and had consistently high L/D values, as a result it was considered the 'best' wing of the high AoA genetic algorithm.

Figure 55 'Best' High AoA Wing

Figure 56 Low AoA Best Wing (Left) and High AoA Best Wing (Right)

The shape of the best wing from the high AoA tests is very different from the best wing of the low AoA tests, as shown in Figure 56. It does have a notch where the second feather recedes, but not in the same place as galliforms do and it only consists of one feather. The retracted second feather divided the trailing edge and creates two protuberances on either side.

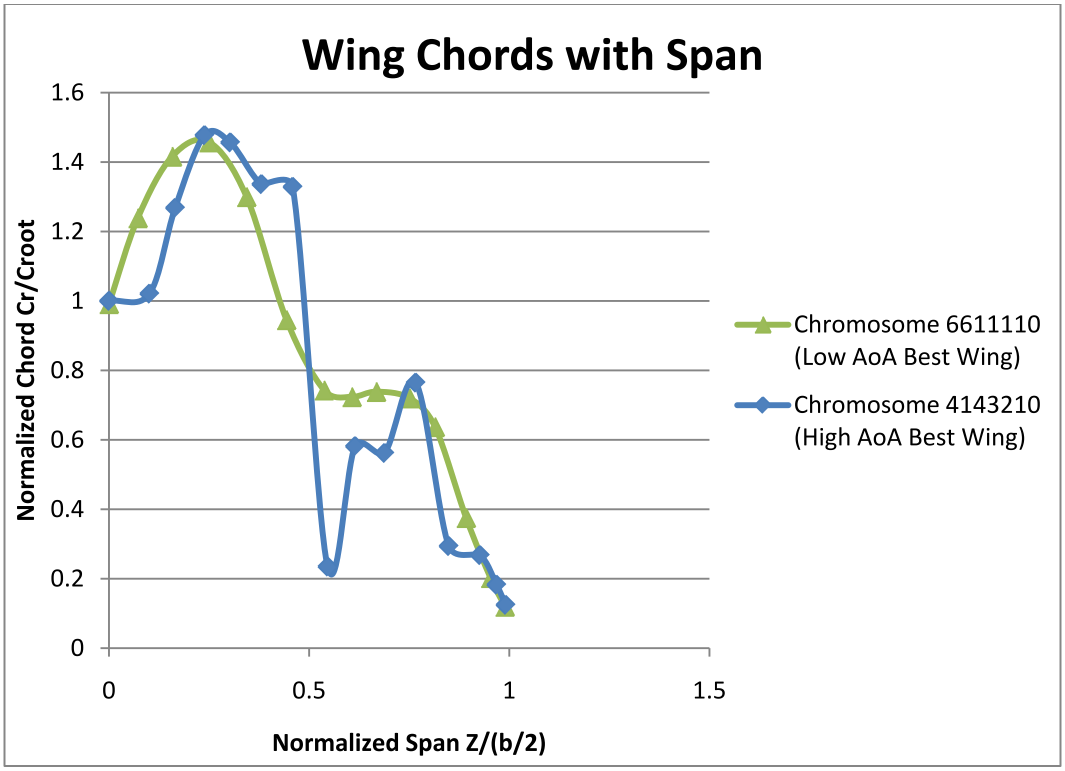

Figure 57 Wing Chords with Span of Best Low AoA and Best High AoA Wings (Present Study)

The chord of the best high AoA wing proved difficult to analyze because of the protruding feathers. Figure 57 shows the chord distribution of the high AoA wing compared with the low AoA wing. While both wings have a notch at the middle of the wing span, there are few other similarities.

The result that different conditions produce different 'best' shapes may prove important for MAV's with variable geometry wings, where MAV designers may wish to change the shape of the wing planform for different flight conditions.

The application of the genetic algorithm technique at high AoA also led to the development of a non conventional planform shape that would generally not be considered as a design alternative for MAV's prior to this study. This highlights one of the advantageous features of genetic algorithms, their ability to find unconventional design solutions.

The following section details the evolution of the wing shapes throughout the generations as the high AoA genetic algorithm proceeded. The original data is located in Appendix

Generation One

A wide variety of wings were produced for the initial generation. Of these the best performing wing was individual 2720312 with an L/D of 3.0. The second best performing wing was individual 6014310 with and L/D of 3.0. Figure 58 shows the highest performing wing of generation one.

Figure 58 Wing 6014310 of Generation One

Generation Two

The 2720312 chromosome was reproduced in generation two, but was one of the worst performers, its earlier performance could have been an error. Unfortunately incorrect data is difficult to determine in the early generations, as the general performance of the wings is unknown. Meanwhile chromosome 6014310 was not carried over. The best performing wing belonged to individual 7643120 with an L/D value of 2.9. Figure 59 shows the highest performing wing of generation two.

Figure 59 Wing 7643120 of Generation Two

Generation Three

The best performing wing was a child 2603120 chromosome, with an L/D value of 2.8. The next highest L/D belonged to chromosome 1515030 with an L/D of 2.8. Chromosome 7643120 was transferred to generation three and still performed well. Figure 60 shows the highest performing wing of generation three.

Figure 60 Wing 2603120 of Generation Three

Generation Four

4025120, a child individual, performed best with an L/D of 2.9. Chromosome 7643120 also was transferred to generation four and performed well. Individual 7655022 performed second best with an L/D value of 2.9. Also of note, there were several individuals with a chromosome of 1035232, which performed notably well. Figure 61 shows the highest performing wing of generation four.

Figure 61 Wing 4025120 of Generation Four

Generation Five

In the later generations error became more prominent. Even with calibration, wing shapes did not always have the same L/D ratio when they were retested. As the wings evolve and poorly performing wings are selected out of the gene pool there is narrower range of L/D values. If this range becomes comparable to the level of noise in the system the ability of the genetic algorithm to select better wings is greatly reduced. This appeared to become an issue around generation five, though it is hard to determine when the noise and range became similar. The highest recorded score belonged to individual 4122120 with an L/D of 2.9, however the generation was dominated by chromosome 1035232 and its children. Figure 62 shows the highest performing wing of generation five.

Figure 62 Wing 4122120 of Generation Five

Generation Six

Individual 4123120 performed best with an impressive L/D of 3.0. The next best performing wing was individual 4312122 with an L/D value of 2.9. These chromosomes and their children would later dominate the following generations. Figure 63 shows the highest performing wing of generation six.

Figure 63 Wing 4123120 of Generation Six

Generation Seven

The best performing individual was 7143122 with and L/D of 2.9. Individual 4342122 was the second best performer with an L/D of 2.8. Figure 64 shows the highest performing wing of generation seven.

Figure 64 Wing 7143122 of Generation Seven

Generation Eight

Individual 4322122 had the highest L/D value of 2.9. The second highest L/D belonged to 5342121 with an L/D of 2.9. This generation was also heavily populated by the 4143120 chromosome, which performed consistently well. Figure 65 shows the highest performing wing of generation eight.

Figure 65 Wing 4322122 of Generation Eight

Generation Nine

The best performing individual in generation nine was individual 7343121 with an L/D of 2.9. The second best performing individual was 4342122 with an L/D of 2.9.

There were worrisome differences between the L/D values of the same chromosomes though, so the relative superiority between the wings is hard to determine. However, most of the ninth generation consisted of the 4322122, 4143120, and 4342122 chromosomes so these are likely the best performing chromosome types. Figure 66 shows the highest performing wing of generation nine.

Figure 66 Wing 7343121 of Generation Nine

Generation Ten

Genetic algorithms are inherently based on random number generation, which can carry the risk of unexpected behavior. Larger populations reduce this risk, but 24 individuals per generation may not be large enough to completely eliminate this risk. After appearing that the 4143120 chromosome was the most optimized, the 7323101 chromosome became more common. Unfortunately due to time constraints the genetic algorithm needed to end soon, and while the new shape performed well, it was not very common throughout generation ten. Generally the 'optimized' solutions for a genetic algorithm are decided when the value of the desired trait reaches a plateau and no longer increases for new generations, or a single chromosome becomes very common in new generations. In generation ten the lift to drag ratio decreased drastically and there was a large variety of chromosomes. While it was possible that new generations could see the new shape become more widespread, experience with the low AoA genetic algorithm suggested it would take at least a few more generations. For the sake of working with a chromosome that had already been heavily observed, the 4143120 chromosome was picked to be studied as the 'best' chromosome.

4.3 Chord Distribution

In this section we study whether the best wings of the of the low AoA study are similar in shape to bird wings from the order Galliformes by measuring their chord length distribution as a function of the location of the wing span. Galliform birds have high wing loadings and low aspect ratios, making them similar in function to MAV wings.

The chord distribution was found for all 'best' wings from the genetic algorithm studies, the Zimmerman wing, bird wings of order Galliformes, and bird wings of a variety of orders. All these can be found in Appendix I.

Comparing the chord distribution of the Zimmerman approximation wing with the two best wings from the low AoA genetic algorithms in Figure 67 shows their differences and similarities. The chords at the wing tip are all similar, while the best low AoA wing of the present study has a region of nearly constant chord length for the region of .5≤ Z/(b/2) ≤.8. This region on the best wing of Day[1] exists for .7≤ Z/(b/2) ≤.8, where Z is the distance from the wing root and b is the full wingspan. Also, both high performing wings have shorter chord lengths than the Zimmerman wing near the wing root.

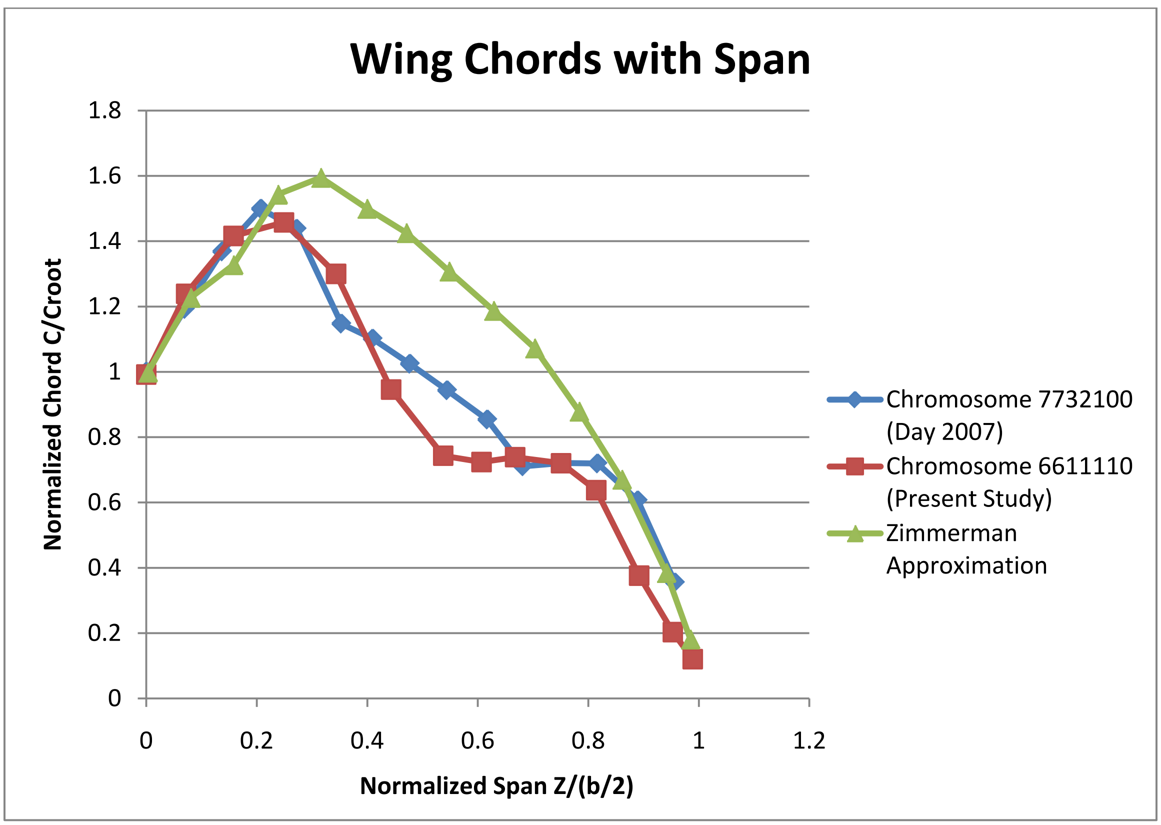

Figure 67 Feathered Wing Chords with Span

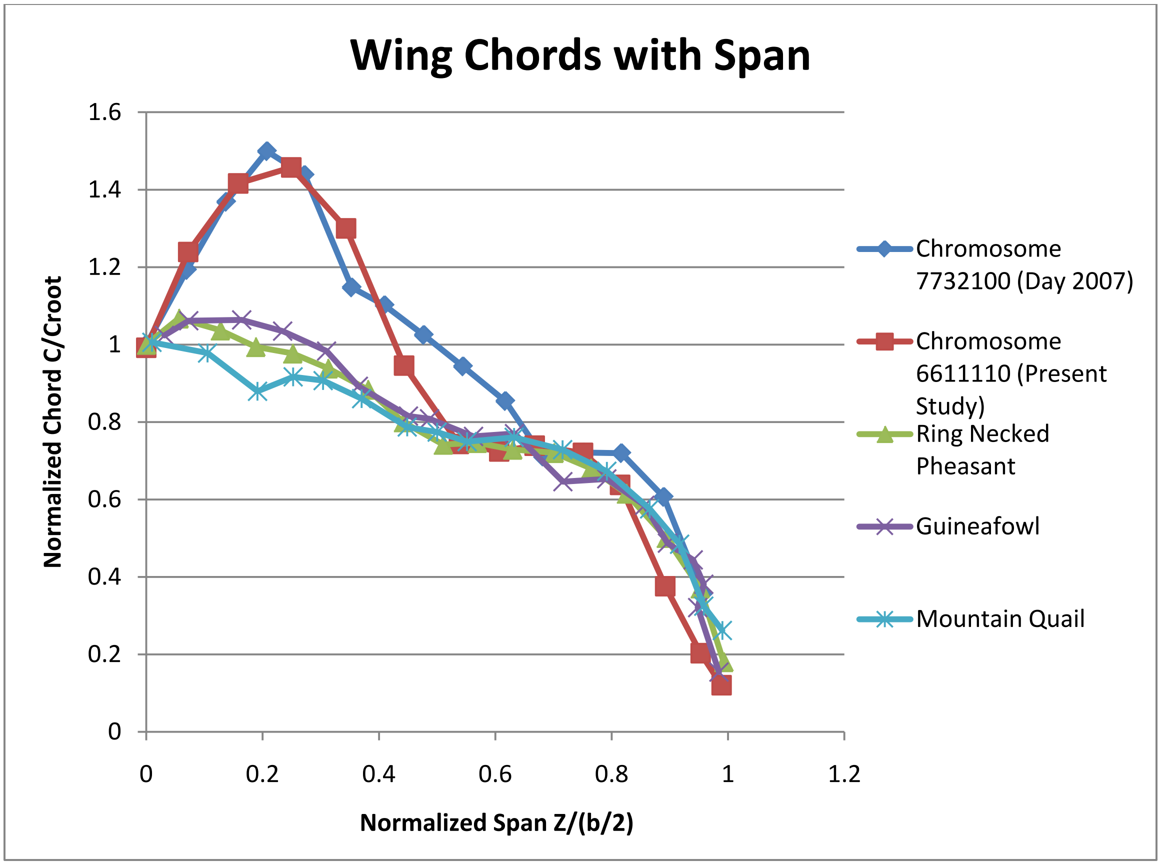

Figure 68 'Best' Low AoA Wings and Galliform Wings

The chord distributions of galliforms compared with the best low AoA wing distributions are shown in Figure 68. All wings have a region of nearly constant chord length from .5≤ Z/(b/2) ≤.8, except for the best wing of Day[1] which has a smaller region of constant chord length.

Next, we show how the specific features of the 'best' wings, including the trailing edge notch, result in a constant chord length region. Figure 69 shows a simplified schematic of the best low AoA (6611110) and galliform wings divided into four regions.

Region 1: Leading edge swept backwards, trailing edge swept back more steeply, chord length increases as Z/(b/2) increases.

Region 2: Leading edge swept back, trailing edge swept forwards, chord length decreases as Z/(b/2) increases.

Region 3: Leading edge swept back, trailing edge sweeps back at the same angle, chord length remains constant with Z/(b/2).

Region 4: Leading edge swept back, trailing edge swept forwards, chord length decreases as Z/(b/2) increases.

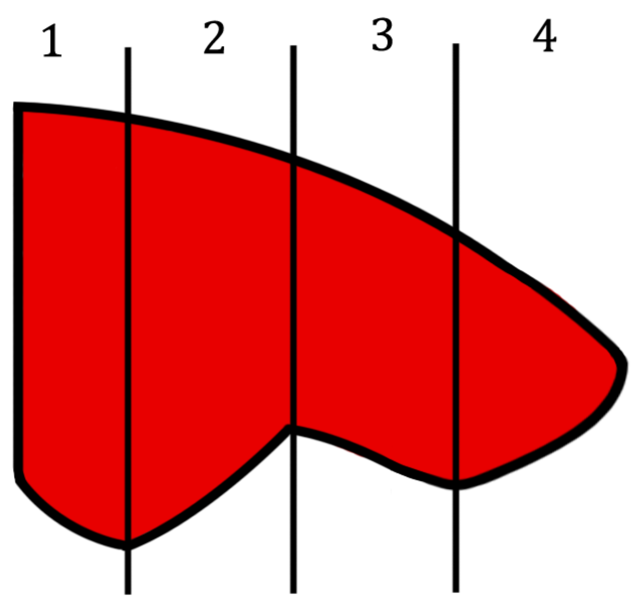

Figure 69 General Structure of Best Low AoA and Galliform Wings

Figure 69 shows how variations in the leading and trailing edge sweep angles in different regions of wing span lead to the chord distribution of Figure 67. In region three, at the trailing edge notch the chord length remains constant since both leading and trailing edges are swept back at the same angle.

The feathered test wing is limited in the shapes it can produce. The feathers can only extend or retract certain amounts. Figure 71 shows the chord distribution of the feathered test wing with all its feathers fully retracted (Figure 70) compared with the best performing wings and the Zimmerman approximation wing. Both high performing low AoA wings had their last feather fully retracted, and the feathers preceding it were either fully retracted, or only extended by one centimeter. Even if the galliform wings were the optimized wing shape for the tested conditions, the feathered test wings could not approach their shape near the wing root.

Figure 70 Wing with Fully Retracted Feathers

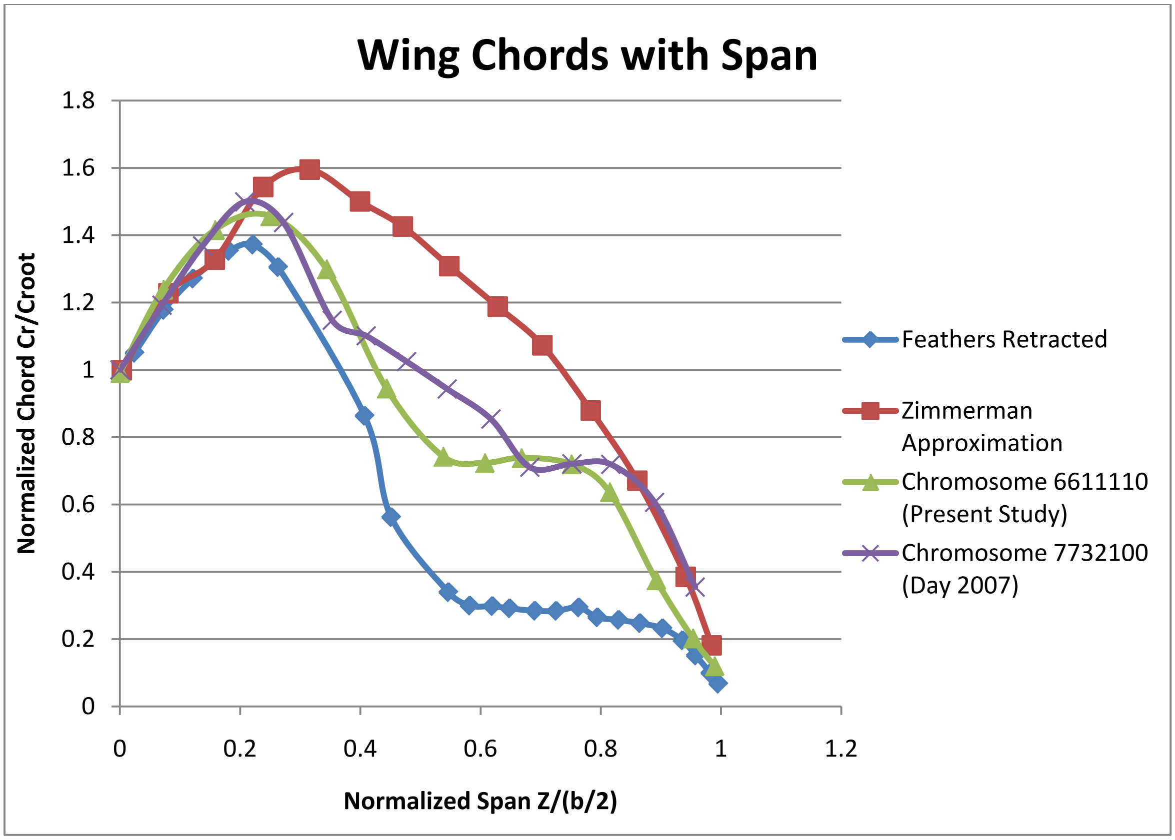

Figure 71 'Best' Low AoA Wings, Zimmerman Approx. Wing, and Fully Retracted Wing

To show whether or not the wings of non-galliform birds had any similarities to the highest performing low AoA wings, the wing chord distributions of non-galliforms were found. Figure 72 shows several example non-galliform wings (Canada goose, goldfinch, and red-tailed hawk) compared to the highest performing low AoA wings. None of the bird wings show any evidence of the constant chord length section seen in certain galliform wings and the high performing low AoA wings.

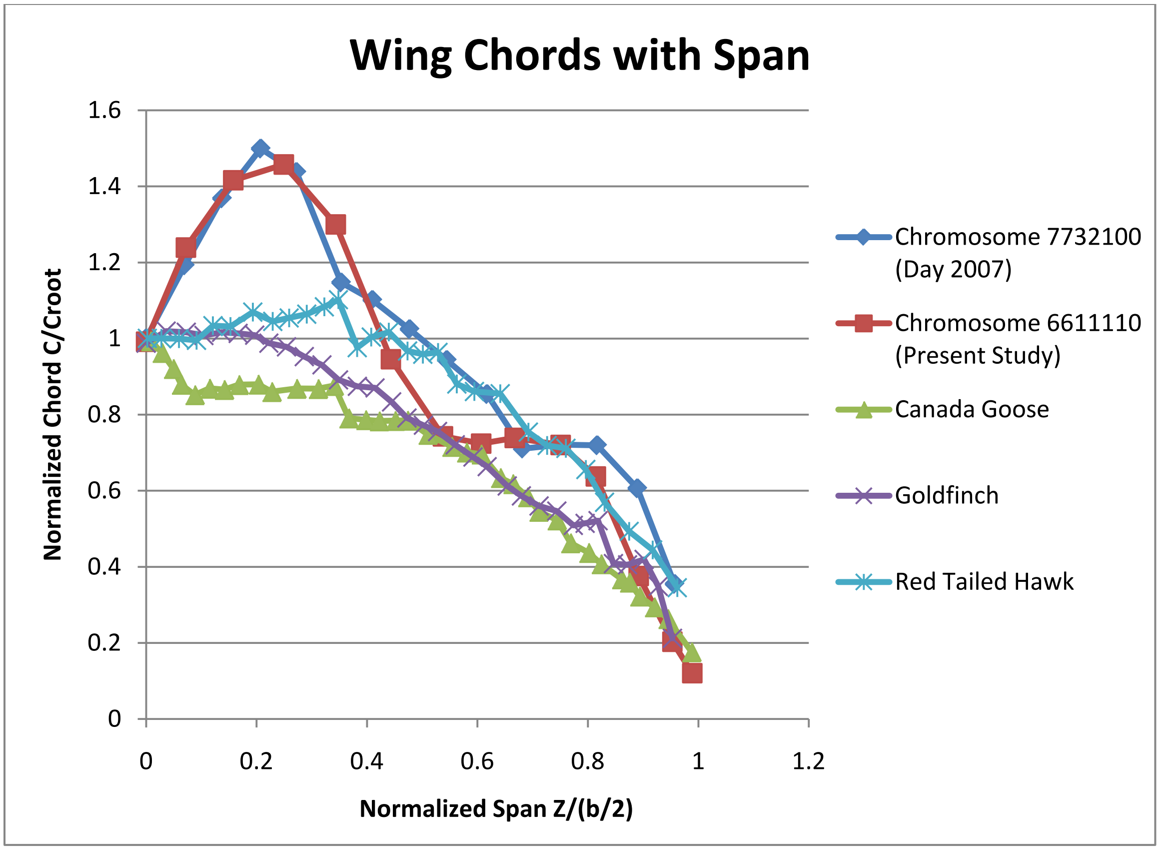

Figure 72 'Best' Low AoA wings and Non-Galliform Wings

The chord distribution of the best high AoA wing was also computed and can be seen in Figure 73, compared with the best low AoA chord distribution. The chord distribution was more difficult to find for this wing because of the two large protuberances on the trailing edge made by the feathers. The chord length is defined as the length from the leading edge to the trailing edge of the wing. Because of the protuberances, there are two leading and trailing edges making the chord length difficult to calculate. There is little similarity between the best high AoA wing and best low AoA wing chord distributions.

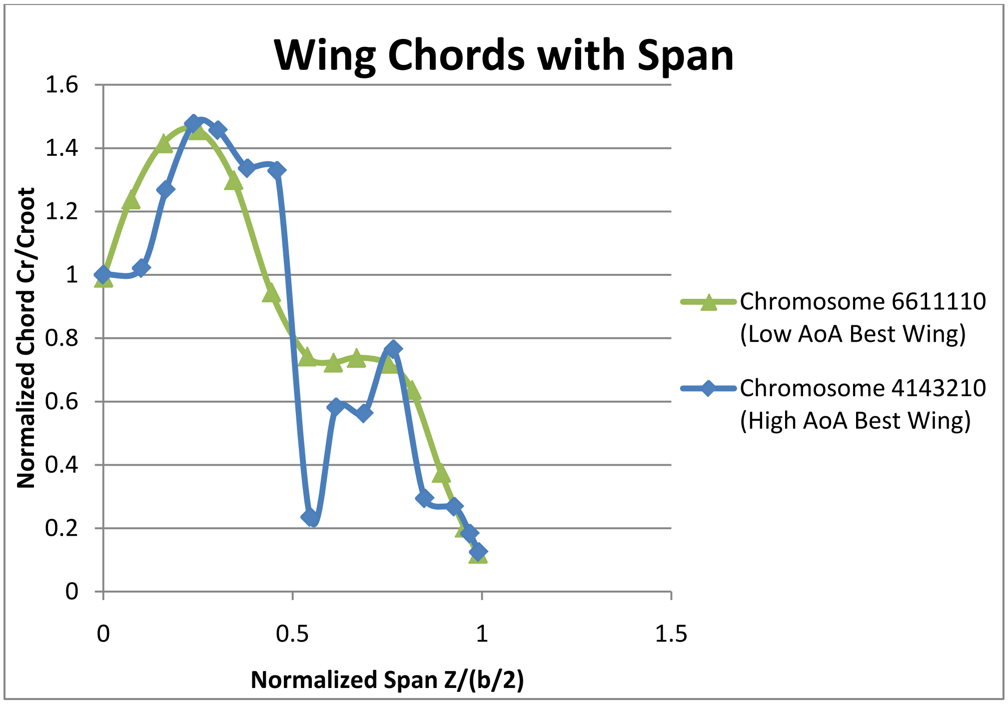

Figure 73 Wing Chord Distributions

4.4 High Angle of Attack Flow Visualization

To study the flow over the aluminum wings at high AoA, the kaolin and kerosene mixture was applied to the flat plate wings, which were then tested at 11.8^0 AoA. Lift and drag were also measured to test whether or not the film significantly disrupted the airflow.

Figures 74 and 75 show that all three wings exhibit the same attached airflow near the leading edge. Behind this, they all exhibit probable separation bubbles (see Figures 7 and 8) near the wing root revealed by circular markings. At the wing tip, another formation was observed, which may be related to wingtip vortices. Between the separation bubble and wing tip there is a line of white kaolin, marking a line where the pressure gradient rapidly changed. This marks the boundary of attached and separated flow. Behind the separation bubbles, the flow is completely separated, evidenced by the textured patterns and tuft studies. Because of its greater velocity gradient near the surface, turbulent flow affects the oil film more than laminar flow[15]. The location of the separation bubble does not vary significantly between wings, although the attached flow region appears larger at the leading edge of the 'best' high AoA wing.

The main difference between the Zimmerman approximation planform and the best high AoA wing was that the high AoA had a second area of attached flow where the oil film is without texture, shown in Figure 74. This could be the effect that gave the feathered best high AoA wing better L/D values, though the aluminum wing L/D tests show the best high AoA aluminum wing as being inferior to the aluminum Zimmerman approximation wing (Figure 79).

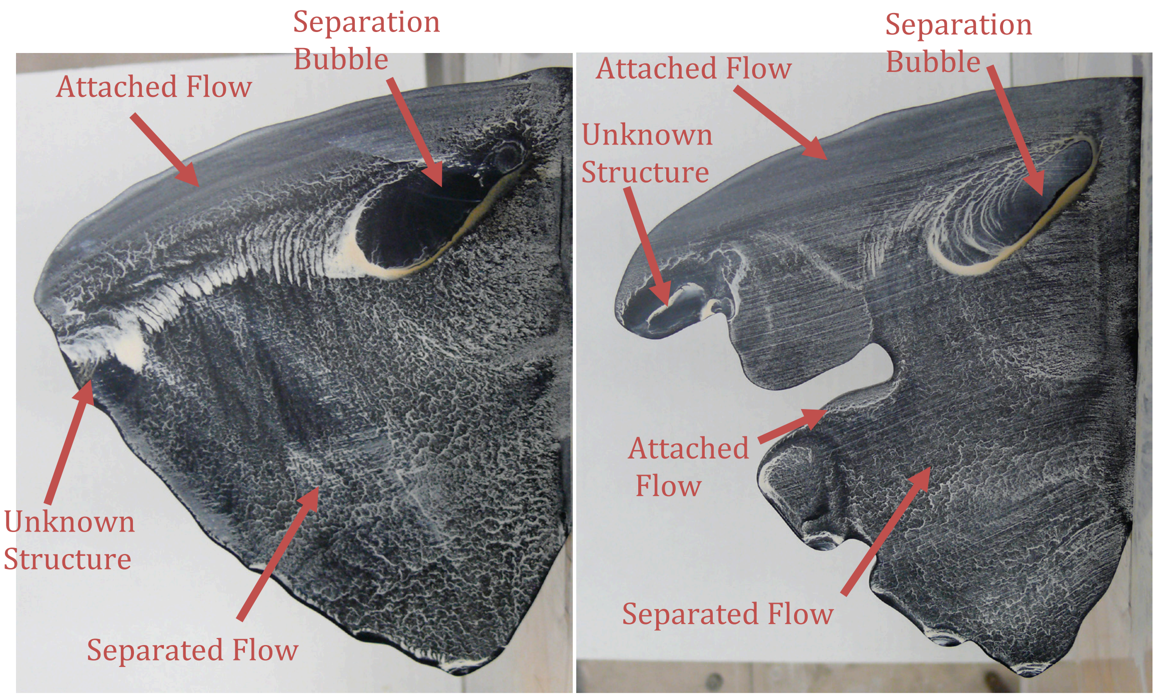

Figure 74 High AoA Film Test with Zimmerman Approximation (Left) and 'Best' High AoA (Right) Wings

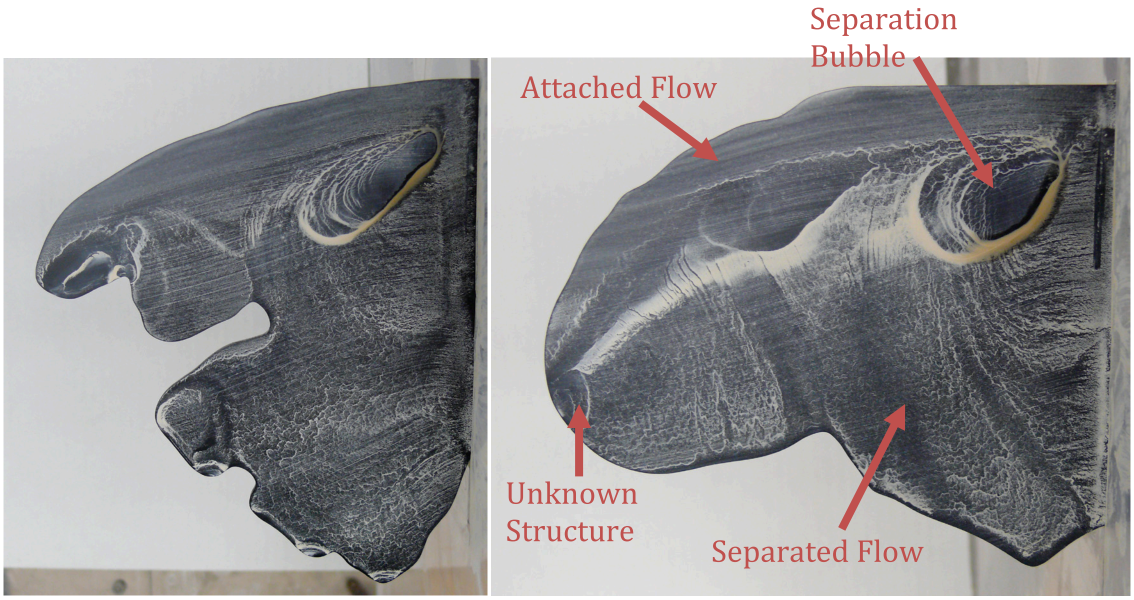

Figure 75 High AoA Film Test with 'Best' High AoA (Left) and Pheasant (Right) Wings

High Angle of Attack Tuft Studies

Figure 76 shows the averaged L/D values of three tests for the tufted and untufted configurations of the feathered test wing at 11.8^0 AoA set to the Zimmerman planform. There is a large difference in coefficients of lift and drag, presumably caused by the tufts. The original data can be found in Appendix J.

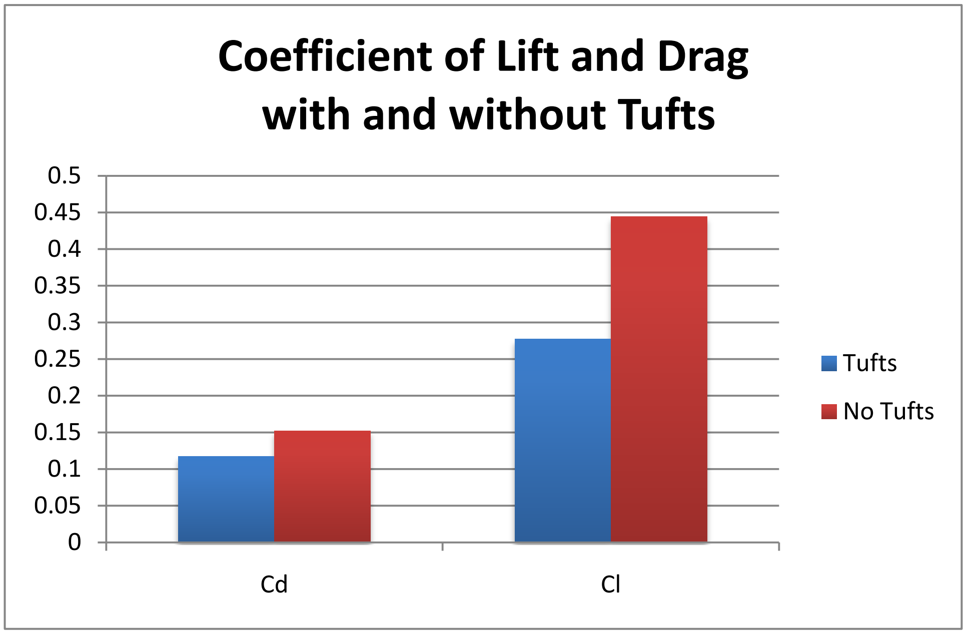

Figure 76 Cl and Cd with and without Tufts

This shows the tuft studies must be conducted with care, as there is always concern that the tufts are disrupting the flow over the wings. Nevertheless, the tuft studies are very valuable in complementing the data from other methods of visualization and were used again on the aluminum wings at 11.8^0 angle of attack.

Due to the concerns about the tufts disrupting the flow, fewer tufts were used for the aluminum wings. Three rows of tufts were used on the leading edge of the wing, and four individual tufts were placed on the trailing edge to monitor flow as it came off the wing.

Figures 77 and 78 show heavily separated airflow; where many of the tufts show local velocities towards the wing tip or even in the opposite direction of the freestream velocity, suggesting separated flow. The leading edge tufts indicate that the leading edge region of the wings does not experience separated flow.

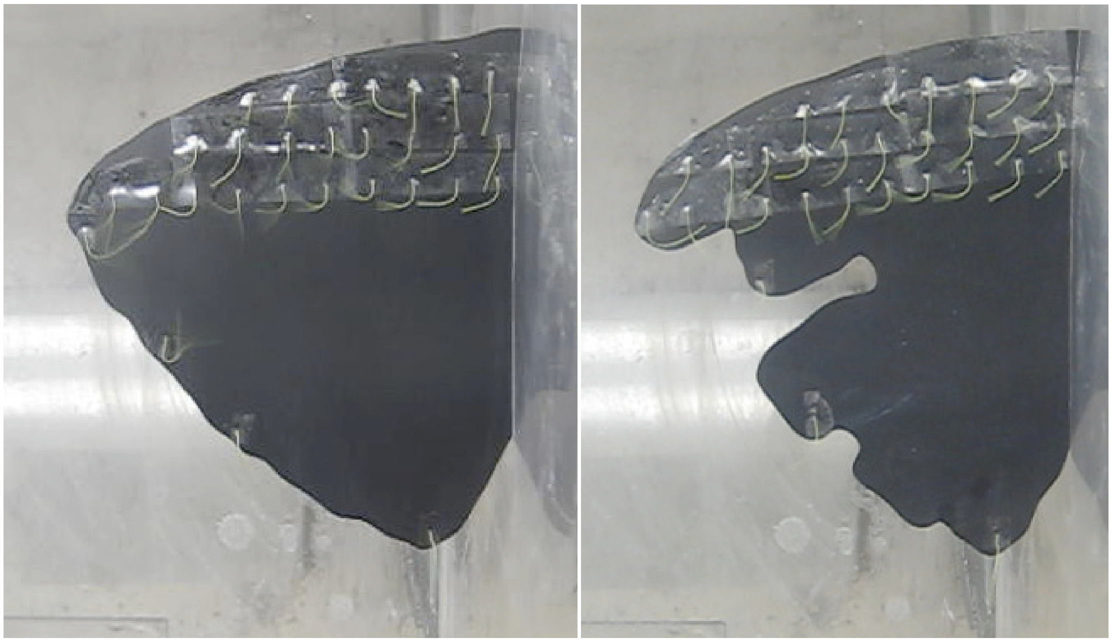

Figure 77 High AoA Tuft Study of Zimmerman Approximation (Left) and 'Best' High AoA (Right) Wings

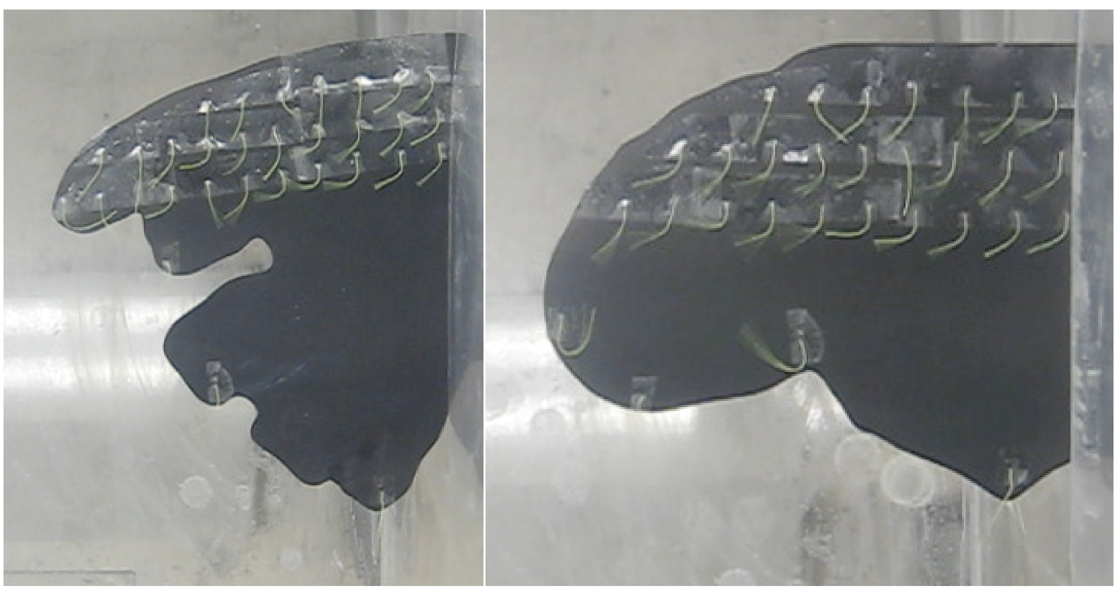

Figure 78 High AoA Tuft Study of 'Best' High AoA (Left) and Pheasant (Right) Wings

Shown in Figure 79, the aluminum Zimmerman wing had the highest average L/D value, followed by the best high AoA wing and then the pheasant wing. This was somewhat unexpected as the Zimmerman approximation wing performed better than the best high AoA configuration, which is the opposite of the results from the feathered wing tests. The aluminum Zimmerman approximation wing also performed much better than the feathered version. It is possible that the ridges and gaps of the feathers affected the airflow over the feathered wings. Appendix K contains the original data.

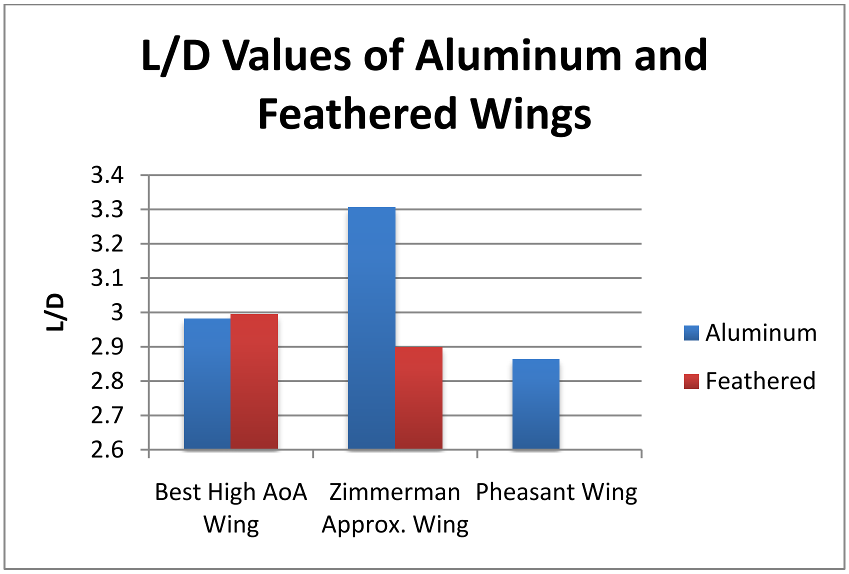

Figure 79 Aluminum Plate L/D Values at High AoA

L/D values were also compared for the aluminum wings with and without oil films and tufts, shown in Figures 80 through 82. The wings showed little change in lift and drag with and without flow visualization confirming that the oil films and tufts do not significantly affect disrupt the airflow over the aluminum wings at low AoA values. Original data can be found in Appendix K.

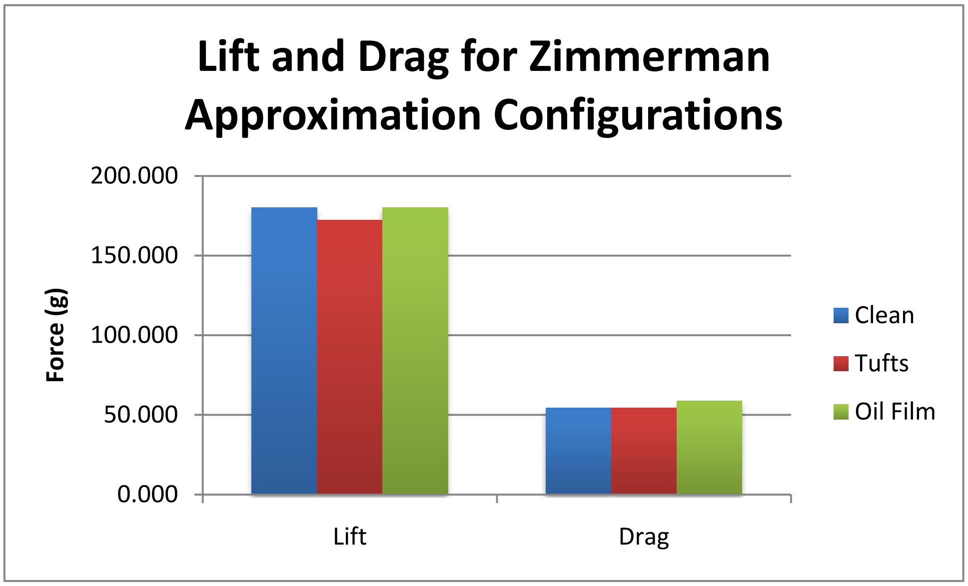

Figure 80 Lift and Drag for Zimmerman Approx. Configurations

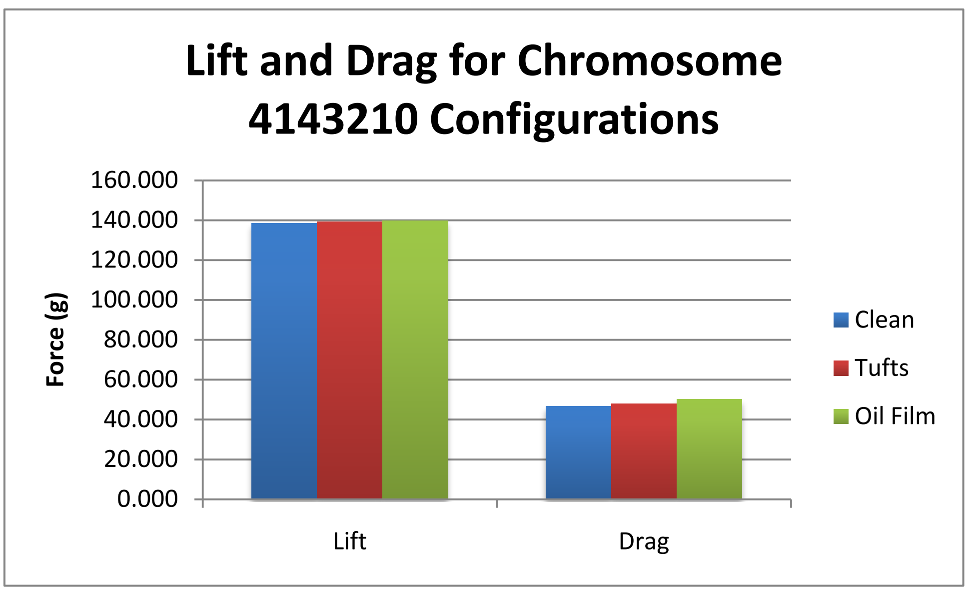

Figure 81 Lift and Drag for 'Best' High AoA Configurations

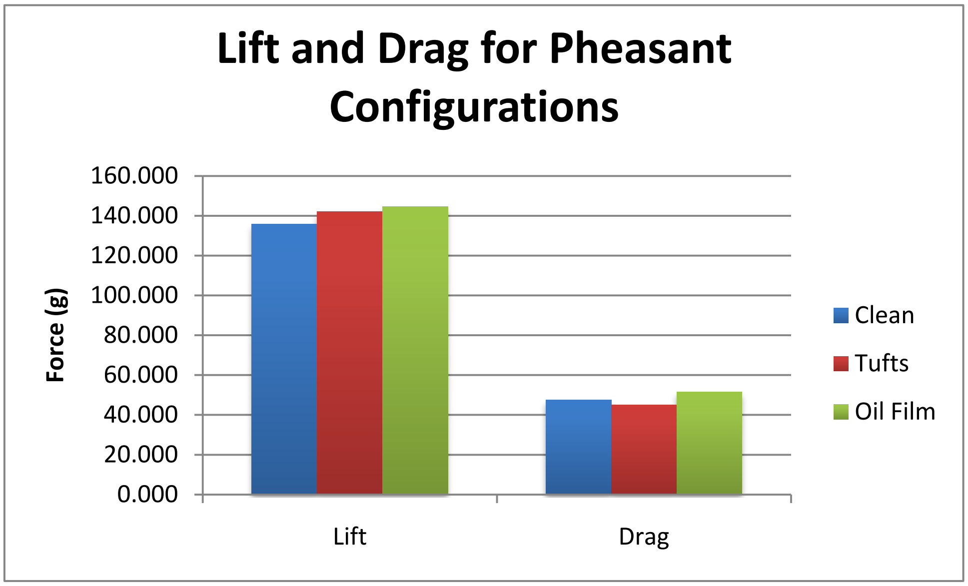

Figure 82 Lift and Drag for Pheasant Configurations

Low Angle of Attack Flow Visualization

Oil film visualization was also performed at 4.6^0 AoA on all three aluminum wings, to view flow patterns for wings at low AoA, shown in Figures 83 and 84.

The most prominent effect on the oil film was the formation of small 'bubbles' on the leading edge of the wings. The tuft studies on the feathered wings and the relatively undisturbed oil film behind the bubbles indicate that the flow was still attached at this AoA. Given the position of the bubbles and the attached airflow, the bubbles are likely separation bubbles.

Most of the streaks oriented from the wing root to tip that were applied by the brushstrokes were not altered by the airflow over the wing. The movement of the oil is related to the boundary layer velocity profile. Laminar flow, with a gradual change from zero to freestream velocity in the boundary layer has a lower velocity near the wing surface, moving it less. Turbulent flow has a more abrupt change from zero to freestream velocity in the boundary layer with higher velocities near the surface, so it will likely move the oil more. As a result turbulent flow is expected to have a greater effect on the oil film[15]. Near the trailing edge of each wing and behind the separation bubbles the brushstrokes are replaced with a different, more textured pattern. This likely shows a turbulent region near on the trailing edge as a result of the transition from laminar to turbulent flow, and behind the separation bubbles because of the obstruction posed by either the oil or the air bubble itself.

Interestingly, the pheasant wing in Figure 84 shows a distinct turbulent region near the trailing edge notch. The turbulent areas on the Zimmerman approximation wing and best high AoA wing are spread out on the trailing edge. What this means is unclear, but the notched pheasant wing seems to be limiting the turbulence to one area around the midspan of the wing. Previous investigations into trailing edge notches have shown that they can decrease drag at low angles of attack[17,29]. The mechanism by which this works is thought to be through inducing small vortices that energize the trailing edge boundary flow. This presents a contradiction. The tuft studies showed that the birdlike low AoA high performing wings had less trailing edge vortices than the Zimmerman approximation. However, the oil film studies show increased turbulence on the pheasant wing thought to be the result of trailing edge vortices. Due to time constraints further investigation was not conducted on this issue, but is an area for future work.

The best high AoA wing showed much evidence of turbulent flow, possibly the result of its odd shape. However, it had very poor L/D values so it is unlikely the turbulence is improving its performance. There is a more distinct separation bubble which possibly increases drag resulting in a lower L/D value.

Each wing exhibits a flow near the wing root that is oriented along the freestream flow direction. The reason for this structure is unknown but could be a result of a disturbance from the interaction between the wing and the wall.

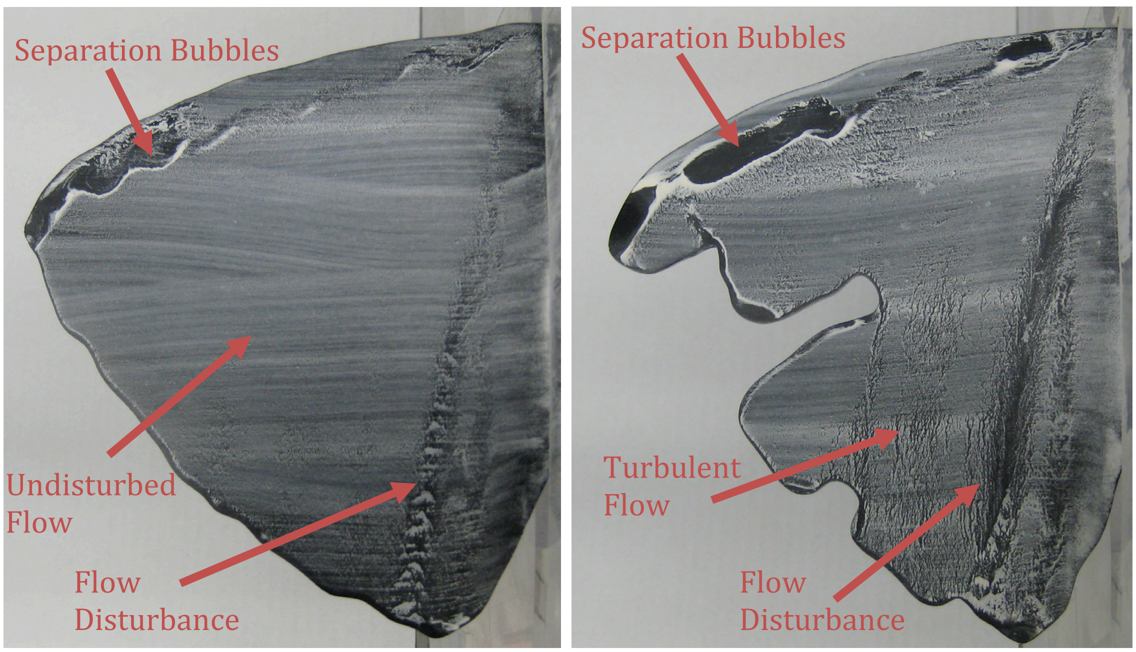

Figure 83 Low AoA Film Test with Zimmerman Approximation (Left) and Best High AoA (Right) Wings

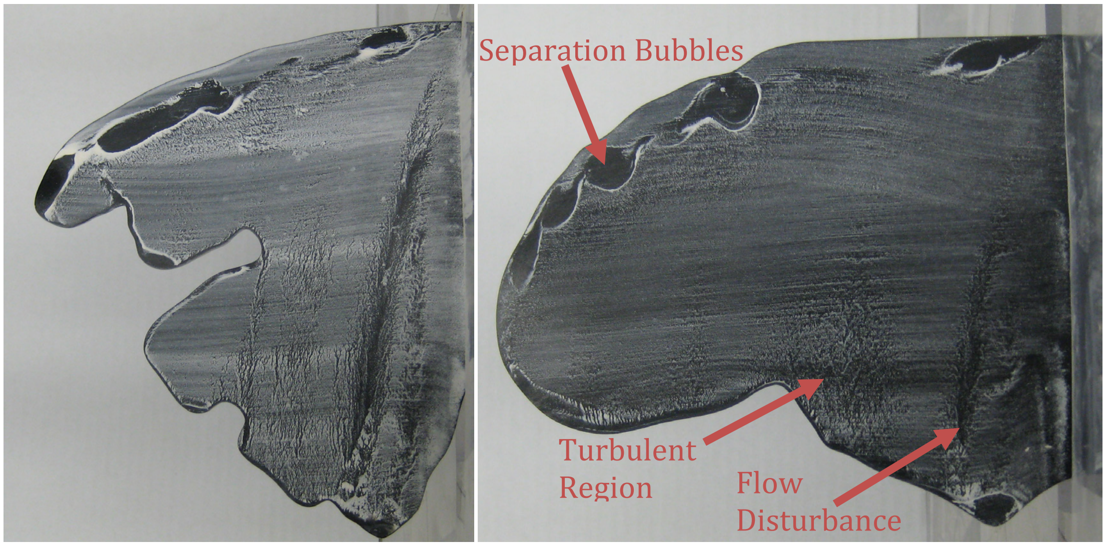

Figure 84 Low AoA Film Test with 'Best' High AoA (Left) and Pheasant (Right) Wings

All three aluminum wings were tested for lift and drag without the application of the oil film in order to find their L/D values. Five tests were done for each wing, and the average L/D values can be seen in Figure 85. The individual test results can be found in Appendix K. For the aluminum wings, the pheasant wing performed best, followed by the Zimmerman approximation wing. The best wing from the high AoA genetic algorithm performed poorly in comparison. The feathered wings showed similar L/D ranges.

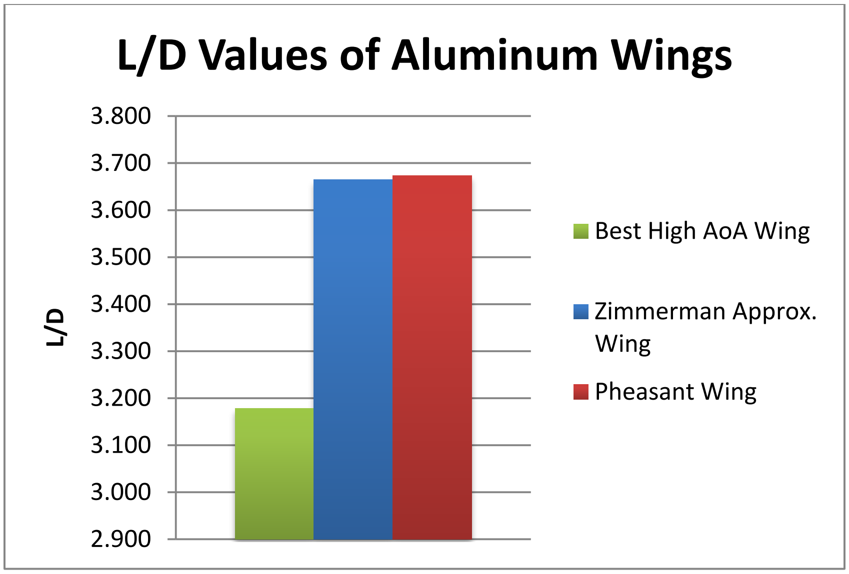

Figure 85 L/D Values at Low AoA

Low Angle of Attack Tuft Studies

Figure 86 shows the tufted Zimmerman approximation wing and best low AoA wing with an AoA of 4.6^0 and a freestream velocity of 18 m/s. Nearly all the tufts are lined up parallel to the freestream velocity, except for a few on the leading edge. These leading edge tufts appear to be oriented towards the wingtip, as though air were sliding from the root of the wing to the tip. It is difficult to see in photographs, but the trailing edge tufts near the middle of the span of the Zimmerman wing are rotating. The rotating tufts can be seen more clearly in video recordings. This rotation is likely due to the formation of wingtip vortices, which are surprisingly more prominent on the middle of the wingspan rather than at the wingtips, a possibility for low aspect ratio wings[6]. No such motion is seen on the best low AoA wing. Aside from the vortices and leading edge flow, the tufts show very little flow patterns.

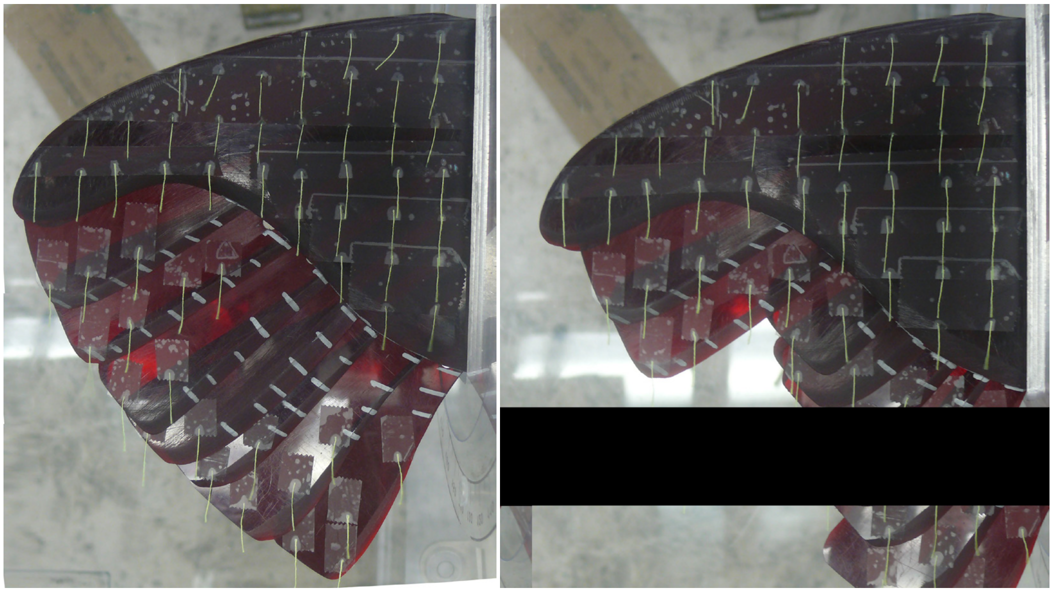

Figure 86 Zimmerman Approximation (Left) and 'Best' Low AoA (Right) Wings of Present Study with Tufts

Figure 87 shows the best wing of the present study compared with the best wing of Day[1]. On both the videos and pictures there was no evidence of wingtip vortices on either wing. However there was a similar wing root to wing tip orientation on some tufts at the leading edge. There also appeared to be more chaotic flow and possible vortices at the trailing edge near the root from video studies.

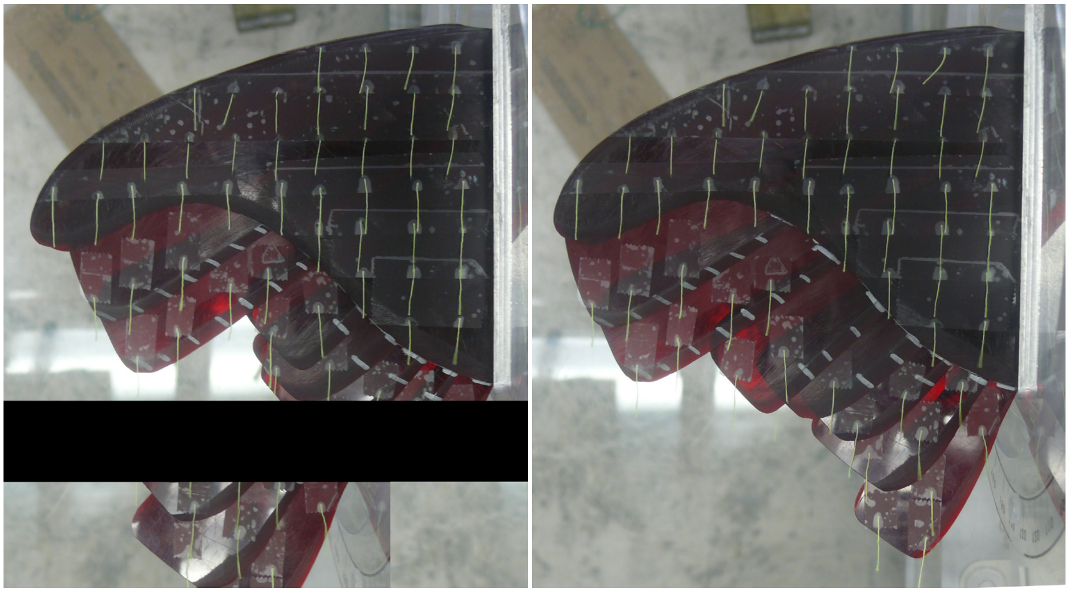

Figure 87 ‘Best’ Low AoA Wings from Present Study (Left) and Day[1] (Right) with Tufts

Unfortunately due to the low speed and low angle of attack there was very little reorientation of the tufts. In the low AoA tests it is also possible that some tufts, once reoriented into a position due to the transient flow during wind tunnel start up were unable to reorient themselves during the steady flow, since the freestream air velocity was too low to reorient them.

However, the Zimmerman approximation wing showed strong vortices near its midspan. In contrast, neither other the highest performing wings from the genetic algorithms showed any evidence of these vortices. Both of these wing planforms have a very different chord length compare to the Zimmerman approximation near the middle of the wingspan, near the location of these vortices. It seems likely that this is not coincidence and that the planforms of the best performing wings from the genetic algorithm are manipulating the formation of these vortices.

5. Conclusions

A summary of the results of this study is provided here.

- A genetic algorithm study was conducted to confirm if the ‘best’ wing from Day[1] from the low AoA genetic algorithm is independent of the initial wing population in the first generation. This was largely confirmed, however, the ‘best’ low AoA wing from the present study proved slightly different and gave a slightly better L/D performance than Day’s[1] ‘best’ wing showing that the low AoA wing from Day[1] was not a global optimum.
- The genetic algorithm study conducted at a high AoA near the stall condition resulted in a significantly different wing planform shape than the ‘best’ low AoA wings. This high AoA wing yielded higher L/D values than the ‘best’ low AoA wings as expected, but its performance was only slightly above that of the Zimmerman approximation wing. Noise in the data measurements also created some problems for the high AoA genetic algorithm.
- Wing chord length distributions of the ‘best’ low AoA wings from the present study were compared to bird wings of the order Galliformes. There was close agreement between the wing planform, shapes of galliform wings and wings from the genetic algorithm study. Both types of wings showed a region of constant chord length from the middle of the wing span to nearly the wing tip associated with a trailing edge notch feature.

- Flow visualization consisting of oil film and tuft studies were conducted on high AoA wing shapes from the genetic algorithm study in addition to a representative galliform wing (ring necked pheasant) and the approximate Zimmerman wing. The high AoA flow visualization showed separated flow for all wings at 11.8^0 AoA. A steady separation bubble preceded the separated flow. The best high AoA wing had two areas of attached flow, one of the leading edge, and one on the leading edge of its extended 'feather.' This is thought to be a reason for the feathered wing's superior performance for the high AoA wing, but this is not conclusive since the aluminum wing used for the flow visualization had lower L/D values than the Zimmerman approximation wing, the opposite of the feathered wing tests. While the flow visualization results were not conclusive in ascertaining why the wings from the genetic algorithm yield higher L/D values, the oil film technique was established as a flow visualization method at WPI to be used in future studies.
- The low AoA flow visualization tests on wings from the genetic algorithm wings, a ring necked pheasant wing, and the approximate Zimmerman wing showed some evidence of vortex manipulation by the best low AoA feathered wings and the pheasant wing. The oil film flow visualization also revealed the location of separation bubbles.

6. Future Work

6.1 Genetic Algorithm

Using cloning with mutation instead of crossover in the genetic algorithms applied in this study could be very useful. In trying to find a purely optimized shape, cloning may be superior in speed. Crossover also tends to optimize for genes that work well with a variety of other genes (given that they will be mixed often) so it is possible that with a wide variety of alleles in a generation the most common and best performing 'children' will not necessarily be the best performing alleles, but alleles that combine well with others while still performing decently. In theory, with enough time sexual selection algorithms would still find the optimal solution, but it may take a longer time. The actual usefulness of crossover in this type of problem is debatable. Focusing instead on mutation may be useful while avoiding the disadvantages of crossover. No crossover at all, or having fewer children produced via crossover are possible solutions, or creating an algorithm that decreases the rate of crossover as the population becomes more uniform. Either tactic would require greater amounts of mutation.

Additionally, a more discerning fitness function would be desirable. Even though removing the difference between the lift/drag of the poorest performing wing and all the other wings allowed for a greater difference between them (and thus more likelihood of the algorithm choosing the better performing wing) it often wasn't enough. An elitist fitness function, where the best wing is always selected for the next generation could be useful.

6.2 Wind Tunnel Testing

Experimental noise was a primary issue in the high AoA test in particular. Though the noise was small enough to merely be a nuisance in the low angle of attack tests, it became a major issue in the high angle tests. There were several issues that came up. Instability due to presumably unsteady airflow patterns over the high AoA wing caused the proximeter readout to vary forcing the average to be estimated. Use of a data acquisition system along with Labview with a time average could mitigate this issue. Varying drag calibration values caused further issues. Even when the test setup was recalibrated every twelve tests, different values would be found that greatly affected the wing's lift/drag ratio. Because the feathers had to be readjusted each test it seems likely that the force in moving them in and out bent the aluminum springs, changing the position and spring constant slightly. Even small changes could cause problems, as the drag values were small. Any future high AoA genetic algorithms would benefit from more accurate drag measurement.

6.3 Flow Visualization

The high AoA flow visualization tests showed flow patterns very clearly. The low AoA tests did not. Personal communications with Jack Ross of the University of Washington suggested that low AoA low airspeed oil film techniques would likely require use of a dye instead of a pigment. Unfortunately there was not enough time to test for that in this project. The best wings from the low AoA genetic algorithms were not tested with oil film flow visualization because there was not enough time apply this to the current study. Better low AoA flow visualization and the high performing planforms made out of aluminum wings would allow more research into why these wings outperformed the others.

7. Works Cited

[1]Day, A. H., "Optimization of a Micro Air Vehicle Planform Using Genetic Algorithms," Masters Thesis *Worcester Polytechnic Institute*, 2007.

[2]Michelson, R. C., "Extraterrestrial Flight," *Neurotechnology for Biomimetic Robots*, edited by Joseph Ayers, MIT Press, Cambridge MA, 2002, pp. 481.

[3]Cubin, N. T., DelSignore, R. C., McCann, R. A., "Trailing Edge Notch Effects on Micro Air Vehicle Performance," *Worcester Polytechnic Institute*, 2007.

[4]Zimmerman, C. H., "Aerodynamic Characteristics of Several Airfoils of Low Aspect Ratio," NACA TN 539, 1935.

[5]Raymer, D. P., "Sizing From a Conceptual Sketch," *Aircraft Design: A Conceptual Approach*, 3rd ed. AIAA, Reston, VA, 1999, pp. 21.

[6]Mueller, T. J., Torres, G. E., "Aerodynamics of Low Aspect Ratio Wings at Low Reynolds Numbers with Applications to Micro Air Vehicle Design and Optimization," *University of Notre Dame Office of Research*, Nov. 2001.

[7]Viieru, D., Albertani, R., Shyy, W., and Ifju, P. G., "Effect of Tip Vortex on Wing Aerodynamics of Micro Air Vehicles," Journal of Aircraft, Vol. 42, No. 6, 2005.

[8]Anderson, J. D. Jr., *Fundamentals of Aerodynamics*, 4th ed. McGraw-Hill, New York, 2007.

[9]Fox, R. W., *Introduction to Fluid Dynamics*, 6th ed., John Wiley & Sons, Inc., 2004.

[10]O'Meara, M. M., and Mueller, T.J., "Laminar Separation Bubble Characteristics on an Airfoil at Low Reynolds Numbers," *AIAA Journal*, Vol. 25, No. 8, 1987, pp. 1033-1041.

[11]Bannasch, R., "From Soaring and Flapping Bird Flight to Innovative Wing and Propeller Constructions," *Progress in Astronautics and Aeronautics*, Vol. 194, pp. 453-471.

[12]Sathaye, S., Yuan, J., and Olinger, D. J., "Lift Distribution on Low-Aspect-Ratio Wings at Low Reynolds Number for Micro-Air Vehicle Applications," *22nd Applied Aerodynamics Conference and Exhibit*, AIAA, Providence, RI, 2004.

[13]Tucker, V. A., "Drag Reduction by Wing Tip Slots in a Gliding Harris' Hawk, Parabuteo Unicinctus," *The Journal of Experimental Biology*, Vol. 198, 1995, pp. 775-781.

[14]Custodio, D., "The Effect of Humpback Whale-like Leading Edge Protruburences on Hydrofoil Performance," *Worcester Polytechnic Institute*, 2007, pp. 22-25

[15]Merzkirch, W., *Flow Visualization*, 2nd ed. Academic Press, Boston, 1987, pp. 82-87.

[16]Yang, W., *Handbook of Flow Visualization,* 2nd ed. Taylor and Francis, New York, 2001, pp. 106.

[17]Van Tyne, J., and Andrew B. J., *Fundamentals of Ornithology*. Dover Publications, Inc., New York, 1971, pp. 351-353.

[18]Drovetski, S., "Influence of the Trailing-Edge Notch on Flight Performance of Galliformes," *The Auk-Journal of American Ornithologists' Union*, Vol. 113, No. 4, 1996, pp. 802-810.

[19]*Slater Museum of Natural History* [online database], 2005, http://digitalcollections.ups.edu/slater/ [retrieved Sep. 2008].

[20]Darwin, Charles, *On the Origin of Species by Means of Natural Selection*, Elecbook, London, 2001.

[21]Mitchell, M., *An Introduction to Genetic Algorithms*, MIT Press, Cambridge, MA, 1996.

[22]Fogel, D. B., *Evolutionary Computation: Toward a New Philosophy of Machine Intelligence,* 2nd ed. IEEE Press, New York, 2000.

[23]Livnat, A., Papadimitriou, C., Dushoff, J., and Feldman, M. W., "A Mixability Theory of the Role of Sex in Evolution," *Proceedings of the National Academy of Sciences in the United States of America*, published online December 10, 2008; Vol. 105, No. 50, 2008, pp. 19803-19808.

[24]Obayashi, S., Oyama, A., and Nakamura, T., "Transonic Wing Shape Optimization Based on Evolutionary Algorithms" *High Performance Computing*, Vol. 1940, Springer-Verlag, Berlin, 2000, pp. 172-181.

[25]Quagliarella, D., and Cioppa, A. D., "Genetic Algorithms Applied to the Aerodynamic Design of Transonic Airfoils," *Aircraft*, Vol. 32, No. 4, pp. 889-890.

[26]Jones, B. R., Crossley, W. A., and Lyrintzis, A. S., "Aerodynamic and Aeroacoustic Optimization of Rotorcraft Airfoils via a Parallel Genetic Algorithm," *Journal of Aircraft*, Vol. 37, No. 6, November-December 2000, pp. 1088-1096.

[27]Popp, K. A., "Experimental Investigation of Reynolds Number and Scale Effects on Parachute Inflation," *Worcester Polytechnic Institute*, 2000, pp. 21.

[28]Blanchard, S., DeFusco, D., & Donoghue, Chris. "Experiments on Trailing Edge Notches for Micro Air Vehicle Wings," *Worcester Polytechnic Institute*, 2006.

[29]Vigen, P., van Dam, C. P., Holmes, B. J., and Howard, F. G., "Wind-Tunnel Investigations of Wings with Serrated Sharp Trailing Edges," *Conference on Low Reynolds Number Aerodynamics*, University of Notre Dame, pp. 295-313.

Appendices

Appendix A: Sample Data Spreadsheets

Sample Spreadsheet with Lift Measurements

	Position Number							Fitness	L/D	voltage	v0	Drag	Lscale	Rscale	Lift
Chromosome #	1	2	3	4	5	6	7	Function		(volts)	(volts)	(g)	(g)	(g)	(g)
1															
2															
3															
4															
5															
6															
7															
8															
9															
10															

Sample Table with Normal Force Measurements

	Position Number							Fitness	L/D	voltage	v0	Drag 1	Lscale	Rscale	Normal	Drag	Lift
Chromosome #	1	2	3	4	5	6	7	Function		(volts)	(volts)	(g)	(g)	(g)	(g)	g	g
1																	
2																	
3																	
4																	
5																	
6																	
7																	
8																	
9																	
10																	

Appendix B: Genetic Algorithm Codes

Initial Population Code

```
popsize=72;
rand('twister',sum(100*clock))
POP=rand(popsize,7);
A=[8, 8, 6, 6, 5, 4, 3];
for i=1:7
    POP(:,i)=A(i)*POP(:,i);
end
InitPopulation=floor(POP);
xlswrite('InitialPopulation.xls', InitPopulation)
```

Selection Roulette Code

```
function parents = selectionroulette(expectation,nParents)
rand('twister',sum(100*clock))
wheel = cumsum(expectation)/sum(expectation);
parents = zeros(1,nParents);
for i = 1:nParents
    r = rand;
    for j = 1:length(wheel)
        if(r < wheel(j))
            parents(i) = j;
            break;
        end
    end
end
```

Genetic Algorithm Code

```
close all
clear all
PopNum=24;
rand('twister',sum(100*clock))
nParents=PopNum/2;
A=[8, 8, 6, 6, 5, 4, 3];
numgen=input('Enter the generation worksheet number for you current population\n')
expectation = xlsread('Populations.xls', numgen, 'I3:I74');%reads fitness values
parents = selectionroulette(expectation,nParents)   %function determines which
                                        %individuals are chosen
                                        %to become parents
OldPop=xlsread('Populations.xls', numgen, 'B2:H74')
NewPop=zeros(PopNum,7);
for i = 1:nParents                          %this for loop places the
   n=parents(i);                           %parents into the next
   NewPop(i,:)=OldPop(n,:);                      %generation of individuals
end

for k = 1:nParents/2                        %loop for each pair of parents
for i = 1:2                              %each parent set makes two children
   for j = 1:7
      r=rand;
      if(r < .5)                            %if statement decideds which parent
         NewPop(nParents+2*(k-1)+i,j) = NewPop(2*(k-1)+1,j);   %contributes each gene
      else
         NewPop(nParents+2*(k-1)+i,j) = NewPop(2*(k-1)+2,j);
      end
%Below is the mutation function, if the random value is less than the mutation fraction,
%the value is mutated to a new random number.
r=rand;
      if(r<.2)
         r=floor(rand*A(j));
         NewPop(nParents+2*(k-1)+i,j) =r;
      end

   end
end
end
numnewgen=numgen+1
xlswrite('Populations.xls', NewPop, numnewgen, 'B2:H25');
```

Appendix C: Flat Plate Wing Models

Zimmerman Approximation Wing

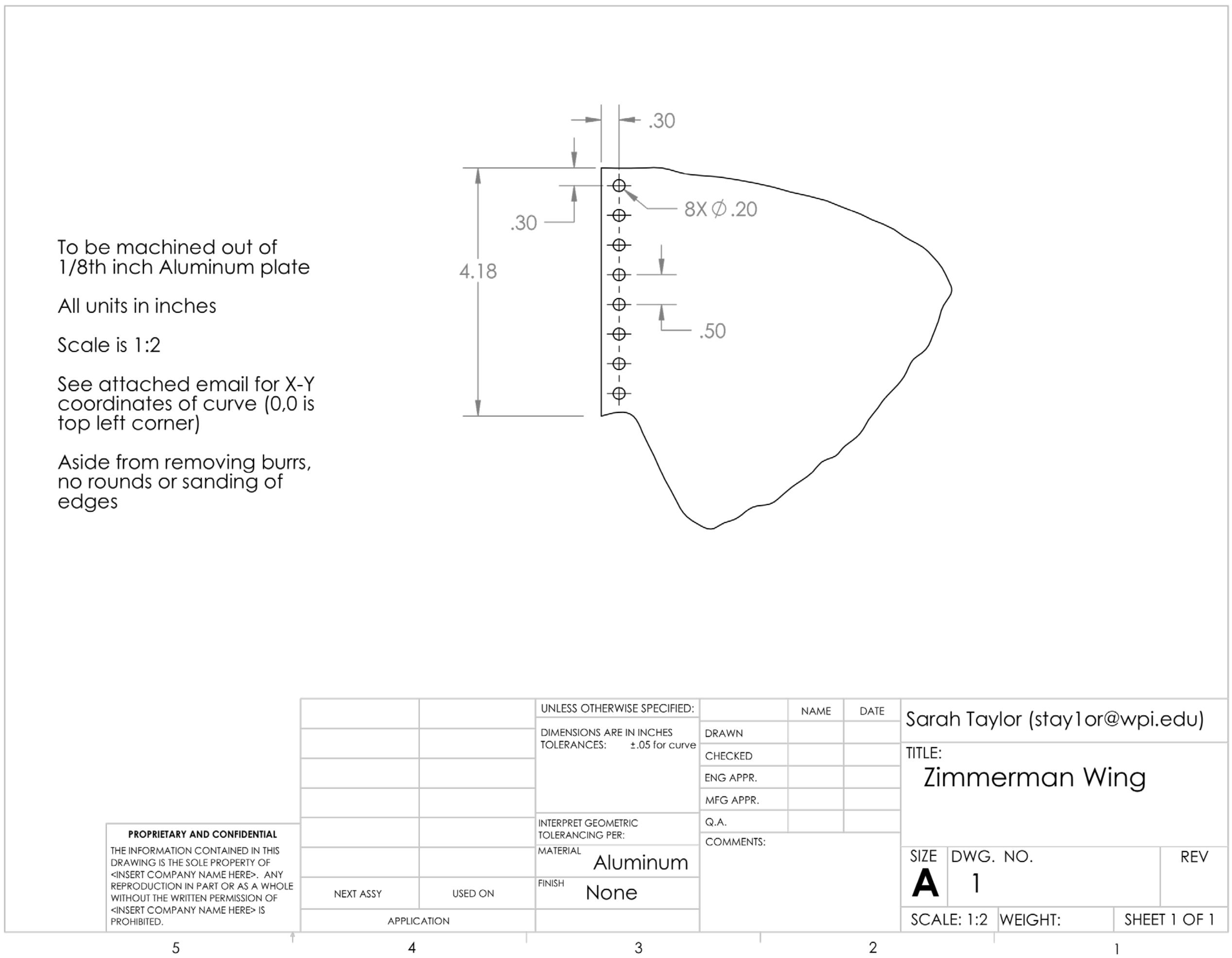

Best High AoA Wing

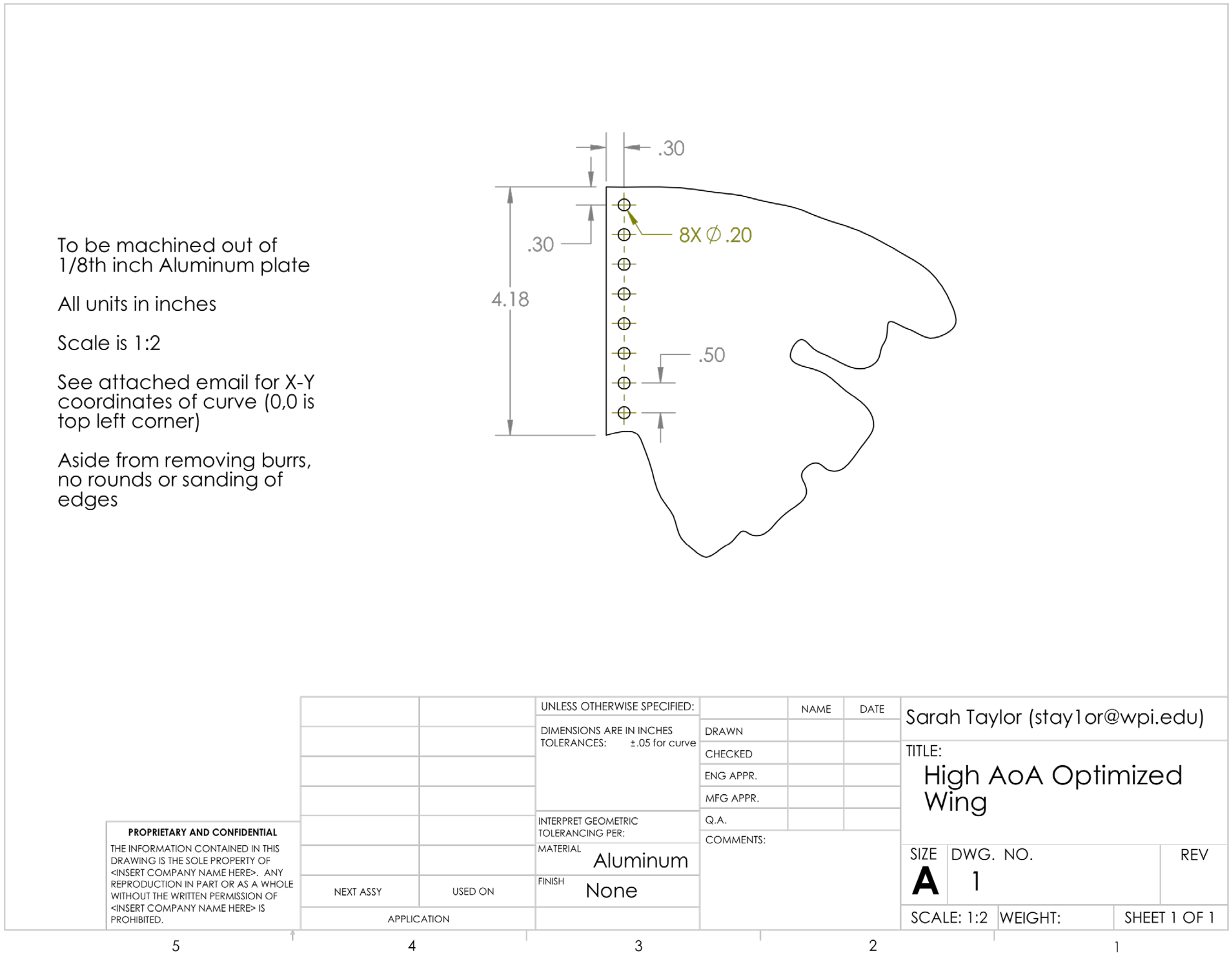

Ring Necked Pheasant Wing

To be machined out of 1/8th inch Aluminum plate

All units in inches

Scale is 1:2

See attached email for X-Y coordinates of curve (0,0 is top left corner)

Aside from removing burrs, no rounds or sanding of edges

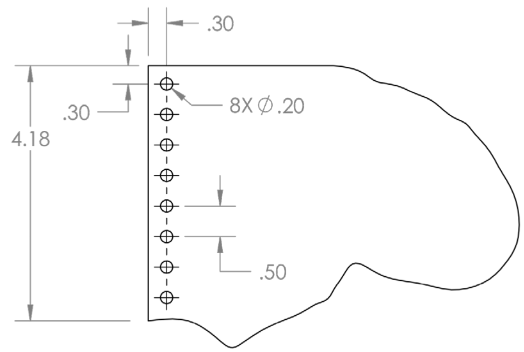

UNLESS OTHERWISE SPECIFIED:

DIMENSIONS ARE IN INCHES
TOLERANCES: ±.05 for curve

INTERPRET GEOMETRIC TOLERANCING PER:

MATERIAL Aluminum

FINISH None

NEXT ASSY | USED ON

APPLICATION

	NAME	DATE
DRAWN		
CHECKED		
ENG APPR.		
MFG APPR.		
Q.A.		

COMMENTS:

Sarah Taylor (stay1or@wpi.edu)

TITLE: Ring Necked Pheasant Wing

SIZE A | DWG. NO. 1 | REV

SCALE: 1:2 | WEIGHT: | SHEET 1 OF 1

5 4 3 2 1

Appendix D: Finding the Wing Chord Distribution

- Take an undistorted (that is, taken directly above the wing) picture of the desired wing and upload it onto a computer. The root should be located on the left of the picture.
- Make an outline of the wing (not including the root) with fifty or more evenly spaced points and record their X and Y positions in two columns. There are some programs (such as in Labview) where this can be done. To achieve consistency take points only at the outer tips of closely packed feathers. This does simplify the wings somewhat, but is required to keep the shapes from becoming too complicated. If the wing has large slots, these may need to be omitted or watched carefully. The Matlab program should not have two potential solutions for the trailing edge of the wing, otherwise it may run into errors. There can also be no duplicate points, that is, no exact same X or Y values.
- Take the coordinate data; make sure it is in a plain text .txt file with only tabs separating the X and Y columns. Save this file in the same directory as the following Matlab programs.
- Run wingshapesinterp.m Make sure there are no errors. If there are errors, check that the wing root is on the left, that the wing outline does not have large slots, and there are no duplicate coordinates. It should work fine it all this is done. If the wing has its root on the right, run wingflip.m. Wingflip.m will ask for the name of your coordinate file and return a version with the wing root on the left.

- If successful the wingshapesinterp.m program will show a preview of the wing chord distribution. Copy the matrix labeled ‘chord’ to get the chord distribution data.
- Paste the chord matrix into Excel (you may need to specify tab delimiters) and plot. You can now compare different chord distributions on the same graph, they have already been normalized by wingshapesinterp.m so you do not need to worry about scaling.

Wing Chord Distribution Code (wingshapesinterp.m)

```
% Sarah Taylor
% WPI Master's Thesis: Biologically Inspired Wing Planform Optimization
% A program to find the normalized chord length versus the normalized span
% in Matlab
% Last update: Jan 2009
%%%%%%%%%%%%%%%%%%%%%%%%%%%
% NOTES
% The wing must have it's root on the left. If it is facing in the opposite
% direction it will not work. Use flipwing.m to flip.
clear all
clc
% Find out which files to get
% Files must consist of the x and y coordinates arranged in a two column
% array (X in column one, and y in column two). The file format must be a
% tab delimited .txt file.
filename=input('What is the name of the desired data set?  \n','s');
filenamevar=strcat(filename,'.txt');
wingarray=dlmread(filenamevar, '\t');
wingdatax=wingarray(:,1);
wingdatay=wingarray(:,2);
% Maximum and minimum x and y values
maxwing=max(wingarray);
minwing=min(wingarray);
maxx=maxwing(1,1);
maxy=maxwing(1,2);
minx=minwing(1,1);
miny=minwing(1,2);
% b=span of one wing (half of total)
b=maxx-minx;
% Leading edge y value at the root
lroot=wingarray(1,2);
% Number of rows in coordinate array
points=length(wingarray);
% trailing edge y value at root
troot=wingarray(points,2);
% Chord at root
croot=lroot-troot;
% Normalizing all coordinates (w.r.t. root chord and b)
normx=(wingdatax-minx)/b;
normy=(wingdatay-troot)/croot;
norm=[normx,normy];
% Finding the wingtip
[tipval, tippointarray]=max(norm);
tippoint=tippointarray(1,1);
tippoint1=tippoint+1;
% Making an array for the leading edge and trailing edge
normtop=norm(1:tippoint,1:2);
normbottom=norm(tippoint1:points,1:2);
% k will be the increment value
k=1;
for k=1:1:tippoint-1,
  % Getting the coordinates of the top point
  xtop=normtop(k,1);
```

```
    ytop=normtop(k,2);
    % Finding the closest x value on the trailing edge
    diffarray=normbottom(:,1) - xtop;
    absdiffarray=abs(diffarray);
    [lownum, closestm]=min(absdiffarray);
    ybottom1=normbottom(closestm,2);
    xbottom1=normbottom(closestm,1);
    % Finding the second point for interpolation
    absdiffarray2=absdiffarray;
    absdiffarray2(closestm,:)=100;
    [lownum2, closestm2]=min(absdiffarray2);
    ybottom2=normbottom(closestm2,2);
    xbottom2=normbottom(closestm2,1);
    % Interpolation
    if xbottom1>xbottom2;
        dir=-1;
    else
        dir=1;
    end
    xdiff=xtop-xbottom1;
    slope=(ybottom2-ybottom1)/(xbottom2-xbottom1);
    ybottom=ybottom1+xdiff*dir*slope;
    % Finding and recording the chord
    ydiff=ytop-ybottom;
    chord1(k,2)=xtop;
    chord1(k,3)=ydiff;
    k=k+1;
end
chord=chord1(:,2:3);
X=chord1(:,2);
Y=chord1(:,3);
scatter(X,Y)
```

Wingflip Code (wingflip.m)

```
% Sarah Taylor
% WPI Master's Thesis: Biologically Inspired Wing Planform Optimization
%A  program to flip the wing if the root is located on the right side
clear all
clc
% Find out which files to get
% Files must consist of the x and y coordinates arranged in a two column
% array (X in column one, and y in column two). The file format must be a
% tab delimited .txt file.
filename=input('What is the name of the desired data set?  \n','s');
filenamevar=strcat(filename,'.txt');
wingarray=dlmread(filenamevar, '\t');
wingdatax=wingarray(:,1);
points=length(wingarray);
for i=1:points
wingdataxnew(i)=(-1)*wingdatax(i);
wingdataxnew(i)=wingdataxnew(i)+20;
wingarray(i,1)=wingdataxnew(i);
end
```

Appendix E: Null Hypothesis

It is known that genetic algorithms will slowly populate new generations with higher performance chromosome. However, the question of what happens when there are no higher performing chromosomes must be answered. Stated another way, how would a genetic algorithm perform if noise completely masked any actual data?

To investigate this idea, the genetic algorithm was run again, however this time the fitness function was produced by a random number generator, set to create values from 0 to .333, similar to the values of the fitness function of the real genetic algorithms. These values were then treated as the fitness function, even though they were not related to the chromosomes and were generated anew each generation.

In the first and second generation the chromosomes were varied as was expected, but in the third generation two chromosomes (one of which happened to be a child of the other) received higher fitness values. These two chromosomes were then duplicated many times over for the fourth generation. From that point on, the gene pool became less varied and more uniform. This continued until generation ten when the experiment was stopped. Generation ten had three instances of chromosome 7552431 and many related chromosomes. While the gene pool in the tenth generation was more varied than the final generations of both high and low AoA tests, to anyone unfamiliar with the process it would appear that the genetic algorithm had bred a 'superior' wing, even when the wing's performance was based entirely on random numbers.

Since this particular genetic algorithm relied heavily on the reshuffling of genes (crossover) to produce variety, it fails in creating diversity once the population is similar.

While neither high nor low AoA final populations looked quite like the randomized population, the high AoA tests do have some worrisome similarities. Primarily, the lack of consistency in later generations, was concerning. The noise was much more of a problem in the high angle of attack tests, perhaps due to instabilities that tend to occur at high angles, or due to the greater influence of the axial force, which historically has proven harder to measure.

To refute the null hypothesis, the most common chromosome from the randomized genetic algorithm was tested in the wind tunnel against several other wings at 11.8^0 AoA. Each wing was tested ten times and their average L/D values were compared to each other.

The most common chromosome of the randomized genetic algorithm was 7552431. This chromosome was tested as a wing shape against several other important wings. The original data can be found at the end of this section.

When tested against the Zimmerman planform, and the most 'best' high AoA wing (4143120), the null hypothesis wing (7552431) performed surprisingly well. In fact, the average lift of the null hypothesis wing was the second highest out of all the tested wings, second only to the most common wing of the high AoA genetic algorithm, shown in Figure 88.

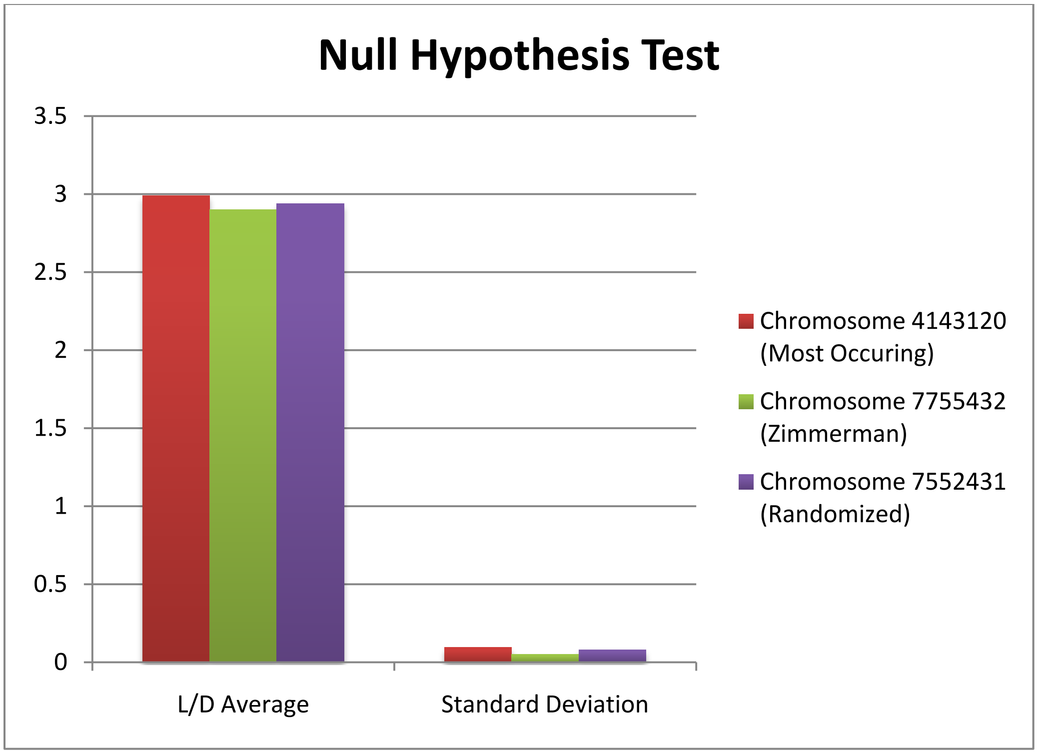

Figure 88 Null Hypothesis Test Results

There is some potential for confusion due to the similarity of the most common chromosome of the randomized algorithm, to the Zimmerman approximation planform. The 7552431 shape has almost all its feathers extended, like the Zimmerman planform, explaining why it performed similarly.

While it is possible that by chance alone, the randomized genetic algorithm found a good wing; it still puts the high angle of attack tests into doubt, especially considering the lack of uniformity in both their final generations. Primarily, this shows that the reduction of noise is of the utmost importance in genetic algorithms.

Randomized Genetic Algorithm

Generation One

	Position Number							Fitness
Chromosome #	-1	-2	-3	-4	-5	-6	-7	Function
1	7	1	4	4	0	0	2	0.125
2	7	1	5	5	4	1	2	0.208
3	0	6	5	3	2	2	0	0.423
4	7	5	2	2	1	3	2	0.351
5	3	5	5	3	3	0	1	0.044
6	3	7	3	3	3	1	0	0.179
7	1	2	4	3	1	2	1	0.172
8	0	2	4	1	1	0	2	0.438
9	2	5	0	0	4	1	1	0.174
10	4	3	1	4	0	2	1	0.010
11	2	7	3	1	0	1	0	0.241
12	4	7	3	5	1	3	1	0.042
13	1	3	4	5	2	2	2	0.086
14	0	1	1	5	4	2	0	0.438
15	7	7	2	4	0	3	0	0.069
16	2	4	4	4	0	2	1	0.340
17	5	0	4	3	4	1	1	0.496
18	7	1	2	2	3	2	1	0.148
19	7	6	1	0	0	0	0	0.429
20	1	0	3	3	1	1	0	0.450
21	6	5	3	1	3	2	0	0.289
22	3	2	2	4	3	3	2	0.171
23	7	3	5	5	3	0	2	0.029
24	5	4	4	3	0	2	0	0.138
25	2	5	3	2	1	2	2	0.016
26	6	4	1	2	3	1	0	0.177
27	6	4	0	0	0	0	2	0.256
28	6	3	4	0	4	2	2	0.117
29	4	4	4	3	1	1	2	0.381
30	0	7	1	3	3	1	0	0.137
31	3	2	5	2	4	3	0	0.184
32	7	6	4	3	0	0	0	0.064
33	6	7	2	5	0	2	0	0.082
34	1	2	0	5	0	1	2	0.108
35	0	6	3	2	3	1	2	0.426
36	0	7	3	5	1	0	1	0.436
37	6	3	4	0	2	0	1	0.123
38	5	7	5	4	3	2	2	0.244
39	6	7	4	4	4	0	1	0.343
40	7	2	0	1	0	2	0	0.200
41	2	3	0	0	2	1	1	0.080
42	2	0	2	1	3	1	2	0.423
43	1	2	2	1	0	0	1	0.475
44	0	1	3	2	2	2	1	0.182
45	0	6	5	2	1	1	0	0.351
46	4	5	2	3	1	1	1	0.241
47	6	3	5	3	0	2	0	0.214
48	5	0	1	4	0	1	0	0.252
49	1	5	3	0	0	0	1	0.026
50	7	0	3	4	2	0	0	0.497
51	4	4	4	4	0	2	0	0.383
52	7	4	3	5	3	1	1	0.259
53	2	0	3	0	4	3	2	0.329
54	5	6	4	0	3	1	0	0.231
55	0	2	0	3	1	2	2	0.284
56	0	3	2	0	4	1	0	0.471
57	0	7	2	1	1	2	1	0.338
58	4	5	3	2	1	1	0	0.181
59	3	7	4	4	3	1	2	0.133
60	0	7	3	1	3	1	2	0.341
61	0	5	1	3	2	0	1	0.333
62	5	2	3	4	2	0	1	0.142
63	5	1	4	0	2	0	1	0.372
64	7	5	5	2	4	3	0	0.226
65	7	5	5	2	2	1	2	0.111
66	3	3	1	4	1	0	2	0.409
67	2	3	2	0	4	1	1	0.364
68	7	2	2	5	0	1	2	0.391
69	5	7	3	2	4	2	2	0.414
70	1	7	2	2	4	1	0	0.118
71	6	6	4	1	3	1	0	0.181
72	4	3	5	4	0	1	1	0.468

Generation Two

Chromosome #	Position Number -1	-2	-3	-4	-5	-6	-7	Fitness Function
1	4	4	4	4	0	2	0	0.314
2	0	6	5	3	2	2	0	0.450
3	0	7	3	5	1	0	1	0.308
4	6	4	0	0	0	0	2	0.228
5	7	5	5	2	4	3	0	0.147
6	4	3	5	4	0	1	1	0.312
7	0	3	2	0	4	1	0	0.311
8	7	0	3	4	2	0	0	0.414
9	3	2	5	2	4	3	0	0.466
10	0	6	5	2	1	1	0	0.369
11	4	4	4	3	1	1	2	0.106
12	7	5	5	2	4	3	0	0.244
13	4	6	5	3	2	2	2	0.420
14	4	4	4	4	0	2	0	0.146
15	0	7	3	5	0	0	0	0.278
16	0	4	0	5	0	0	2	0.055
17	4	5	5	2	4	3	1	0.218
18	7	3	1	2	4	3	0	0.109
19	0	0	3	0	4	1	0	0.017
20	0	3	2	0	2	0	0	0.368
21	7	2	5	2	4	1	0	0.138
22	0	2	1	2	1	1	0	0.123
23	7	5	3	2	1	2	0	0.171
24	4	4	5	2	4	1	0	0.296

Generation Three

Chromosome #	Position Number -1	-2	-3	-4	-5	-6	-7	Fitness Function
1	0	7	3	5	1	0	1	0.103
2	0	3	2	0	2	0	0	0.023
3	4	5	5	2	4	3	1	0.455
4	7	5	5	2	4	3	0	0.495
5	7	5	5	2	4	3	0	0.082
6	7	0	3	4	2	0	0	0.134
7	4	6	5	3	2	2	2	0.134
8	7	0	3	4	2	0	0	0.084
9	0	7	3	5	1	0	1	0.464
10	4	6	5	3	2	2	2	0.065
11	0	7	3	5	1	0	1	0.339
12	3	2	5	2	4	3	0	0.230
13	3	3	2	5	1	0	1	0.260
14	6	3	2	0	2	0	0	0.309
15	5	6	5	2	2	3	0	0.291
16	7	5	5	2	4	3	1	0.029
17	7	5	5	2	3	0	0	0.350
18	5	5	3	4	2	3	0	0.443
19	4	6	5	3	2	2	0	0.393
20	4	0	5	4	2	0	0	0.201
21	0	0	3	5	2	0	2	0.182
22	4	1	2	5	2	2	2	0.311
23	0	0	5	1	4	0	1	0.057
24	0	7	5	2	0	3	1	0.380

Generation Four

Chromosome #	Position Number -1	-2	-3	-4	-5	-6	-7	Fitness Function
1	0	7	5	2	0	3	1	0.010353497
2	4	1	2	5	2	2	2	0.450712287
3	3	2	5	2	4	3	0	0.199947866
4	7	5	5	2	4	3	0	0.413216368
5	4	1	2	5	2	2	2	0.094080476
6	0	7	5	2	0	3	1	0.192727367
7	7	5	5	2	3	0	0	0.295931546
8	3	2	5	2	4	3	0	0.330546234
9	4	5	5	2	4	3	1	0.277483027
10	7	5	5	2	4	3	0	0.198060571
11	5	5	3	4	2	3	0	0.003380845
12	6	3	2	0	2	0	0	0.101887137
13	6	7	5	5	2	2	2	0.100930295
14	4	1	5	5	4	3	1	0.366268882
15	7	2	5	2	4	1	0	0.450855893
16	7	2	5	2	4	3	0	0.22329605
17	4	7	2	5	2	0	1	0.073858526
18	0	7	2	5	0	3	1	0.054585433
19	3	2	5	2	4	0	0	0.113895354
20	7	2	0	2	3	0	0	0.062457235
21	4	5	5	2	3	3	1	0.107785625
22	7	5	5	2	4	3	1	0.091395544
23	6	2	2	4	2	1	0	0.140286296
24	6	0	3	4	2	0	0	0.469157254

Generation Five

Chromosome #	Position Number -1	-2	-3	-4	-5	-6	-7	Fitness Function
1	7	5	5	2	3	0	0	0.379
2	7	5	5	2	4	3	0	0.391
3	3	2	5	2	4	0	0	0.385
4	4	1	2	5	2	2	2	0.137
5	4	1	2	5	2	2	2	0.030
6	7	2	0	2	3	0	0	0.323
7	4	1	5	5	4	3	1	0.336
8	3	2	5	2	4	3	0	0.211
9	7	5	5	2	4	3	1	0.273
10	6	0	3	4	2	0	0	0.247
11	0	7	5	2	0	3	1	0.104
12	7	2	5	2	4	1	0	0.196
13	4	5	5	2	4	3	0	0.231
14	7	5	5	0	4	0	0	0.310
15	3	2	5	2	2	0	2	0.212
16	6	2	3	5	4	2	0	0.271
17	6	2	2	2	3	3	2	0.367
18	4	1	0	2	2	0	2	0.322
19	5	2	5	5	4	3	0	0.476
20	4	1	5	5	2	0	2	0.186
21	6	5	5	4	4	0	2	0.064
22	6	0	5	4	4	3	1	0.428
23	7	7	5	2	0	1	1	0.358
24	6	2	5	2	4	1	1	0.478

Generation Six

Chromosome #	-1	-2	-3	-4	-5	-6	-7	Fitness Function
	Position Number							
1	7	2	0	2	3	0	0	0.110
2	7	5	5	0	4	0	0	0.378
3	6	2	5	2	4	1	1	0.472
4	5	2	5	5	4	3	0	0.087
5	4	1	2	5	2	2	2	0.392
6	7	7	5	2	0	1	1	0.109
7	7	5	5	2	3	0	0	0.085
8	6	0	5	4	4	3	1	0.351
9	6	5	5	4	4	0	2	0.387
10	7	5	5	2	4	3	0	0.369
11	6	2	5	2	4	1	1	0.394
12	7	7	5	2	0	1	1	0.185
13	0	2	0	2	4	0	0	0.265
14	7	2	5	2	3	0	0	0.098
15	6	2	5	3	4	1	0	0.007
16	6	2	5	2	4	3	0	0.457
17	2	1	2	2	1	2	1	0.302
18	7	1	2	1	0	1	1	0.064
19	6	5	5	2	3	0	0	0.115
20	7	5	5	2	4	0	0	0.464
21	7	4	5	2	4	0	2	0.021
22	6	5	5	2	4	0	2	0.430
23	6	3	5	2	0	1	1	0.375
24	6	2	5	2	0	1	1	0.376

Generation Seven

Chromosome #	-1	-2	-3	-4	-5	-6	-7	Fitness Function
	Position Number							
1	7	5	5	2	4	3	0	0.081
2	2	1	2	2	1	2	1	0.219
3	7	5	5	0	4	0	0	0.117
4	6	0	5	4	4	3	1	0.299
5	0	2	0	2	4	0	0	0.115
6	2	1	2	2	1	2	1	0.400
7	6	2	5	2	4	1	1	0.464
8	6	0	5	4	4	3	1	0.156
9	4	1	2	5	2	2	2	0.462
10	7	5	5	2	4	3	0	0.287
11	6	2	5	2	4	1	1	0.300
12	2	1	2	2	1	2	1	0.341
13	7	1	2	1	1	3	0	0.448
14	7	1	5	2	4	3	0	0.233
15	7	0	5	4	4	0	0	0.343
16	6	0	5	0	4	3	1	0.385
17	2	2	0	2	1	2	1	0.323
18	0	5	2	5	1	2	0	0.454
19	6	0	5	4	3	1	1	0.239
20	6	0	5	4	4	3	1	0.379
21	7	1	5	1	2	3	0	0.395
22	7	5	2	5	2	3	0	0.118
23	5	4	2	2	4	1	1	0.188
24	3	2	0	2	4	1	1	0.102

Generation Eight

Chromosome #	Position Number -1	-2	-3	-4	-5	-6	-7	Fitness Function
1	7	5	5	2	4	3	0	0.300
2	6	2	5	2	4	1	1	0.226
3	6	0	5	0	4	3	1	0.043
4	6	0	5	0	4	3	1	0.036
5	2	2	0	2	1	2	1	0.332
6	0	5	2	5	1	2	0	0.029
7	7	1	5	1	2	3	0	0.362
8	6	0	5	0	4	3	1	0.059
9	2	2	0	2	1	2	1	0.361
10	6	0	5	4	4	3	1	0.331
11	7	5	5	2	4	3	0	0.464
12	7	0	5	4	4	0	0	0.105
13	6	0	5	5	4	1	0	0.029
14	7	5	5	2	4	1	0	0.382
15	5	0	5	0	4	3	1	0.359
16	6	0	5	0	1	1	1	0.151
17	0	5	2	5	1	2	0	0.273
18	5	5	2	5	0	2	0	0.359
19	6	0	5	1	2	3	1	0.236
20	1	5	4	0	2	3	0	0.158
21	6	7	5	4	4	2	1	0.003
22	2	7	0	4	1	2	0	0.311
23	7	0	5	2	1	3	0	0.395
24	3	5	3	2	4	3	0	0.037

Generation Nine

Chromosome #	Position Number -1	-2	-3	-4	-5	-6	-7	Fitness Function
1	7	1	5	1	2	3	0	0.297
2	7	5	5	2	4	3	0	0.309
3	2	7	0	4	1	2	0	0.204
4	0	5	2	5	1	2	0	0.451
5	7	5	5	2	4	3	0	0.154
6	7	0	5	2	1	3	0	0.054
7	6	0	5	1	2	3	1	0.290
8	2	7	0	4	1	2	0	0.274
9	2	2	0	2	1	2	1	0.146
10	7	5	5	2	4	3	0	0.039
11	7	5	5	2	4	1	0	0.083
12	1	5	4	0	2	3	0	0.234
13	3	1	5	2	4	3	0	0.174
14	7	3	5	2	4	3	0	0.492
15	2	6	2	2	1	2	0	0.422
16	7	3	0	4	1	2	0	0.020
17	7	0	5	2	1	3	0	0.051
18	7	5	5	2	4	3	1	0.473
19	2	7	0	4	2	3	0	0.032
20	6	7	0	4	2	2	0	0.175
21	2	2	0	2	1	3	1	0.160
22	7	5	0	2	1	3	0	0.202
23	7	5	4	0	2	1	0	0.294
24	1	5	5	2	0	3	0	0.371

Generation Ten

	Position Number							Fitness
Chromosome #	-1	-2	-3	-4	-5	-6	-7	Function
1	1	5	5	2	0	3	0	0.326
2	7	5	5	2	4	3	1	0.047
3	7	1	5	1	2	3	0	0.413
4	6	7	0	4	2	2	0	0.433
5	7	5	5	2	4	3	1	0.341
6	2	7	0	4	1	2	0	0.177
7	7	5	5	2	4	3	1	0.406
8	1	5	5	2	0	3	0	0.441
9	7	5	4	0	2	1	0	0.322
10	1	5	4	0	2	3	0	0.239
11	2	2	0	2	1	3	1	0.044
12	2	6	2	2	1	2	0	0.487
13	1	5	5	2	0	1	1	0.355
14	2	5	5	4	0	3	0	0.222
15	7	1	0	4	2	2	0	0.481
16	6	7	0	4	2	3	0	0.474
17	1	5	5	4	4	3	1	0.289
18	7	5	5	2	1	2	2	0.287
19	1	5	5	2	0	1	0	0.157
20	1	5	5	2	0	3	0	0.202
21	7	5	4	0	2	3	0	0.310
22	7	5	4	0	2	2	0	0.229
23	2	2	0	2	2	3	1	0.490
24	2	2	2	2	1	3	0	0.050

Null Hypothesis Tests

	Position Number							L/D	voltage	v0	Drag 1	Lscale	Rscale	Normal	Drag	Lift
	-1	-2	-3	-4	-5	-6	-7		(volts)	(volts)	(g)	(g)	(g)	(g)	g	g
Most Occurring	4	1	4	3	1	2	0	2.731	12.903	12.162	18.037	45.6	62.6	108.2	40.164	109.682
	4	1	4	3	1	2	0	3.074	12.907	12.363	13.242	45.5	62.8	108.3	35.389	108.778
	4	1	4	3	1	2	0	2.970	12.91	12.312	14.557	45.1	63.1	108.2	36.683	108.954
	4	1	4	3	1	2	0	3.048	12.92	12.363	13.558	45.3	63	108.3	35.705	108.844
	4	1	4	3	1	2	0	2.963	12.915	12.313	14.654	45.1	63.1	108.2	36.780	108.975
	4	1	4	3	1	2	0	3.080	12.916	12.377	13.120	45.2	62.7	107.9	35.185	108.361
	4	1	4	3	1	2	0	3.035	12.921	12.358	13.705	45.2	62.9	108.1	35.811	108.679
	4	1	4	3	1	2	0	2.995	12.921	12.34	14.143	45.4	62.1	107.5	36.126	108.183
	4	1	4	3	1	2	0	2.985	12.918	12.333	14.240	45	62.3	107.3	36.182	108.007
	4	1	4	3	1	2	0	2.992	12.915	12.333	14.167	44.8	62.6	107.4	36.130	108.090
	4	1	4	3	1	2	0	3.017	12.918	12.35	13.826	45	62.3	107.3	35.769	107.921
Zimmerman	7	7	5	5	4	3	2	2.798	13.047	12.121	23.083	65.4	81.5	146.9	53.124	148.618
	7	7	5	5	4	3	2	2.915	13.051	12.22	20.715	64.2	82.3	146.5	50.674	147.732
	7	7	5	5	4	3	2	2.869	13.047	12.179	21.638	64.8	82	146.8	51.658	148.218
	7	7	5	5	4	3	2	2.919	13.024	12.201	20.516	49.2	96.4	145.6	50.290	146.809
	7	7	5	5	4	3	2	2.892	13.038	12.187	21.214	67.4	79.5	146.9	51.254	148.227
	7	7	5	5	4	3	2	2.866	13.037	12.168	21.662	64	82.6	146.6	51.642	148.027
	7	7	5	5	4	3	2	2.896	13.032	12.185	21.114	65	81.8	146.8	51.134	148.109
	7	7	5	5	4	3	2	2.903	13.02	12.18	20.940	64.7	81.7	146.4	50.878	147.681
	7	7	5	5	4	3	2	2.963	13.017	12.226	19.718	65	80.6	145.6	49.493	146.642
	7	7	5	5	4	3	2	2.972	13.012	12.224	19.643	65.2	81.1	146.3	49.561	147.312
Randomized Algorithm	7	5	5	2	4	3	1	2.767	12.855	11.926	22.693	63.9	76.7	140.6	51.445	142.370
	7	5	5	2	4	3	1	2.989	12.86	12.098	18.613	64.4	76.4	140.8	47.406	141.713
	7	5	5	2	4	3	1	3.008	12.869	12.124	18.198	64.2	75.9	140.1	46.848	140.941
	7	5	5	2	4	3	1	2.980	12.873	12.1	18.882	64.6	77	141.6	47.839	142.552
	7	5	5	2	4	3	1	2.996	12.873	12.111	18.613	63.8	77.9	141.7	47.590	142.594
	7	5	5	2	4	3	1	2.994	12.882	12.12	18.613	64.9	76.5	141.4	47.529	142.300
	7	5	5	2	4	3	1	2.825	12.878	11.997	21.520	64.8	75.6	140.4	50.231	141.929
	7	5	5	2	4	3	1	2.952	12.882	12.093	19.273	65.3	75.6	140.9	48.086	141.949
	7	5	5	2	4	3	1	2.953	12.883	12.094	19.273	63.2	77.8	141	48.107	142.047
	7	5	5	2	4	3	1	2.932	12.883	12.081	19.590	65.7	74.9	140.6	48.343	141.721

Appendix F: Angle of Attack Tests with Best Low AoA and Zimmerman Wings

Zimmerman Approximation

	L/D	voltage	v0	Drag 1	Lscale	Rscale	Normal	Drag	Lift	Cl	Date 2008
AoA		(volts)	(volts)	(g)	(g)	(g)	(g)	(g)	(g)		
2	1.395	10.331	9.992	8.879	1.2	11.5	12.7	9.323	13.002	0.042081	27-Jan
4	1.111	11.186	10.083	28.891	10.0	22.7	32.7	31.172	34.641	0.112112	27-Jan
6	2.985	12.176	11.673	13.175	25.0	30.6	55.6	18.987	56.680	0.183441	27-Jan
8	2.980	13.152	12.491	17.314	33.6	51.8	85.4	29.199	87.002	0.281576	27-Jan
10	2.719	14.408	13.514	23.417	48.8	67.3	116.1	43.577	118.465	0.383403	27-Jan
12	2.665	15.272	14.306	25.302	68.7	77.6	146.3	55.720	148.481	0.480548	27-Jan
14	2.358	9.84	8.62	31.955	67.7	100.9	168.6	72.743	171.559	0.555238	27-Jan
16	1.756	10.807	9.591	31.851	43.0	55.0	98.0	58.863	103.337	0.334441	27-Jan

Best Low AoA 7732100 (Day 2007)

	L/D	voltage	v0	Drag 1	Lscale	Rscale	Normal	Drag	Lift	Cl	Date 2008
AoA		(volts)	(volts)	(g)	(g)	(g)	(g)	(g)	(g)		
2	1.344	10.221	9.971	6.548	0.1	8.9	9.0	6.862	9.223	0.02985	27-Jan
4	2.823	11.153	10.821	8.696	9.2	20.7	29.9	10.782	30.435	0.098501	27-Jan
6	3.430	12.134	11.693	11.551	22.7	37.7	60.4	17.865	61.283	0.198338	27-Jan
8	2.845	13.11	12.526	15.297	30.8	38.8	69.6	24.983	71.072	0.23002	27-Jan
10	2.874	14.308	13.577	19.147	44.3	62.0	106.3	37.606	108.061	0.349732	27-Jan
12	2.633	15.236	14.368	22.736	54.8	73.0	127.8	49.307	129.840	0.420216	27-Jan
14	2.425	9.638	8.674	25.250	51.2	92.0	143.2	59.893	145.242	0.470064	27-Jan
16	1.348	10.568	9.641	24.281	21.3	22.4	43.7	36.326	48.970	0.158486	27-Jan

Best Low AoA 6611110 (Present Study)

	L/D	voltage	v0	Drag 1	Lscale	Rscale	Normal	Drag	Lift	Cl	Date 2008
AoA		(volts)	(volts)	(g)	(g)	(g)	(g)	(g)	(g)		
2	1.815	10.219	9.972	6.470	2.5	9.8	12.3	6.899	12.518	0.040515	27-Jan
4	2.984	11.167	10.834	8.722	10.5	21.7	32.2	10.968	32.731	0.105933	27-Jan
6	3.481	12.13	11.702	11.211	22.7	37.3	60.0	17.482	60.850	0.196935	27-Jan
8	2.981	13.091	12.491	15.716	30.0	47.6	77.6	26.516	79.054	0.255851	27-Jan
10	2.917	14.277	13.614	17.366	40.4	59.1	99.5	34.644	101.050	0.327042	27-Jan
12	2.722	15.152	14.413	19.357	49.7	68.1	117.8	43.849	119.340	0.386235	27-Jan
14	2.525	9.586	8.768	21.426	49.0	86.6	135.6	54.230	136.914	0.443112	27-Jan
16	1.049	10.596	9.633	25.224	13.7	14.9	28.6	33.107	34.725	0.112384	27-Jan

Appendix G: Low AoA Genetic Algorithm

Generation #1

	Position Number							Fitness	L/D	voltage	v0	Drag	Lscale	Rscale	Lift	Date 2008
Chromosome #	(1)	(2)	(3)	(4)	(5)	(6)	(7)	Function		(volts)	(volts)	(g)	(g)	(g)	(g)	
1	2	7	1	1	1	0	2	0.55	3.550	10.842	10.435	15.832	20.5	35.7	56.2	22-Dec
2	2	2	2	2	3	3	0	0.33	3.331	10.859	10.464	15.249	17.1	33.7	50.8	21-Dec
3	7	4	2	5	3	0	1	0.24	3.241	10.834	10.449	14.717	15.0	32.7	47.7	21-Dec
4	2	0	5	0	1	1	1	0.30	3.295	10.854	10.476	14.535	16.1	31.8	47.9	21-Dec
5	2	4	4	3	2	2	0	0.36	3.357	10.86	10.464	15.250	16.6	34.6	51.2	20-Dec
6	5	1	2	2	2	3	0	0.45	3.447	10.839	10.466	13.781	15.3	32.2	47.5	21-Dec
7	2	4	0	1	2	1	2	0.44	3.441	10.823	10.42	15.488	18.0	35.3	53.3	22-Dec
8	2	1	5	0	4	2	1	0.11	3.110	10.874	10.48	14.986	14.7	31.9	46.6	21-Dec
9	4	2	5	5	1	3	2	0.23	3.233	10.692	10.298	15.186	17.1	32.0	49.1	20-Dec
10	1	6	5	3	0	1	2	0.22	3.221	10.866	10.466	15.398	16.2	33.4	49.6	21-Dec
11	4	0	2	2	3	1	2	0.31	3.308	10.76	10.392	14.300	15.6	31.7	47.3	20-Dec
12	4	7	2	1	2	2	0	0.42	3.415	10.684	10.267	16.396	19.7	36.3	56.0	20-Dec
13	7	2	5	5	4	2	1	0.12	3.118	10.658	10.252	15.457	16.1	32.1	48.2	20-Dec
14	3	1	0	2	4	2	1	0.15	3.150	10.669	10.295	14.287	14.1	30.9	45.0	20-Dec
15	5	0	0	1	0	0	1	0.38	3.376	10.893	10.551	13.389	14.7	30.5	45.2	20-Dec
16	3	4	5	3	4	0	0	0.30	3.296	10.851	10.45	15.563	17.0	34.3	51.3	20-Dec
17	3	6	4	2	1	0	1	0.41	3.409	10.845	10.453	15.402	18.3	34.2	52.5	20-Dec
18	7	1	5	4	4	0	1	0.11	3.110	10.845	10.446	15.177	14.8	32.4	47.2	20-Dec
19	2	4	2	0	4	2	2	0.25	3.245	10.852	10.46	15.129	15.6	33.5	49.1	20-Dec
20	6	1	4	3	1	0	2	0.23	3.226	10.824	10.457	14.135	14.6	31.0	45.6	20-Dec
21	6	7	3	5	0	3	1	0.21	3.211	10.843	10.434	15.727	15.8	34.7	50.5	20-Dec
22	0	3	5	1	0	2	2	0.14	3.144	10.891	10.492	15.233	14.2	33.7	47.9	20-Dec
23	5	3	2	4	0	0	1	0.26	3.265	10.85	10.477	14.427	14.0	33.1	47.1	20-Dec
24	2	5	1	3	4	1	0	0.28	3.280	10.868	10.458	15.884	15.5	36.6	52.1	20-Dec
25	6	1	3	2	4	1	2	0.11	3.112	10.836	10.456	14.458	13.1	31.9	45.0	20-Dec
26	2	6	2	4	0	0	0	0.33	3.334	10.859	10.465	15.355	15.9	35.3	51.2	20-Dec
27	0	0	0	1	0	2	1	0.34	3.343	10.869	10.484	15.018	16.9	33.3	50.2	20-Dec
28	0	1	5	5	4	1	0	0.05	3.047	10.717	10.267	17.002	16.6	35.2	51.8	20-Dec
29	4	7	1	5	1	1	2	0.30	3.297	10.792	10.377	16.107	17.5	35.6	53.1	20-Dec
30	6	7	3	1	3	2	1	0.39	3.395	10.778	10.359	16.438	19.5	36.3	55.8	20-Dec
31	4	4	2	1	3	1	1	0.31	3.313	10.751	10.355	15.396	17.3	33.7	51.0	20-Dec
32	4	0	0	1	3	1	1	0.19	3.189	10.86	10.502	13.734	13.5	30.3	43.8	20-Dec
33	6	6	3	1	3	2	1	0.43	3.433	10.882	10.482	15.759	18.8	35.3	54.1	20-Dec
34	7	6	2	0	1	1	1	0.48	3.477	10.847	10.467	15.043	18.2	34.1	52.3	20-Dec
35	5	5	3	2	3	2	2	0.46	3.455	10.856	10.45	16.034	19.4	36.0	55.4	20-Dec
36	4	3	1	1	3	2	2	0.37	3.366	10.844	10.468	14.705	16.5	33.0	49.5	20-Dec
37	7	7	5	0	0	0	0	0.36	3.356	10.846	10.476	14.453	15.8	32.7	48.5	20-Dec

38	4	5	1	2	0	2	0	0.38	3.380	10.823	10.443	14.883	17.1	33.2	50.3	20-Dec
39	3	2	5	2	1	1	0	0.27	3.269	10.83	10.46	14.317	14.9	31.9	46.8	20-Dec
40	7	3	4	0	2	3	1	0.17	3.168	10.81	10.448	13.856	13.8	30.1	43.9	20-Dec
41	1	1	4	3	0	2	0	0.23	3.225	10.836	10.46	14.480	15.0	31.7	46.7	20-Dec
42	7	0	1	4	1	1	1	0.20	3.202	10.84	10.488	13.522	13.1	30.2	43.3	20-Dec
43	6	4	0	3	3	2	1	0.36	3.356	10.868	10.492	14.689	16.3	33.0	49.3	20-Dec
44	1	3	4	1	4	0	1	0.26	3.257	10.866	10.478	14.858	15.1	33.3	48.4	20-Dec
45	0	5	0	1	4	2	1	0.28	3.279	10.893	10.497	15.340	16.6	33.7	50.3	21-Dec
46	1	2	3	3	2	3	2	0.31	3.312	10.89	10.49	15.550	17.0	34.5	51.5	21-Dec
47	2	1	4	2	3	1	0	0.36	3.359	10.863	10.476	15.123	17.3	33.5	50.8	21-Dec
48	4	4	3	3	1	0	2	0.50	3.499	10.842	10.464	15.002	18.8	33.7	52.5	21-Dec
49	0	2	2	5	0	0	0	0.27	3.272	10.871	10.496	14.516	15.1	32.4	47.5	21-Dec
50	5	6	4	0	2	1	1	0.35	3.351	10.862	10.466	15.460	17.2	34.6	51.8	21-Dec
51	4	3	4	4	2	0	1	0.33	3.331	10.865	10.472	15.310	16.8	34.2	51.0	21-Dec
52	7	2	1	1	0	3	0	0.18	3.176	10.816	10.47	13.255	13.0	29.1	42.1	21-Dec
53	6	7	4	1	2	0	2	0.39	3.387	10.86	10.466	15.443	18.0	34.3	52.3	21-Dec
54	3	2	3	5	2	3	0	0.26	3.262	10.881	10.487	15.235	16.0	33.7	49.7	21-Dec
55	0	5	3	4	1	3	0	0.33	3.327	10.892	10.489	15.692	17.3	34.9	52.2	21-Dec
56	7	2	5	3	2	1	2	0.26	3.257	10.843	10.472	14.337	15.4	31.3	46.7	21-Dec
57	4	4	4	4	0	2	1	0.32	3.318	10.862	10.48	14.860	16.5	32.8	49.3	21-Dec
58	5	2	0	3	1	1	2	0.25	3.251	10.841	10.485	13.749	14.7	30.0	44.7	21-Dec
59	2	3	3	3	1	2	0	0.38	3.379	10.872	10.482	15.273	17.0	34.6	51.6	21-Dec
60	6	6	0	0	2	3	1	0.39	3.386	10.853	10.471	14.972	17.0	33.7	50.7	21-Dec
61	3	3	0	5	3	3	1	0.33	3.333	10.92	10.518	15.663	18.3	33.9	52.2	21-Dec
62	1	4	3	4	2	0	2	0.30	3.296	10.876	10.475	15.563	17.0	34.3	51.3	21-Dec
63	5	3	4	5	2	0	1	0.27	3.269	10.855	10.47	14.897	15.9	32.8	48.7	21-Dec
64	6	5	4	4	0	2	1	0.31	3.314	10.821	10.433	15.087	17.0	33.0	50.0	21-Dec
65	5	2	1	2	0	0	2	0.32	3.324	10.817	10.463	13.780	15.7	30.1	45.8	21-Dec
66	6	2	4	5	4	0	0	0.11	3.112	10.841	10.45	14.876	14.5	31.8	46.3	21-Dec
67	3	7	3	2	1	1	0	0.17	3.168	10.993	10.607	14.774	10.0	36.8	46.8	21-Dec
68	6	0	0	5	0	0	1	0.20	3.200	10.86	10.506	13.595	13.8	29.7	43.5	21-Dec
69	6	3	5	3	3	1	2	0.12	3.121	10.732	10.334	15.156	15.6	31.7	47.3	21-Dec
70	3	6	1	4	3	1	2	0.26	3.263	10.77	10.346	16.396	18.6	34.9	53.5	21-Dec
71	1	1	4	1	2	1	1	0.23	3.227	10.761	10.366	15.215	16.8	32.3	49.1	21-Dec
72	5	2	5	2	2	0	1	0.17	3.167	10.744	10.357	14.810	15.8	31.1	46.9	21-Dec

Generation #2

Chromosome #	Position Number (1)	(2)	(3)	(4)	(5)	(6)	(7)	Fitness Function	L/D	voltage (volts)	v0 (volts)	Drag (g)	Lscale (g)	Rscale (g)	Lift (g)	Date 2007
1	4	4	2	1	3	1	1	0.37	3.370	10.821	10.428	14.985	15.9	34.6	50.5	22-Dec
2	0	1	5	5	4	1	0	0.39	3.389	10.91	10.486	16.201	21.6	33.3	54.9	22-Dec
3	6	6	3	1	3	2	1	0.54	3.536	10.894	10.484	15.923	19.5	36.8	56.3	22-Dec
4	2	3	3	3	1	2	0	0.08	3.080	10.882	10.491	14.448	10.9	33.6	44.5	22-Dec
5	7	3	4	0	2	3	1	0.31	3.310	10.857	10.487	14.016	14.8	31.6	46.4	22-Dec
6	1	1	4	1	2	1	1	0.45	3.450	10.886	10.501	14.811	17.4	33.7	51.1	22-Dec
7	7	6	2	0	1	1	1	0.59	3.594	10.869	10.491	14.776	18.5	34.6	53.1	22-Dec
8	4	7	1	5	1	1	2	0.40	3.398	10.873	10.479	15.069	17.1	34.1	51.2	22-Dec
9	5	3	4	5	2	0	1	0.33	3.334	10.863	10.476	14.698	15.9	33.1	49.0	22-Dec
10	2	4	2	0	4	2	2	0.35	3.350	10.882	10.492	14.838	16.2	33.5	49.7	22-Dec
11	2	4	2	0	4	2	2	0.34	3.343	10.883	10.492	14.865	16.4	33.3	49.7	22-Dec
12	6	7	4	1	2	0	2	0.46	3.460	10.883	10.483	15.405	18.1	35.2	53.3	22-Dec
13	6	1	4	5	4	1	2	0.20	3.203	10.876	10.475	15.015	15.5	32.6	48.1	22-Dec
14	4	2	2	5	0	1	0	0.26	3.257	10.853	10.491	13.633	14.1	30.3	44.4	22-Dec
15	2	3	3	1	2	2	0	0.54	3.544	10.878	10.497	14.812	18.1	34.4	52.5	22-Dec
16	4	6	3	3	1	2	1	0.62	3.620	10.884	10.486	15.606	20.3	36.2	56.5	22-Dec
17	7	1	4	1	2	3	0	0.24	3.240	10.851	10.484	13.797	14.0	30.7	44.7	22-Dec
18	7	3	4	2	2	3	1	0.34	3.344	10.855	10.479	14.296	15.5	32.3	47.8	22-Dec
19	7	6	2	0	1	1	1	0.51	3.505	10.864	10.48	14.863	17.6	34.5	52.1	22-Dec
20	4	6	1	0	1	1	2	0.61	3.615	10.892	10.503	15.243	19.4	35.7	55.1	22-Dec
21	5	4	4	0	2	1	2	0.51	3.507	10.871	10.488	14.827	16.4	35.6	52.0	22-Dec
22	5	0	4	0	2	2	1	0.25	3.253	10.865	10.491	14.080	14.5	31.3	45.8	22-Dec
23	6	4	4	1	4	2	2	0.36	3.362	10.859	10.471	14.782	16.1	33.6	49.7	22-Dec
24	2	4	2	1	4	2	2	0.35	3.353	10.883	10.488	15.033	16.0	34.4	50.4	22-Dec

Generation #3

Chromosome #	Position Number (1)	(2)	(3)	(4)	(5)	(6)	(7)	Fitness Function	L/D	voltage (volts)	v0 (volts)	Drag (g)	Lscale (g)	Rscale (g)	Lift (g)	Date 2007
1	7	6	2	0	1	1	1	0.46	3.562	10.906	10.529	14.684	18.2	34.1	52.3	28-Dec
2	2	3	3	1	2	2	0	0.37	3.470	10.917	10.535	14.727	17.3	33.8	51.1	28-Dec
3	2	4	2	1	4	2	2	0.23	3.326	10.924	10.531	14.913	16.0	33.6	49.6	28-Dec
4	6	1	4	5	4	1	2	0.02	3.119	10.943	10.549	14.620	14.8	30.8	45.6	28-Dec
5	6	6	3	1	3	2	1	0.28	3.381	10.952	10.553	15.232	18.2	33.3	51.5	28-Dec
6	2	3	3	1	2	2	0	0.35	3.452	10.941	10.563	14.544	16.9	33.3	50.2	28-Dec
7	7	1	4	1	2	3	0	0.13	3.230	10.912	10.55	13.593	13.7	30.2	43.9	28-Dec
8	4	2	2	5	0	1	0	0.14	3.236	10.918	10.552	13.753	14.4	30.1	44.5	28-Dec
9	5	3	4	5	2	0	1	0.17	3.275	10.927	10.541	14.566	15.6	32.1	47.7	28-Dec
10	5	0	4	0	2	2	1	0.17	3.273	10.925	10.559	13.809	14.9	30.3	45.2	28-Dec
11	2	3	3	1	2	2	0	0.39	3.486	10.941	10.56	14.716	17.8	33.5	51.3	28-Dec
12	4	6	3	3	1	2	1	0.45	3.546	10.939	10.543	15.398	19.5	35.1	54.6	28-Dec
13	2	6	3	0	2	1	1	0.36	3.462	10.948	10.552	15.253	18.5	34.3	52.8	28-Dec
14	7	3	3	0	2	1	0	0.20	3.304	10.899	10.544	13.439	14.0	30.4	44.4	28-Dec
15	2	4	2	1	4	1	2	0.18	3.281	10.951	10.553	15.028	15.3	34.0	49.3	28-Dec
16	6	4	2	5	4	1	2	0.19	3.288	10.943	10.535	15.419	16.2	34.5	50.7	28-Dec
17	6	6	1	1	2	2	0	0.29	3.390	10.8	10.404	15.133	17.3	34.0	51.3	28-Dec
18	2	6	3	5	3	2	1	0.25	3.350	10.941	10.511	16.360	18.6	36.2	54.8	28-Dec
19	4	3	4	1	2	1	0	0.25	3.351	10.896	10.514	14.535	15.9	32.8	48.7	28-Dec
20	4	2	3	5	2	1	0	0.11	3.213	10.837	10.446	14.657	15.3	31.8	47.1	28-Dec
21	5	3	4	0	2	2	1	0.12	3.221	10.819	10.445	14.032	14.6	30.6	45.2	28-Dec
22	5	5	4	5	2	0	1	0.19	3.292	10.844	10.435	15.463	16.9	34.0	50.9	28-Dec
23	2	3	3	0	1	2	1	0.28	3.382	10.951	10.577	14.280	16.0	32.3	48.3	28-Dec
24	2	6	3	3	2	2	1	0.36	3.465	10.968	10.553	15.990	19.7	35.7	55.4	28-Dec

Generation #4

Chromosome #	Position Number (1)	(2)	(3)	(4)	(5)	(6)	(7)	Fitness Function	L/D	voltage (volts)	v0 (volts)	Drag (g)	Lscale (g)	Rscale (g)	Lift (g)	Date 2007
1	6	6	1	1	2	2	0	0.25	3.505	10.964	10.59	14.667	17.9	33.5	51.4	31-Dec
2	2	6	3	3	2	2	1	0.19	3.444	11.008	10.604	15.737	19.1	35.1	54.2	31-Dec
3	2	6	3	5	3	2	1	0.11	3.355	11.012	10.594	16.124	18.8	35.3	54.1	31-Dec
4	2	3	3	1	2	2	0	0.17	3.422	10.985	10.612	14.494	16.8	32.8	49.6	31-Dec
5	2	3	3	1	2	2	0	0.17	3.420	10.985	10.611	14.530	16.7	33.0	49.7	31-Dec
6	5	3	4	0	2	2	1	0.00	3.252	10.962	10.604	13.654	14.5	29.9	44.4	31-Dec
7	7	6	2	0	1	1	1	0.24	3.494	10.958	10.6	14.023	17.0	32.0	49.0	31-Dec
8	6	6	1	1	2	2	0	0.23	3.485	10.971	10.597	14.635	17.7	33.3	51.0	31-Dec
9	2	3	3	0	1	2	1	0.13	3.380	10.983	10.612	14.350	16.3	32.2	48.5	31-Dec
10	5	3	4	0	2	2	1	0.06	3.312	10.966	10.605	13.859	15.1	30.8	45.9	31-Dec
11	2	6	3	0	2	1	1	0.15	3.404	10.991	10.61	14.776	17.7	32.6	50.3	31-Dec
12	6	6	1	1	2	2	0	0.29	3.541	10.983	10.618	14.373	17.5	33.4	50.9	31-Dec
13	5	6	1	1	2	3	1	0.26	3.511	11.01	10.629	14.952	18.3	34.2	52.5	31-Dec
14	1	6	1	3	2	2	1	0.18	3.430	11.014	10.625	15.130	18.4	33.5	51.9	31-Dec
15	2	3	3	1	3	2	0	0.13	3.380	10.985	10.611	14.466	16.3	32.6	48.9	31-Dec
16	2	3	3	1	2	2	1	0.21	3.461	10.983	10.615	14.361	17.2	32.5	49.7	31-Dec
17	5	3	4	0	2	2	1	0.09	3.338	10.965	10.604	13.899	15.6	30.8	46.4	31-Dec
18	5	3	4	0	2	2	0	0.07	3.319	10.96	10.604	13.678	14.9	30.5	45.4	31-Dec
19	7	6	1	1	2	2	1	0.27	3.521	10.967	10.599	14.458	17.9	33.0	50.9	31-Dec
20	6	6	1	0	1	2	0	0.40	3.646	11.094	10.736	14.264	18.4	33.6	52.0	31-Dec
21	2	3	3	0	1	2	1	0.10	3.351	10.928	10.558	14.265	15.9	31.9	47.8	31-Dec
22	2	3	0	0	1	2	1	0.23	3.481	11.001	10.636	14.277	16.9	32.8	49.7	31-Dec
23	6	6	4	0	2	3	1	0.07	3.317	10.995	10.612	14.712	16.1	32.7	48.8	31-Dec
24	2	6	3	2	2	1	0	0.19	3.444	11.023	10.628	15.387	18.2	34.8	53.0	31-Dec

Generation #5

Chromosome #	Position Number (1)	(2)	(3)	(4)	(5)	(6)	(7)	Fitness Function	L/D	voltage (volts)	v0 (volts)	Drag (g)	Lscale (g)	Rscale (g)	Lift (g)	Date 2008
1	6	6	1	1	2	2	0	0.42	3.670	10.994	10.625	13.678	16.9	33.3	50.2	1-Jan
2	5	6	1	1	2	3	1	0.42	3.668	10.996	10.612	14.231	17.9	34.3	52.2	1-Jan
3	7	6	2	0	1	1	1	0.38	3.632	10.973	10.609	13.435	16.4	32.4	48.8	1-Jan
4	6	6	1	1	2	2	0	0.44	3.688	10.99	10.614	13.966	17.5	34.0	51.5	1-Jan
5	2	3	0	0	1	2	1	0.40	3.646	10.992	10.627	13.493	16.6	32.6	49.2	1-Jan
6	6	6	1	1	2	2	0	0.41	3.659	10.991	10.613	13.994	17.4	33.8	51.2	1-Jan
7	2	3	3	0	1	2	1	0.30	3.546	10.991	10.623	13.452	15.7	32.0	47.7	1-Jan
8	6	6	1	1	2	2	0	0.42	3.669	10.986	10.611	13.899	17.4	33.6	51.0	1-Jan
9	7	6	1	1	2	2	1	0.38	3.625	10.948	10.574	13.793	17.0	33.0	50.0	1-Jan
10	7	6	1	1	2	2	1	0.41	3.657	10.946	10.581	13.509	16.8	32.6	49.4	1-Jan
11	6	6	4	0	2	3	1	0.24	3.492	10.96	10.577	13.916	16.0	32.6	48.6	1-Jan
12	6	6	1	0	1	2	0	0.43	3.683	10.951	10.586	13.550	17.0	32.9	49.9	1-Jan
13	5	6	1	1	0	1	1	0.48	3.725	10.953	10.586	13.690	17.9	33.1	51.0	1-Jan
14	6	6	1	3	2	3	1	0.36	3.611	10.961	10.579	14.066	17.4	33.4	50.8	1-Jan
15	6	6	2	0	1	2	1	0.42	3.669	10.951	10.584	13.602	17.3	32.6	49.9	1-Jan
16	7	6	1	0	1	1	2	0.42	3.672	10.94	10.583	13.236	16.9	31.7	48.6	1-Jan
17	6	3	0	1	1	1	0	0.37	3.620	10.926	10.594	12.237	14.7	29.6	44.3	1-Jan
18	2	0	0	0	1	0	1	0.33	3.580	10.831	10.474	13.100	16.9	30.0	46.9	1-Jan
19	6	3	1	1	4	2	2	0.00	3.251	10.802	10.443	12.703	12.9	28.4	41.3	1-Jan
20	2	3	1	1	2	2	0	0.63	3.885	10.981	10.649	12.614	17.2	31.8	49.0	1-Jan
21	7	6	1	1	2	2	2	0.44	3.686	10.918	10.544	13.889	17.8	33.4	51.2	1-Jan
22	7	0	1	1	2	2	1	0.23	3.480	10.884	10.549	12.155	14.3	28.0	42.3	1-Jan
23	6	6	4	0	4	3	0	0.15	3.400	10.925	10.539	13.882	15.4	31.8	47.2	1-Jan
24	6	6	4	0	1	3	1	0.25	3.498	10.918	10.543	13.635	16.1	31.6	47.7	1-Jan

Generation #6

Chromosome #	(1)	(2)	(3)	(4)	(5)	(6)	(7)	Fitness Function	L/D	voltage (volts)	v0 (volts)	Drag (g)	Lscale (g)	Rscale (g)	Lift (g)	Date 2008
	Position Number															
1	7	6	1	0	1	1	2	0.16	3.553	10.781	10.415	14.326	18.1	32.8	50.9	3-Jan
2	5	6	1	1	0	1	1	0.17	3.565	10.793	10.428	14.306	17.7	33.3	51.0	3-Jan
3	7	6	1	1	2	2	1	0.19	3.582	10.856	10.48	14.767	18.9	34.0	52.9	3-Jan
4	7	6	1	1	2	2	1	0.18	3.567	10.854	10.475	14.859	19.0	34.0	53.0	3-Jan
5	7	6	1	1	2	2	2	0.18	3.566	10.857	10.48	14.779	18.7	34.0	52.7	3-Jan
6	6	6	1	1	2	2	0	0.21	3.604	10.879	10.502	14.843	19.0	34.5	53.5	3-Jan
7	7	6	1	0	1	1	2	0.17	3.562	10.835	10.461	14.655	19.2	33.0	52.2	3-Jan
8	7	6	1	1	2	2	2	0.17	3.561	10.86	10.483	14.771	18.7	33.9	52.6	3-Jan
9	5	6	1	1	0	1	1	0.18	3.568	10.798	10.427	14.547	18.4	33.5	51.9	3-Jan
10	7	6	1	1	2	2	1	0.13	3.523	10.786	10.412	14.590	18.0	33.4	51.4	3-Jan
11	2	3	1	1	2	2	0	0.14	3.530	10.845	10.472	14.562	18.0	33.4	51.4	3-Jan
12	6	6	1	1	2	2	0	0.11	3.504	10.837	10.458	14.754	18.3	33.4	51.7	3-Jan
13	7	6	1	1	1	1	1	0.22	3.605	10.817	10.45	14.451	19.1	33.0	52.1	3-Jan
14	7	6	1	0	0	1	1	0.12	3.506	10.803	10.447	13.862	17.3	31.3	48.6	3-Jan
15	7	6	5	1	2	2	0	0.04	3.427	10.837	10.456	14.706	16.8	33.6	50.4	3-Jan
16	7	6	1	1	2	2	1	0.18	3.575	10.825	10.45	14.715	18.7	33.9	52.6	3-Jan
17	7	6	1	2	2	1	0	0.40	3.789	10.801	10.457	13.831	19.8	32.6	52.4	3-Jan
18	7	6	1	1	2	2	2	0.16	3.549	10.825	10.452	14.595	18.2	33.6	51.8	3-Jan
19	7	6	1	3	2	2	2	0.14	3.532	10.828	10.451	14.723	18.1	33.9	52.0	3-Jan
20	7	6	1	1	1	1	0	0.25	3.640	10.802	10.442	14.231	18.5	33.3	51.8	3-Jan
21	5	6	1	1	2	1	1	0.20	3.591	10.759	10.375	15.095	19.4	34.8	54.2	3-Jan
22	7	3	3	1	2	1	1	0.01	3.396	10.741	10.385	13.694	15.7	30.8	46.5	3-Jan
23	4	3	1	1	3	2	0	0.08	3.471	10.86	10.499	14.002	16.4	32.2	48.6	3-Jan
24	6	6	1	1	2	2	0	0.23	3.618	10.881	10.506	14.787	19.0	34.5	53.5	3-Jan

Generation #7

	Position Number							Fitness	L/D	voltage	v0	Drag	Lscale	Rscale	Lift	Date 2008
Chromosome #	(1)	(2)	(3)	(4)	(5)	(6)	(7)	Function		(volts)	(volts)	(g)	(g)	(g)	(g)	
1	7	6	1	1	2	2	1	0.31	3.704	10.851	10.49	13.633	18.1	32.4	50.5	4-Jan
2	7	6	1	0	1	1	2	0.35	3.743	10.846	10.491	13.466	18.6	31.8	50.4	4-Jan
3	2	3	1	1	2	2	0	0.37	3.764	10.878	10.523	13.498	18.1	32.7	50.8	4-Jan
4	2	3	1	1	2	2	0	0.33	3.720	10.878	10.517	13.657	18.3	32.5	50.8	4-Jan
5	7	6	1	2	2	1	0	0.45	3.836	10.887	10.526	13.841	19.8	33.3	53.1	4-Jan
6	7	6	1	1	1	1	0	0.48	3.871	10.88	10.527	13.589	19.4	33.2	52.6	4-Jan
7	4	3	1	1	3	2	0	0.20	3.586	10.794	10.437	13.302	16.7	31.0	47.7	4-Jan
8	6	6	1	1	2	2	0	0.21	3.596	10.803	10.434	13.765	18.5	31.0	49.5	4-Jan
9	5	6	1	1	2	1	1	0.39	3.779	10.812	10.434	14.397	20.4	34.0	54.4	4-Jan
10	7	6	1	1	2	2	1	0.22	3.614	10.764	10.388	14.055	18.1	32.7	50.8	4-Jan
11	7	6	1	1	2	2	2	0.20	3.594	10.765	10.392	13.911	17.3	32.7	50.0	4-Jan
12	6	6	1	1	2	2	0	0.25	3.638	10.782	10.405	14.130	18.3	33.1	51.4	4-Jan
13	7	6	1	0	1	1	1	0.24	3.633	10.776	10.413	13.598	17.6	31.8	49.4	4-Jan
14	7	6	1	1	1	1	1	0.32	3.709	10.781	10.415	13.830	18.5	32.8	51.3	4-Jan
15	2	3	2	1	2	0	0	0.31	3.700	10.924	10.561	13.702	17.8	32.9	50.7	4-Jan
16	2	3	1	1	2	2	0	0.37	3.757	10.923	10.558	13.867	18.8	33.3	52.1	4-Jan
17	7	6	1	1	0	1	0	0.37	3.758	10.842	10.494	13.224	18.0	31.7	49.7	4-Jan
18	5	6	2	1	1	1	0	0.20	3.585	10.732	10.336	14.754	19.0	33.9	52.9	4-Jan
19	6	3	1	1	2	2	0	0.23	3.624	10.913	10.576	12.611	15.7	30.0	45.7	4-Jan
20	6	6	1	1	3	3	0	0.07	3.455	10.723	10.325	14.615	17.3	33.2	50.5	4-Jan
21	7	6	1	1	2	1	1	0.26	3.645	10.758	10.385	13.991	18.1	32.9	51.0	4-Jan
22	7	6	1	1	2	1	1	0.24	3.626	10.757	10.382	14.037	18.0	32.9	50.9	4-Jan
23	6	6	1	2	2	2	2	0.25	3.636	10.768	10.379	14.577	19.2	33.8	53.0	4-Jan
24	7	6	1	1	2	2	0	0.22	3.610	10.816	10.446	13.824	17.3	32.6	49.9	4-Jan

Generation #8

	Position Number							Fitness	L/D	voltage	v0	Drag	Lscale	Rscale	Lift	Date 2008
Chromosome #	(1)	(2)	(3)	(4)	(5)	(6)	(7)	Function		(volts)	(volts)	(g)	(g)	(g)	(g)	
1	2	3	2	1	2	0	0	0.24	3.612	10.975	10.618	13.730	17.3	32.3	49.6	4-Jan
2	7	6	1	0	1	1	1	0.22	3.593	10.886	10.527	13.777	18.0	31.5	49.5	4-Jan
3	7	6	1	1	0	1	0	0.25	3.622	10.909	10.559	13.475	17.0	31.8	48.8	4-Jan
4	7	6	1	1	1	1	0	0.30	3.675	10.916	10.557	13.905	18.2	32.9	51.1	4-Jan
5	2	3	1	1	2	2	0	0.25	3.623	10.902	10.535	14.132	18.0	33.2	51.2	4-Jan
6	7	6	1	0	1	1	2	0.28	3.645	10.915	10.554	13.936	18.5	32.3	50.8	4-Jan
7	7	6	1	1	1	1	0	0.21	3.579	10.789	10.428	13.832	17.9	31.6	49.5	4-Jan
8	6	3	1	1	2	2	0	0.08	3.446	10.786	10.437	13.175	15.6	29.8	45.4	4-Jan
9	7	6	1	1	2	2	1	0.17	3.542	10.8	10.43	14.118	17.8	32.2	50.0	4-Jan
10	7	6	1	1	2	2	1	0.17	3.542	10.8	10.43	14.118	17.8	32.2	50.0	4-Jan
11	2	3	1	1	2	2	0	0.28	3.651	10.903	10.54	14.023	18.0	33.2	51.2	4-Jan
12	7	6	1	1	2	2	1	0.17	3.538	10.798	10.429	14.074	17.7	32.1	49.8	4-Jan
13	7	3	3	0	2	0	1	-0.07	3.298	10.775	10.433	12.703	13.9	28.0	41.9	4-Jan
14	2	6	3	1	2	2	1	0.15	3.519	10.888	10.484	15.375	19.5	34.6	54.1	4-Jan
15	7	6	0	1	1	1	0	0.12	3.490	10.783	10.431	13.353	16.0	30.6	46.6	4-Jan
16	7	6	1	1	0	1	0	0.13	3.504	10.784	10.431	13.413	16.2	30.8	47.0	4-Jan
17	7	3	1	0	1	1	2	0.16	3.528	10.882	10.548	12.725	15.9	29.0	44.9	4-Jan
18	2	6	4	1	0	1	2	0.00	3.373	10.91	10.53	14.230	16.0	32.0	48.0	4-Jan
19	6	6	1	1	1	1	0	0.31	3.676	10.909	10.548	13.984	18.6	32.8	51.4	4-Jan
20	6	6	1	1	2	2	0	0.23	3.596	10.918	10.55	14.127	17.7	33.1	50.8	4-Jan
21	7	6	5	3	2	2	1	0.09	3.456	10.907	10.515	14.815	17.8	33.4	51.2	4-Jan
22	7	6	5	1	2	2	1	0.08	3.448	10.898	10.514	14.500	17.2	32.8	50.0	4-Jan
23	7	6	1	1	2	2	1	0.23	3.598	10.899	10.527	14.285	18.4	33.0	51.4	4-Jan
24	2	3	1	1	2	2	1	0.20	3.568	10.899	10.535	13.930	17.0	32.7	49.7	4-Jan

Generation #9

Chromosome #	Position Number (1)	(2)	(3)	(4)	(5)	(6)	(7)	Fitness Function	L/D	voltage (volts)	v0 (volts)	Drag (g)	Lscale (g)	Rscale (g)	Lift (g)	Date 2008
1	7	6	1	1	1	1	0	0.36	3.757	11.039	10.682	13.626	18.4	32.8	51.2	7-Jan
2	6	6	1	1	1	1	0	0.42	3.817	11.048	10.686	13.912	19.3	33.8	53.1	7-Jan
3	2	3	2	1	2	0	0	0.23	3.630	11.071	10.707	13.693	16.9	32.8	49.7	7-Jan
4	7	6	1	1	1	1	0	0.37	3.767	11.033	10.671	13.832	18.9	33.2	52.1	7-Jan
5	2	3	1	1	2	2	0	0.31	3.706	11.06	10.691	14.002	18.4	33.5	51.9	7-Jan
6	7	6	1	1	0	1	0	0.33	3.730	11.038	10.68	13.621	18.2	32.6	50.8	7-Jan
7	7	6	1	1	0	1	0	0.35	3.744	11.038	10.682	13.568	18.2	32.6	50.8	7-Jan
8	7	6	1	1	2	2	1	0.27	3.667	11.04	10.674	13.826	17.8	32.9	50.7	7-Jan
9	6	6	1	1	1	1	0	0.42	3.815	11.045	10.682	13.947	19.3	33.9	53.2	7-Jan
10	7	6	1	1	1	1	0	0.56	3.960	11.0029	10.672	12.930	18.5	32.7	51.2	7-Jan
11	2	3	1	1	2	2	0	0.28	3.671	11.066	10.702	13.757	17.6	32.9	50.5	7-Jan
12	6	6	1	1	1	1	0	0.44	3.830	11.027	10.658	14.203	20.2	34.2	54.4	7-Jan
13	6	6	1	1	1	3	0	0.31	3.708	11.031	10.658	14.157	18.7	33.8	52.5	7-Jan
14	7	6	1	1	1	1	0	0.42	3.811	10.993	10.633	13.827	19.5	33.2	52.7	7-Jan
15	2	3	2	1	1	0	0	0.29	3.681	11.03	10.666	13.773	17.7	33.0	50.7	7-Jan
16	2	3	2	1	2	0	0	0.20	3.598	11.023	10.656	13.757	16.9	32.6	49.5	7-Jan
17	4	7	1	5	2	2	0	0.00	3.399	11.017	10.631	14.151	15.7	32.4	48.1	7-Jan
18	1	6	1	3	2	1	0	0.20	3.591	11.083	10.703	14.232	18.1	33.0	51.1	7-Jan
19	7	6	5	1	2	2	1	0.08	3.471	11.03	10.655	13.858	16.1	32.0	48.1	7-Jan
20	7	6	1	1	2	1	1	0.29	3.683	11.03	10.667	13.738	17.9	32.7	50.6	7-Jan
21	7	6	1	1	1	3	0	0.25	3.645	11.032	10.665	13.829	17.7	32.7	50.4	7-Jan
22	2	6	1	1	1	1	0	0.32	3.716	11.066	10.692	14.208	19.1	33.7	52.8	7-Jan
23	2	6	1	1	2	1	2	0.26	3.653	11.081	10.7	14.371	18.9	33.6	52.5	7-Jan
24	2	6	1	1	2	2	0	0.23	3.625	11.079	10.699	14.288	18.3	33.5	51.8	7-Jan

Generation #10

	Position Number							Fitness	L/D	voltage	v0	Drag	Lscale	Rscale	Lift	Date 2008
Chromosome #	(1)	(2)	(3)	(4)	(5)	(6)	(7)	Function		(volts)	(volts)	(g)	(g)	(g)	(g)	
1	7	6	1	1	1	1	0	0.32	3.705	11.048	10.693	13.683	18.0	32.7	50.7	8-Jan
2	2	3	1	1	2	2	0	0.30	3.686	11.077	10.713	13.999	18.2	33.4	51.6	8-Jan
3	7	6	1	1	2	1	1	0.36	3.751	11.059	10.693	14.182	19.5	33.7	53.2	8-Jan
4	6	6	1	1	1	1	0	0.39	3.782	11.062	10.703	13.960	19.3	33.5	52.8	8-Jan
5	6	6	1	1	1	1	0	0.41	3.804	11.062	10.706	13.879	19.3	33.5	52.8	8-Jan
6	6	6	1	1	1	1	0	0.42	3.809	11.063	10.707	13.887	19.3	33.6	52.9	8-Jan
7	2	3	2	1	2	0	0	0.07	3.456	10.94	10.564	14.092	16.5	32.2	48.7	8-Jan
8	2	6	1	1	2	1	2	0.16	3.549	10.952	10.554	15.073	19.5	34.0	53.5	8-Jan
9	2	3	2	1	2	0	0	0.11	3.498	10.944	10.572	14.008	16.6	32.4	49.0	8-Jan
10	2	6	1	1	2	1	2	0.19	3.581	10.973	10.574	15.164	19.9	34.4	54.3	8-Jan
11	2	3	2	1	2	0	0	0.12	3.512	10.951	10.581	13.953	16.9	32.1	49.0	8-Jan
12	7	6	1	1	0	1	0	0.26	3.645	10.99	10.631	13.744	17.9	32.2	50.1	8-Jan
13	2	6	1	1	1	1	0	0.26	3.655	11.03	10.653	14.448	19.0	33.8	52.8	8-Jan
14	2	6	1	2	2	1	0	0.21	3.601	11.033	10.651	14.551	18.7	33.7	52.4	8-Jan
15	6	6	4	1	2	1	1	0.16	3.545	11.02	10.637	14.498	18.1	33.3	51.4	8-Jan
16	6	6	1	1	1	1	1	0.32	3.710	11.016	10.647	14.231	19.4	33.4	52.8	8-Jan
17	6	7	1	5	1	1	0	-0.04	3.353	11.001	10.63	13.748	15.0	31.1	46.1	8-Jan
18	0	6	1	1	1	1	0	0.23	3.621	11.059	10.68	14.470	18.8	33.6	52.4	8-Jan
19	2	3	1	1	2	0	2	0.18	3.568	11.046	10.679	13.928	17.3	32.4	49.7	8-Jan
20	2	5	2	5	2	1	0	0.18	3.574	11.052	10.663	14.773	18.5	34.3	52.8	8-Jan
21	2	0	1	1	2	0	1	0.00	3.391	11.046	10.691	13.210	14.8	30.0	44.8	8-Jan
22	2	3	2	1	2	3	2	0.18	3.566	11.062	10.688	14.190	17.6	33.0	50.6	8-Jan
23	2	6	2	1	2	0	0	0.20	3.594	11.064	10.681	14.578	18.5	33.9	52.4	8-Jan
24	7	6	2	1	2	0	0	0.23	3.620	11.034	10.67	13.895	17.6	32.7	50.3	8-Jan

Generation #11

Chromosome #	(1)	(2)	(3)	(4)	(5)	(6)	(7)	Fitness Function	L/D	voltage (volts)	v0 (volts)	Drag (g)	Lscale (g)	Rscale (g)	Lift (g)	Date 2008
	Position Number															
1	2	3	2	1	2	0	0	0.15	3.542	11.035	10.664	14.229	17.5	32.9	50.4	10-Jan
2	6	6	1	1	1	1	1	0.29	3.676	11.023	10.65	14.525	19.5	33.9	53.4	10-Jan
3	2	3	2	1	2	0	0	0.13	3.524	11.086	10.722	13.933	16.8	32.3	49.1	10-Jan
4	7	6	1	1	0	1	0	0.18	3.573	11.034	10.685	13.433	16.7	31.3	48.0	10-Jan
5	6	6	1	1	1	1	0	0.26	3.652	11.048	10.687	14.019	18.4	32.8	51.2	10-Jan
6	6	6	1	1	1	1	0	0.28	3.674	11.049	10.691	13.937	18.4	32.8	51.2	10-Jan
7	2	6	1	1	1	1	0	0.23	3.619	11.13	10.755	14.508	18.9	33.6	52.5	10-Jan
8	2	6	1	1	2	1	2	0.17	3.559	11.135	10.757	14.526	18.4	33.3	51.7	10-Jan
9	6	6	1	1	1	1	0	0.26	3.654	11.077	10.712	14.177	18.9	32.9	51.8	10-Jan
10	2	6	1	1	2	1	2	0.11	3.505	11.069	10.685	14.666	18.2	33.2	51.4	10-Jan
11	6	6	1	1	1	1	0	0.27	3.656	11.055	10.691	14.141	18.7	33.0	51.7	10-Jan
12	7	6	2	1	2	0	0	0.15	3.539	11.027	10.66	14.071	17.6	32.2	49.8	10-Jan
13	6	6	1	1	2	0	0	0.17	3.555	11.029	10.668	13.867	17.2	32.1	49.3	10-Jan
14	1	6	1	1	0	1	1	0.11	3.500	11.089	10.708	14.544	18.1	32.8	50.9	10-Jan
15	2	6	1	5	0	0	0	-0.06	3.335	11.08	10.704	14.094	15.3	31.7	47.0	10-Jan
16	7	3	1	1	2	0	2	0.05	3.439	11.056	10.717	12.853	15.2	29.0	44.2	10-Jan
17	6	6	1	1	3	1	0	0.09	3.476	11.054	10.683	14.125	16.8	32.3	49.1	10-Jan
18	6	6	1	2	1	2	0	0.20	3.594	11.054	10.689	14.081	18.0	32.6	50.6	10-Jan
19	2	6	5	1	1	1	0	0.06	3.448	11.125	10.746	14.385	16.7	32.9	49.6	10-Jan
20	2	6	1	1	2	1	0	0.20	3.589	11.104	10.721	14.767	19.0	34.0	53.0	10-Jan
21	2	6	1	1	1	1	0	0.28	3.667	11.101	10.721	14.781	19.8	34.4	54.2	10-Jan
22	6	6	1	1	1	1	2	0.21	3.603	11.034	10.661	14.405	19.1	32.8	51.9	10-Jan
23	6	6	1	1	1	0	1	0.28	3.674	11.034	10.669	14.209	19.3	32.9	52.2	10-Jan
24	7	6	0	1	2	3	0	0.04	3.431	11.023	10.653	14.017	16.6	31.5	48.1	10-Jan

Appendix H: High AoA Genetic Algorithm

Generation #1

	Position Number							Fitness	L/D	voltage	v0	Drag 1	Lscale	Rscale	Normal	Drag	Lift	Date 2008
Chromosome #	-1	-2	-3	-4	-5	-6	-7	Function		(volts)	(volts)	(g)	(g)	(g)	(g)	g	g	
1	6	1	4	0	1	1	0	0.282	2.573	15.016	14.168	21.325	49	62.4	111.4	44.106	113.501	Sept 28
2	4	5	2	4	4	0	1	0.000	2.292	15.08	14.135	23.764	45.8	51.2	97	43.600	99.915	Sept 28
3	0	5	4	1	1	0	0	0.246	2.537	15.045	14.191	21.476	45.8	62.9	108.7	43.704	110.889	Sept 28
4	4	6	3	5	0	3	2	0.111	2.402	15.085	14.141	23.739	50.1	56.7	106.8	45.579	109.502	Sept 28
5	5	4	2	2	3	3	2	0.091	2.383	15.055	14.054	25.172	50.5	60.8	111.3	47.933	114.207	Sept 28
6	2	6	0	3	1	0	0	0.343	2.635	15.055	14.239	20.520	50	63.1	113.1	43.648	114.997	Sept 28
7	3	3	4	1	2	0	2	0.341	2.633	14.975	14.151	20.721	48.3	65.7	114	44.034	115.920	Sept 28
8	0	3	3	1	2	0	2	0.339	2.631	15.14	14.417	18.181	39.9	60	99.9	38.610	101.587	Sept 28
9	3	4	3	1	2	0	1	0.306	2.598	15.135	14.337	20.067	43.1	64	107.1	41.969	109.029	Sept 28
10	3	1	4	5	3	0	0	0.244	2.535	15.129	14.275	21.476	44.9	63.6	108.5	43.663	110.694	Sept 28
11	0	7	2	3	4	0	2	0.188	2.479	15.27	14.236	26.002	54.1	71	125.1	51.584	127.888	Sept 28
12	0	2	2	2	2	2	1	0.360	2.652	15.105	14.339	19.263	45	62.8	107.8	41.307	109.546	Sept 28
13	4	0	3	2	1	2	2	0.384	2.675	15.11	14.324	19.766	46.8	66.1	112.9	42.853	114.643	Sept 28
14	5	6	3	1	3	2	1	0.145	2.437	15.157	14.199	24.091	45.7	66	111.7	46.933	114.372	Sept 28
15	1	2	5	2	3	3	2	0.145	2.437	15.195	14.273	23.186	44.3	63.2	107.5	45.169	110.072	Sept 28
16	3	7	2	0	4	2	1	0.167	2.459	15.17	14.169	25.172	51.7	67.3	119	49.507	121.744	Sept 28
17	1	2	2	3	3	3	1	0.299	2.590	15.077	14.261	20.520	45.5	63.3	108.8	42.769	110.788	Sept 28
18	4	5	5	1	4	1	2	0.272	2.564	15.218	14.277	23.663	51.5	71.1	122.6	48.735	124.953	Sept 28
19	5	6	0	0	0	1	0	0.307	2.599	15.138	14.246	22.431	53	66.8	119.8	46.930	121.954	Sept 28
20	7	1	4	0	1	0	2	0.277	2.569	15.15	14.173	24.569	58.2	69.6	127.8	50.703	130.232	Sept 28
21	5	1	5	2	3	3	2	0.316	2.607	15.166	14.24	23.286	56	69.3	125.3	48.909	127.517	Sept 28
22	4	3	4	4	0	3	1	0.334	2.626	15.099	14.204	22.507	55.3	67.8	123.1	47.680	125.200	Sept 28
23	1	7	3	5	1	1	2	0.368	2.659	15.307	14.413	23.417	57.3	74.6	131.9	50.390	134.005	Sept 30
24	5	1	1	0	1	1	0	0.592	2.884	15.083	14.502	15.218	42.6	62	104.6	36.608	105.569	Sept 30
25	4	1	5	4	3	3	0	0.500	2.792	15.205	14.455	19.645	53.7	70.7	124.4	45.084	125.875	Sept 30
26	0	3	1	1	4	3	0	0.346	2.638	15.092	14.326	20.064	46.6	64.3	110.9	42.742	112.748	Sept 30
27	3	5	5	4	1	2	2	0.260	2.551	15.3	14.289	26.481	58.5	77.2	135.7	54.231	138.364	Sept 30
28	6	0	1	4	0	3	0	0.380	2.672	15.146	14.347	20.928	51.6	67.6	119.2	45.304	121.053	Sept 30
29	1	4	0	5	2	1	0	0.326	2.617	15.074	14.275	20.928	48.6	65	113.6	44.159	115.571	Sept 30
30	7	3	0	2	4	0	1	0.317	2.609	15.239	14.317	24.150	56	74.1	130.1	50.755	132.396	Sept 30
31	0	6	1	2	3	0	2	0.370	2.661	15.278	14.435	22.081	52.4	72.2	124.6	47.561	126.580	Sept 30
32	4	4	2	0	4	2	2	0.462	2.754	15.197	14.436	19.933	51.5	70.5	122	44.881	123.586	Sept 30
33	2	3	5	3	4	1	2	0.208	2.499	15.231	14.258	25.486	54.4	70.4	124.8	51.007	127.487	Sept 30
34	0	4	4	5	3	3	2	0.172	2.464	15.294	14.268	26.874	55	72.6	127.6	52.968	130.518	Sept 30
35	2	4	2	5	4	1	2	0.398	2.689	15.221	14.432	20.666	50.8	68.7	119.5	45.104	121.292	Sept 30
36	1	5	3	1	4	3	1	0.620	2.912	14.956	14.28	17.706	58.2	66.6	124.8	43.228	125.862	Sept 30
37	7	2	4	3	4	3	0	0.487	2.779	15.223	14.555	17.497	46.5	63	109.5	39.889	110.841	Sept 30

38	4	3	2	5	3	0	2	0.201	2.493	15.22	14.389	21.766	42.9	63.1	106	43.443	108.307	Sept 30
39	3	0	3	5	2	3	2	0.339	2.631	15.211	14.45	19.933	45.1	64.4	109.5	42.325	111.350	Sept 30
40	7	4	2	0	3	2	1	0.366	2.658	15.244	14.458	20.588	49.6	66.2	115.8	44.268	117.654	Sept 30
41	2	1	5	5	0	1	2	0.571	2.863	15.232	14.592	16.764	47.7	65.4	113.1	39.892	114.212	Sept 30
42	7	5	0	0	4	3	1	0.270	2.561	15.177	14.341	21.897	48.5	64.7	113.2	45.046	115.382	Sept 30
43	4	7	0	5	3	3	0	0.076	2.367	15.58	14.389	31.196	69.4	66.7	136.1	59.028	139.741	Sept 30
44	6	2	0	5	2	2	1	0.500	2.791	15.217	14.484	19.199	52.2	69.3	121.5	44.046	122.943	Sept 30
45	0	3	2	3	1	3	0	0.188	2.479	14.93	14.136	19.515	36.2	57.7	93.9	38.717	95.993	Oct 7
46	6	0	1	4	3	1	0	0.642	2.934	15.023	14.416	14.919	44.1	63.2	107.3	36.861	108.149	Oct 7
47	7	1	1	5	1	2	1	0.319	2.611	15.088	14.186	22.169	51.3	68.4	119.7	46.648	121.802	Oct 7
48	3	0	2	5	4	3	0	0.511	2.803	14.921	14.247	16.566	45	60.9	105.9	38.222	107.123	Oct 7
49	7	5	3	3	2	0	1	0.356	2.648	15.155	14.21	23.226	55.7	73.8	129.5	49.708	131.616	Oct 7
50	5	7	2	3	3	3	0	0.477	2.769	14.98	14.097	21.702	59.3	75.3	134.6	49.228	136.289	Oct 7
51	3	3	5	1	2	1	0	0.459	2.751	11.28	10.622	16.853	48.1	54.8	102.9	37.896	104.246	Oct 7
52	7	7	2	1	4	1	0	0.439	2.731	15.016	14.101	22.489	59.6	75.3	134.9	50.075	136.747	Oct 7
53	1	0	5	3	1	1	2	0.503	2.795	14.75	14.115	15.607	41.5	57.6	99.1	35.873	100.266	Oct 7
54	1	0	3	5	4	1	0	0.273	2.564	14.748	13.97	19.122	40.9	58.2	99.1	39.387	101.000	Oct 7
55	4	2	3	1	4	2	0	0.415	2.706	14.735	13.965	18.925	47.9	63.2	111.1	41.645	112.706	Oct 7
56	6	6	5	3	4	2	2	0.413	2.705	14.948	14.024	22.710	59.6	73.5	133.1	49.928	135.032	Oct 7
57	7	3	5	5	0	0	0	0.491	2.783	14.875	14.035	20.646	57	72.7	129.7	47.169	131.272	Oct 7
58	4	4	4	0	1	3	1	0.489	2.781	14.792	14.071	17.721	46.3	64.8	111.1	40.440	112.454	Oct 7
59	0	6	2	4	2	1	2	0.403	2.695	14.937	14.066	21.407	54.9	69.5	124.4	46.847	126.243	Oct 7
60	4	7	1	3	0	0	0	0.377	2.669	14.864	14.002	21.186	51.8	68.5	120.3	45.787	122.184	Oct 7
61	0	5	4	5	3	0	1	0.453	2.745	14.855	14.079	19.073	47.8	68	115.8	42.753	117.337	Oct 7
62	4	2	4	0	3	2	2	0.349	2.640	14.785	13.969	20.056	46.5	64.6	111.1	42.775	112.942	Oct 7
63	7	6	4	3	1	2	0	0.493	2.784	14.873	14.001	21.432	60	74.8	134.8	48.998	136.429	Oct 7
64	5	6	5	3	0	3	1	0.529	2.821	14.889	14.045	20.744	61.8	73	134.8	48.310	136.285	Oct 7
65	2	5	2	1	0	2	1	0.211	2.503	14.812	13.909	22.194	45.2	63.8	109	44.484	111.333	Oct 7
66	7	3	2	1	3	2	1	0.465	2.756	14.868	14.053	20.031	53.4	69.5	122.9	45.164	124.488	Oct 7
67	1	0	3	2	1	3	2	0.334	2.626	14.815	14.109	17.352	38.7	56.2	94.9	36.759	96.520	Oct 7
68	3	6	3	3	1	0	2	0.400	2.692	14.91	14.066	20.744	51.7	68.5	120.2	45.324	121.993	Oct 7
69	2	7	2	0	3	1	2	0.670	2.962	14.918	14.28	15.681	49.7	66	115.7	39.341	116.531	Oct 7
70	4	6	5	2	2	2	1	0.335	2.627	14.922	13.985	23.030	55.1	71	126.1	48.817	128.246	Oct 7
71	1	5	1	5	0	3	0	0.432	2.723	14.809	14.064	18.311	46.6	62.5	109.1	40.621	110.620	Oct 7
72	3	7	1	3	0	2	1	0.447	2.738	14.905	14.114	19.441	50.6	66.8	117.4	43.449	118.981	Oct 7

Generation #2

Chromosome #	Position Number -1	-2	-3	-4	-5	-6	-7	Fitness Function	L/D	voltage (volts)	v0 (volts)	Drag 1 (g)	Lscale (g)	Rscale (g)	Normal (g)	Drag (g)	Lift (g)	Date 2008
1	3	0	3	5	2	3	2	0.035	2.622	15.941	15.222	18.240	46.1	53.3	99.4	38.567	101.110	Oct 22
2	1	7	3	5	1	1	2	0.035	2.622	16.043	15.168	22.198	58.4	62.6	121	46.942	123.080	Oct 22
3	1	5	3	1	4	3	1	0.016	2.602	15.994	15.151	21.386	54.1	60.5	114.6	44.821	116.646	Oct 22
4	6	2	0	5	2	2	1	0.057	2.644	15.984	15.188	20.194	54	58.2	112.2	43.138	114.048	Oct 22
5	7	2	4	3	4	3	0	0.186	2.772	16.025	15.213	20.600	63.1	65.1	128.2	46.816	129.794	Oct 22
6	1	5	1	5	0	3	0	0.186	2.773	15.864	15.162	17.809	53.4	57.5	110.9	40.488	112.277	Oct 22
7	2	7	2	0	3	1	2	0.041	2.627	16.01	15.17	21.310	55.4	61.3	116.7	45.175	118.686	Oct 22
8	4	0	3	2	1	2	2	0.106	2.693	15.982	15.302	17.251	46.3	53.8	100.1	37.721	101.589	Oct 22
9	2	6	0	3	1	0	0	0.129	2.716	15.95	15.226	18.367	50.7	58	108.7	40.596	110.240	Oct 22
10	2	7	2	0	3	1	2	0.000	2.587	16.018	15.167	21.589	53.9	60.2	114.1	44.922	116.199	Oct 22
11	7	6	4	3	1	2	0	0.271	2.857	16.016	15.269	18.951	62.2	65	127.2	44.963	128.471	Oct 22
12	0	5	4	5	3	0	1	0.044	2.631	16.008	15.206	20.346	51.9	59.9	111.8	43.209	113.688	Oct 22
13	4	7	3	2	2	3	2	0.202	2.789	16.055	15.276	19.762	60.6	64.2	124.8	45.284	126.291	Oct 22
14	1	0	3	5	2	3	2	0.093	2.680	15.89	15.206	17.352	47	52.5	99.5	37.700	101.022	Oct 22
15	6	6	1	5	2	1	1	0.002	2.589	16.022	15.092	23.593	60.3	64.6	124.9	49.135	127.189	Oct 22
16	1	2	3	1	4	2	1	0.079	2.665	15.991	15.29	17.784	46.4	54.3	100.7	38.376	102.287	Oct 22
17	7	5	4	5	0	3	1	0.111	2.697	16.065	15.173	22.629	64.5	67.3	131.8	49.582	133.742	Oct 22
18	7	2	4	3	2	3	2	0.076	2.663	16.024	15.151	22.147	60.3	64.8	125.1	47.730	127.083	Oct 22
19	2	0	2	2	4	1	2	0.137	2.723	15.877	15.271	15.374	41.1	50.5	91.6	34.105	92.876	Oct 22
20	4	1	2	2	1	2	0	0.245	2.832	15.855	15.27	14.841	44.9	52.5	97.4	34.759	98.442	Oct 22
21	7	7	2	3	1	0	1	0.211	2.797	16.01	15.217	20.118	62.9	65.1	128	46.293	129.498	Oct 22
22	2	6	2	3	3	0	2	0.098	2.684	15.98	15.207	19.610	52.5	60.4	112.9	42.698	114.611	Oct 22
23	7	5	4	5	3	0	1	0.083	2.670	16.065	15.169	22.731	62.4	66.8	129.2	49.152	131.218	Oct 22
24	2	5	4	5	1	2	0	0.214	2.801	15.959	15.268	17.530	52.5	59.4	111.9	40.413	113.197	Oct 22

Generation #3

Chromosome #	Position Number -1	-2	-3	-4	-5	-6	-7	Fitness Function	L/D	voltage (volts)	v0 (volts)	Drag 1 (g)	Lscale (g)	Rscale (g)	Normal (g)	Drag (g)	Lift (g)	Date 2008
1	2	6	2	3	3	0	2	0.227215	2.69099	16.005	15.301	20.271	55.2	62.2	117.4	44.279	119.154	Oct 23
2	2	6	2	3	3	0	2	0.107393	2.57117	16.011	15.227	22.5745	55.4	62.3	117.7	46.644	119.929	Oct 23
3	2	5	4	5	1	2	0	0.169747	2.63352	15.981	15.221	21.8834	58	62.5	120.5	46.525	122.525	Oct 23
4	1	0	3	5	2	3	2	0.055571	2.51935	16.012	15.299	20.5301	48.4	53.9	102.3	41.450	104.427	Oct 23
5	2	6	0	3	1	0	0	0.075027	2.5388	15.949	15.198	21.6243	51.2	58.4	109.6	44.037	111.801	Oct 23
6	7	6	4	3	1	2	0	0.146254	2.61003	16.052	15.197	24.6189	65.5	67.3	132.8	51.776	135.137	Oct 23
7	1	5	1	5	0	3	0	0.294086	2.75786	15.952	15.32	18.1978	52.8	59	111.8	41.060	113.239	Oct 23
8	2	5	4	5	1	2	0	0.047073	2.51085	15.955	15.144	23.3519	54.8	60.7	115.5	46.971	117.938	Oct 23
9	4	1	2	2	1	2	0	0.263458	2.72723	15.892	15.317	16.5566	45.6	53.4	99	36.802	100.367	Oct 23
10	4	7	3	2	2	3	2	0	2.46378	16.076	15.149	26.692	61.4	65.3	126.7	52.602	129.599	Oct 23
11	6	2	0	5	2	2	1	0.155084	2.61886	15.979	15.259	20.7317	53.9	58.8	112.7	43.778	114.649	Oct 23
12	4	7	3	2	2	3	2	0.11323	2.57701	16.076	15.239	24.1006	61.4	64.9	126.3	49.928	128.666	Oct 23
13	2	6	2	1	3	0	2	0.16427	2.62805	16.022	15.297	20.8756	53.9	60.5	114.4	44.270	116.344	Oct 23
14	2	3	2	3	3	0	2	0.209025	2.6728	15.936	15.309	18.0538	46.8	56.1	102.9	39.096	104.497	Oct 23
15	1	5	3	5	2	3	0	0.236678	2.70045	16	15.284	20.6165	57.9	62.5	120.4	45.238	122.163	Oct 23
16	6	5	4	5	2	2	2	0.144105	2.60788	16.074	15.229	24.3309	63.8	67.2	131	51.120	133.315	Oct 23
17	7	6	4	3	1	2	0	0.023839	2.48761	16.054	15.111	27.1527	64.4	67.2	131.6	54.064	134.491	Oct 23
18	2	6	0	3	1	2	0	0.326885	2.79066	15.916	15.312	17.3916	51.5	58.5	110	39.886	111.309	Oct 23
19	1	5	1	5	0	1	2	0.104336	2.56811	15.939	15.207	21.0772	50.9	58.7	109.6	43.490	111.687	Oct 23
20	1	5	1	5	1	3	1	0.156698	2.62047	15.962	15.236	20.9044	53.7	60.1	113.8	44.176	115.762	Oct 23
21	4	7	2	2	2	3	1	0.049031	2.51281	16.024	15.152	25.1084	60	64.4	124.4	50.548	127.017	Oct 23
22	4	2	3	2	2	2	1	0.146912	2.61069	15.919	15.226	19.9542	49.7	58	107.7	41.978	109.593	Oct 23
23	6	7	3	4	2	2	2	0.131709	2.59548	16.045	15.166	25.3099	66	68.8	134.8	52.876	137.239	Oct 23
24	5	1	3	2	2	3	1	0.089318	2.55309	15.908	15.167	21.3364	51.2	58.3	109.5	43.729	111.643	Oct 23

Generation #4

	Position Number							Fitness	L/D	voltage	v0	Drag 1	Lscale	Rscale	Normal	Drag	Lift	Date 2008
Chromosome #	-1	-2	-3	-4	-5	-6	-7	Function		(volts)	(volts)	(g)	(g)	(g)	(g)	(g)	(g)	
1	2	6	2	1	3	0	2	0.124	2.738	15.903	15.132	19.287	54.8	61.6	116.4	43.090	117.969	Oct 24
2	4	1	2	2	1	2	0	0.062	2.676	15.763	15.077	17.160	44.6	53.5	98.1	37.221	99.612	Oct 24
3	4	2	3	2	2	2	1	0.000	2.614	15.817	15.0247	19.819	49.7	57.6	107.3	41.762	109.173	Oct 24
4	1	0	3	5	2	3	2	0.242	2.856	15.859	15.252	15.184	48.1	53.7	101.8	36.002	102.821	Oct 24
5	4	1	2	2	1	2	0	0.185	2.799	15.77	15.144	15.659	45.8	54	99.8	36.068	100.962	Oct 24
6	1	0	3	5	2	3	2	0.215	2.829	15.875	15.261	15.359	47.1	53.4	100.5	35.911	101.585	Oct 24
7	1	5	1	5	1	3	1	0.207	2.821	15.926	15.221	17.636	54.1	60.5	114.6	41.071	115.862	Oct 24
8	4	1	2	2	1	2	0	0.115	2.729	15.871	15.217	16.360	44.1	53.9	98	36.400	99.347	Oct 24
9	6	5	4	5	2	2	2	0.047	2.661	16.055	15.133	23.064	63.1	67	130.1	49.669	132.169	Oct 24
10	7	6	4	3	1	2	0	0.189	2.804	15.988	15.172	20.412	63.5	67.1	130.6	47.119	132.104	Oct 24
11	4	1	2	2	1	2	0	0.174	2.788	15.83	15.202	15.709	45.4	53.7	99.1	35.975	100.288	Oct 24
12	1	5	3	5	2	3	0	0.052	2.666	15.953	15.115	20.963	56.7	62.1	118.8	45.257	120.669	Oct 24
13	4	6	2	3	3	0	2	0.103	2.718	15.985	15.182	20.087	55.9	63.2	119.1	44.443	120.780	Oct 24
14	2	0	2	2	1	2	0	0.065	2.679	15.843	15.207	15.910	40.6	50.6	91.2	34.560	92.596	Oct 24
15	1	2	3	5	2	3	1	0.125	2.739	15.938	15.231	17.686	50.2	56.7	106.9	39.546	108.336	Oct 24
16	1	2	3	5	2	1	1	0.127	2.742	15.914	15.242	16.810	46.8	55	101.8	37.628	103.161	Oct 24
17	4	0	2	5	1	2	0	0.299	2.913	15.889	15.301	14.709	48.7	55.1	103.8	35.936	104.679	Oct 24
18	1	0	3	2	2	2	2	0.029	2.643	15.96	15.282	16.960	42.7	51.5	94.2	36.224	95.752	Oct 24
19	1	3	1	2	1	3	1	0.162	2.776	15.92	15.287	15.834	45	53.9	98.9	36.059	100.118	Oct 24
20	4	1	5	5	4	2	0	0.011	2.625	16.008	15.158	21.263	55.5	60.7	116.2	45.025	118.186	Oct 24
21	7	6	5	5	0	2	2	0.259	2.873	16.097	15.285	20.312	68.5	69.8	138.3	48.594	139.621	Oct 24
22	7	1	4	3	1	2	2	0.132	2.746	16.006	15.213	19.837	58.1	62.5	120.6	44.499	122.196	Oct 24
23	1	1	3	5	2	3	0	0.152	2.766	15.883	15.228	16.385	47.4	54	101.4	37.121	102.680	Oct 24
24	4	3	3	5	2	2	0	0.182	2.796	15.912	15.201	17.786	53.3	59.7	113	40.894	114.328	Oct 24

Generation #5

Chromosome #	Position Number -1	-2	-3	-4	-5	-6	-7	Fitness Function	L/D	voltage (volts)	v0 (volts)	Drag 1 (g)	Lscale (g)	Rscale (g)	Normal (g)	Drag (g)	Lift (g)	Date 2008
1	1	1	3	5	2	3	0	0	2.655	15.885	15.171	17.847	47	53.1	100.1	38.317	101.713	Oct 24
2	1	0	3	5	2	3	2	0.092	2.747	15.922	15.257	16.622	48.1	53	101.1	37.297	102.436	Oct 24
3	1	0	3	5	2	3	2	0.035	2.689	15.929	15.231	17.447	47.9	53	100.9	38.081	102.413	Oct 24
4	4	1	2	2	1	2	0	0.018	2.672	15.834	15.148	17.147	44.9	52.8	97.7	37.127	99.218	Oct 24
5	7	6	4	3	1	2	0	0.002	2.656	16.052	15.127	23.121	63.4	66.5	129.9	49.685	131.985	Oct 24
6	1	1	3	5	2	3	0	0.003	2.658	15.938	15.231	17.672	46.6	52.8	99.4	37.999	100.991	Oct 24
7	4	1	2	2	1	2	0	0.043	2.698	15.859	15.18	16.972	45.5	53.4	98.9	37.197	100.356	Oct 24
8	7	1	4	3	1	2	2	0.156	2.810	15.98	15.244	18.397	57	61.4	118.4	42.609	119.741	Oct 24
9	1	1	3	5	2	3	0	0.034	2.689	15.892	15.166	18.147	50.6	54.3	104.9	39.599	106.474	Oct 24
10	4	1	2	2	1	2	0	0.144	2.798	15.829	15.219	15.248	44.5	52.6	97.1	35.104	98.233	Oct 24
11	4	1	2	2	1	2	0	0.229	2.883	15.857	15.284	14.323	45.2	53.2	98.4	34.445	99.313	Oct 24
12	1	5	1	5	1	3	1	0.011	2.665	15.966	15.162	20.097	53.8	60	113.8	43.368	115.594	Oct 24
13	1	4	0	1	4	1	2	0.029	2.684	15.93	15.223	17.672	46.5	55.2	101.7	38.469	103.243	Oct 24
14	1	0	3	5	2	3	2	0.115	2.769	15.902	15.247	16.372	48.5	53.1	101.6	37.149	102.873	Oct 24
15	1	0	3	5	1	2	2	0.049	2.704	15.886	15.214	16.797	46.4	52	98.4	36.920	99.830	Oct 24
16	1	0	3	2	3	3	0	0.056	2.710	15.864	15.212	16.297	44.3	51.7	96	35.929	97.376	Oct 24
17	7	1	4	5	4	2	0	0.063	2.718	15.972	15.136	20.897	60.8	63.1	123.9	46.234	125.647	Oct 24
18	7	1	3	3	2	2	1	0.181	2.835	15.987	15.254	18.322	58	62.6	120.6	42.984	121.879	Oct 24
19	4	1	4	3	1	2	0	0.189	2.844	15.83	15.205	15.623	48.3	55.3	103.6	36.808	104.674	Oct 24
20	4	3	4	2	1	2	2	0.113	2.767	15.91	15.201	17.722	51.7	58.1	109.8	40.176	111.182	Oct 24
21	1	1	3	2	1	2	0	0.128	2.783	15.778	15.192	14.648	42.1	49.9	92	33.461	93.116	Oct 24
22	1	1	3	3	1	3	0	0.074	2.729	15.813	15.197	15.398	42.1	50.1	92.2	34.252	93.468	Oct 24
23	4	5	1	3	1	2	0	0.171	2.826	15.895	15.223	16.797	51.1	58.5	109.6	39.210	110.793	Oct 24
24	1	5	5	2	1	3	0	0.175	2.830	15.973	15.27	17.572	54.7	60.4	115.1	41.110	116.339	Oct 24

Generation #6

	Position Number							Fitness	L/D	voltage	v0	Drag 1	Lscale	Rscale	Normal	Drag	Lift	Date 2008
Chromosome #	-1	-2	-3	-4	-5	-6	-7	Function		(volts)	(volts)	(g)	(g)	(g)	(g)	(g)	(g)	
1	4	1	4	3	1	2	0	0.215	2.745	12.082	11.48	16.255	45.8	52.9	98.7	36.438	100.010	Oct 24
2	1	0	3	5	2	3	2	0.072	2.601	12.178	11.493	18.496	47.3	51.7	99	38.741	100.772	Oct 24
3	7	1	3	3	2	2	1	0.072	2.601	12.168	11.42	20.197	51.3	56.8	108.1	42.303	110.035	Oct 24
4	7	1	3	3	2	2	1	0.124	2.654	12.17	11.453	19.360	51.5	57	108.5	41.548	110.252	Oct 24
5	7	1	4	3	1	2	2	0.247	2.776	12.188	11.52	18.037	54.3	58.3	112.6	41.063	113.989	Oct 24
6	1	0	3	5	2	3	2	0.102	2.632	12.104	11.454	17.551	45.9	50.6	96.5	37.285	98.127	Oct 24
7	1	5	5	2	1	3	0	0.099	2.628	12.173	11.418	20.386	53	58.7	111.7	43.228	113.598	Oct 24
8	1	1	3	2	1	2	0	0.031	2.560	12.014	11.387	16.930	39.9	47.5	87.4	34.803	89.090	Oct 24
9	1	1	3	2	1	2	0	0.000	2.529	12.067	11.426	17.308	39.1	47.9	87	35.099	88.777	Oct 24
10	4	3	4	2	1	2	2	0.151	2.681	12.103	11.448	17.686	47.1	54.4	101.5	38.442	103.050	Oct 24
11	4	1	4	3	1	2	0	0.264	2.793	12.095	11.492	16.282	49	54.2	103.2	37.386	104.421	Oct 24
12	4	1	2	2	1	2	0	0.176	2.705	12.052	11.442	16.471	45.3	51.3	96.6	36.225	97.999	Oct 24
13	5	0	1	5	0	3	2	0.133	2.662	11.248	10.606	16.986	44.7	51.2	95.9	36.597	97.422	Oct 24
14	4	0	3	3	1	3	0	0.314	2.843	11.225	10.665	14.816	46.1	52.1	98.2	34.898	99.220	Oct 24
15	7	6	3	1	2	2	1	0.129	2.659	11.378	10.538	22.225	61.2	63.9	125.1	47.807	127.099	Oct 24
16	7	3	0	3	2	2	1	0.303	2.832	11.3	10.678	16.457	51.2	56.8	108	38.542	109.156	Oct 24
17	7	1	3	5	2	3	1	0.218	2.747	11.315	10.605	18.785	55.5	58.8	114.3	42.159	115.809	Oct 24
18	7	0	5	5	2	3	2	0.285	2.814	11.343	10.645	18.468	59.3	60	119.3	42.864	120.637	Oct 24
19	1	1	3	2	1	2	0	0.141	2.671	11.189	10.611	15.293	39.3	47.7	87	33.084	88.356	Oct 24
20	1	7	3	2	1	1	0	0.271	2.801	11.301	10.656	17.065	51.7	57.2	108.9	39.335	110.164	Oct 24
21	4	3	1	2	1	2	0	0.287	2.816	11.212	10.649	14.896	44.4	52	96.4	34.609	97.475	Oct 24
22	4	3	1	2	1	2	2	0.385	2.914	11.251	10.747	13.335	42.5	51.7	94.2	32.598	94.995	Oct 24
23	4	1	4	3	1	2	0	0.299	2.829	11.225	10.649	15.240	46.7	53	99.7	35.628	100.777	Oct 24
24	4	1	2	3	1	2	0	0.462	2.991	11.212	10.745	12.356	43	50.6	93.6	31.497	94.203	Oct 24

Generation #7

	Position Number							Fitness	L/D	voltage	v0	Drag 1	Lscale	Rscale	Normal	Drag	Lift	Date 2008
Chromosome #	-1	-2	-3	-4	-5	-6	-7	Function		(volts)	(volts)	(g)	(g)	(g)	(g)	(g)	(g)	
1	4	3	1	2	1	2	2	0.014	2.670	11.256	10.585	17.496	46.2	53.3	99.5	37.843	101.052	Nov 7
2	4	3	4	2	1	2	2	0.219	2.876	11.298	10.696	15.697	50.5	56.6	107.1	37.598	108.116	Nov 7
3	7	1	3	3	2	2	1	0.114	2.771	11.338	10.638	18.252	54.4	59	113.4	41.442	114.817	Nov 7
4	4	3	4	2	1	2	2	0.062	2.719	11.285	10.607	17.678	49	55.9	104.9	39.130	106.376	Nov 7
5	4	1	4	3	1	2	0	0.149	2.805	11.273	10.656	16.088	48.4	54.7	103.1	37.171	104.282	Nov 7
6	4	1	4	3	1	2	0	0.066	2.723	11.299	10.636	17.287	48.4	54.6	103	38.350	104.435	Nov 7
7	4	3	1	2	1	2	2	0.100	2.757	11.288	10.672	16.062	45.5	53.1	98.6	36.225	99.872	Nov 7
8	4	3	1	2	1	2	2	0.136	2.792	11.287	10.687	15.644	45.8	53.3	99.1	35.910	100.274	Nov 7
9	4	1	4	3	1	2	0	0.159	2.815	11.282	10.668	16.009	49	54.5	103.5	37.175	104.657	Nov 7
10	5	0	1	5	0	3	2	0.051	2.708	11.298	10.632	17.365	48.6	53.5	102.1	38.244	103.570	Nov 7
11	7	1	4	3	1	2	2	0.233	2.890	11.332	10.702	16.427	54.8	58.7	113.5	39.637	114.533	Nov 7
12	4	3	1	2	1	2	2	0.178	2.835	11.284	10.712	14.914	45.4	52.7	98.1	34.975	99.143	Nov 7
13	1	3	1	2	1	2	2	0.035	2.692	11.31	10.694	16.407	43.5	51.6	95.1	35.855	96.518	Nov 7
14	4	3	4	2	1	2	2	0.058	2.715	11.37	10.687	18.192	51.2	56.4	107.6	40.195	109.127	Nov 7
15	4	3	3	2	1	1	0	0.024	2.681	11.321	10.673	17.259	45.8	53.3	99.1	37.525	100.611	Nov 7
16	4	3	4	2	1	3	2	0.031	2.688	11.39	10.677	18.991	52.4	57.3	109.7	41.424	111.349	Nov 7
17	4	1	4	3	1	2	0	0.077	2.734	11.334	10.701	16.860	47.6	53.8	101.4	37.596	102.779	Nov 7
18	4	2	4	3	1	2	0	0.001	2.658	11.333	10.643	18.378	48.6	54.8	103.4	39.523	105.054	Nov 7
19	4	3	2	2	1	2	1	0.101	2.758	11.335	10.73	16.114	45.6	53.4	99	36.359	100.274	Nov 7
20	4	1	1	2	3	2	2	0.000	2.657	11.333	10.703	16.780	43.5	50.8	94.3	36.064	95.813	Nov 7
21	5	0	4	5	0	3	2	0.117	2.774	11.37	10.727	17.126	51.3	55.4	106.7	38.946	108.023	Nov 7
22	5	0	4	5	1	2	1	0.041	2.698	11.36	10.682	18.059	49.9	55.3	105.2	39.572	106.749	Nov 7
23	7	2	1	2	1	2	2	0.120	2.777	11.355	10.73	16.647	49.4	54.6	104	37.914	105.280	Nov 7
24	4	3	1	2	2	2	2	0.020	2.677	11.39	10.727	17.659	47.2	53.8	101	38.313	102.555	Nov 7

Generation #8

	Position Number							Fitness	L/D	voltage	v0	Drag 1	Lscale	Rscale	Normal	Drag	Lift	Date 2008
Chromosome #	-1	-2	-3	-4	-5	-6	-7	Function		(volts)	(volts)	(g)	(g)	(g)	(g)	(g)	(g)	
1	4	3	1	2	1	2	2	0.037	2.630	11.398	10.709	18.197	46.5	53.4	99.9	38.626	101.590	Nov. 8
2	4	3	4	2	1	2	2	0.193	2.786	11.428	10.791	16.824	49.8	56.2	106	38.500	107.275	Nov. 8
3	4	1	4	3	1	2	0	0.223	2.816	11.412	10.805	16.031	49.3	54.4	103.7	37.238	104.858	Nov. 8
4	4	1	4	3	1	2	0	0.220	2.813	11.427	10.813	16.216	49.6	55	104.6	37.607	105.777	Nov. 8
5	4	3	4	2	1	2	2	0.050	2.643	11.44	10.707	19.359	50.9	56.6	107.5	41.343	109.273	Nov. 8
6	7	1	4	3	1	2	2	0.235	2.828	11.475	10.808	17.616	56.1	59.1	115.2	41.174	116.446	Nov. 8
7	4	1	4	3	1	2	0	0.000	2.593	11.52	10.777	19.623	49.3	55	104.3	40.952	106.195	Nov. 8
8	4	3	4	2	1	2	2	0.079	2.672	11.512	10.798	18.857	51	56.4	107.4	40.820	109.070	Nov. 8
9	4	3	1	2	1	2	2	0.160	2.753	11.498	10.882	16.269	46.2	53.3	99.5	36.617	100.796	Nov. 8
10	4	3	4	2	1	2	2	0.131	2.725	11.513	10.832	17.986	50.4	56.9	107.3	39.928	108.790	Nov. 8
11	4	3	3	2	1	1	0	0.130	2.723	11.463	10.82	16.982	47	54.2	101.2	37.677	102.609	Nov. 8
12	4	3	2	2	1	2	1	0.186	2.779	11.473	10.855	16.322	47.8	54.4	102.2	37.221	103.450	Nov. 8
13	4	3	4	4	1	3	2	0.222	2.815	11.533	10.864	17.367	54	58.3	112.3	40.332	113.555	Nov. 8
14	4	3	0	2	0	2	2	0.092	2.685	11.483	10.819	17.237	46.3	53	99.3	37.544	100.803	Nov. 8
15	4	1	4	3	3	2	0	0.167	2.760	11.435	10.764	17.419	51.3	55.9	107.2	39.341	108.574	Nov. 8
16	4	1	4	3	1	2	0	0.251	2.844	11.416	10.812	15.680	49.7	54.3	104	36.947	105.078	Nov. 8
17	7	3	4	3	1	2	1	0.192	2.785	11.471	10.747	18.795	57.5	60.8	118.3	42.987	119.727	Nov. 8
18	3	1	4	2	1	2	2	0.133	2.726	11.438	10.801	16.537	46.3	52.5	98.8	36.741	100.167	Nov. 8
19	4	3	4	2	1	2	2	0.226	2.819	11.458	10.824	16.459	50.8	56	106.8	38.299	107.981	Nov. 8
20	5	3	4	2	1	2	1	0.305	2.898	11.468	10.854	15.939	53.3	57.7	111	38.639	111.984	Nov. 8
21	4	3	4	2	1	2	2	0.283	2.876	11.45	10.85	15.576	50.2	56.1	106.3	37.314	107.308	Nov. 8
22	4	3	0	2	1	2	2	0.100	2.694	11.444	10.789	17.004	45.9	52.8	98.7	37.188	100.166	Nov. 8
23	4	3	2	2	1	1	1	0.199	2.792	11.435	10.817	16.043	47.5	54.1	101.6	36.820	102.805	Nov. 8
24	4	3	2	2	1	2	2	0.335	2.928	11.439	10.887	14.330	48.3	54.2	102.5	35.291	103.328	Nov. 8

Generation #9

	Position Number							Fitness	L/D	voltage	v0	Drag 1	Lscale	Rscale	Normal	Drag	Lift	Date 2008
Chromosome #	-1	-2	-3	-4	-5	-6	-7	Function		(volts)	(volts)	(g)	(g)	(g)	(g)	(g)	(g)	
1	5	3	4	2	1	2	1	0.052	2.715	11.5	10.755	19.527	56.8	58.7	115.5	43.146	117.139	Nov. 9
2	4	3	2	2	1	1	1	0.170	2.833	11.482	10.85	16.565	52.8	56	108.8	38.815	109.961	Nov. 9
3	4	3	2	2	1	2	2	0.227	2.890	11.485	10.885	15.727	53	55.7	108.7	37.955	109.688	Nov. 9
4	4	3	2	2	1	1	1	0.073	2.736	11.484	10.861	16.329	42.9	55.5	98.4	36.452	99.732	Nov. 9
5	4	3	4	2	1	2	2	0.107	2.770	11.499	10.804	18.217	55.9	57.2	113.1	41.345	114.516	Nov. 9
6	4	3	4	2	1	2	2	0.156	2.819	11.5	10.834	17.457	56.1	57.1	113.2	40.605	114.455	Nov. 9
7	7	3	4	3	1	2	1	0.187	2.850	11.502	10.794	18.557	62.3	61.4	123.7	43.854	124.963	Nov. 9
8	7	3	4	3	1	2	1	0.239	2.902	11.508	10.831	17.745	62.8	61.2	124	43.102	125.087	Nov. 9
9	4	3	4	2	1	2	2	0.232	2.895	11.494	10.869	16.382	56.7	57	113.7	39.633	114.720	Nov. 9
10	4	1	4	3	1	2	0	0.174	2.836	11.476	10.847	16.487	53.9	54.7	108.6	38.695	109.749	Nov. 9
11	7	1	4	3	1	2	2	0.216	2.878	11.509	10.833	17.719	62	59.2	121.2	42.504	122.340	Nov. 9
12	4	3	4	2	1	2	2	0.195	2.857	11.498	10.85	16.985	57.1	56.9	114	40.297	115.139	Nov. 9
13	5	3	3	5	1	2	1	0.196	2.859	11.473	10.78	17.778	60.9	58.6	119.5	42.216	120.689	Nov. 9
14	5	1	4	2	1	2	1	0.101	2.764	11.38	10.74	16.419	47.7	53.7	101.4	37.154	102.687	Nov. 9
15	4	3	2	2	1	1	2	0.103	2.766	11.352	10.746	15.546	44.2	52	96.2	35.219	97.415	Nov. 9
16	0	3	3	2	1	1	2	0.080	2.743	11.365	10.758	15.572	43	51.4	94.4	34.876	95.658	Nov. 9
17	4	5	4	2	1	2	2	0.198	2.860	11.4	10.767	16.239	52	57.3	109.3	38.590	110.383	Nov. 9
18	4	3	4	0	1	2	2	0.090	2.752	11.384	10.726	16.880	48.8	54.4	103.2	37.984	104.546	Nov. 9
19	7	3	2	3	1	0	1	0.203	2.865	11.381	10.745	16.316	52.9	57.4	110.3	38.872	111.378	Nov. 9
20	7	3	4	3	1	2	1	0.165	2.828	11.388	10.709	17.419	54.6	59.3	113.9	40.711	115.132	Nov. 9
21	4	1	4	2	2	2	2	0.170	2.833	11.387	10.775	15.700	49	54.1	103.1	36.784	104.201	Nov. 9
22	4	1	1	2	1	2	2	0.063	2.725	11.35	10.757	15.213	41.8	49	90.8	33.781	92.059	Nov. 9
23	4	1	4	2	1	2	2	0.054	2.717	11.383	10.729	16.778	46.8	52.6	99.4	37.105	100.804	Nov. 9
24	4	1	0	2	1	2	2	0.000	2.663	11.343	10.733	15.649	40.3	48.1	88.4	33.726	89.801	Nov. 9

Generation #10

	Position Number							Fitness	L/D	voltage	v0	Drag 1	Lscale	Rscale	Normal	Drag	Lift	Date 2008
Chromosome #	-1	-2	-3	-4	-5	-6	-7	Function		(volts)	(volts)	(g)	(g)	(g)	(g)	(g)	(g)	
1	5	3	3	5	1	2	1	0.122	2.775	11.265	10.623	17.340	51.2	57	108.2	39.467	109.536	Nov. 9
2	7	3	4	3	1	2	1	0.139	2.793	11.275	10.594	18.394	56	60.6	116.6	42.238	117.979	Nov. 9
3	4	3	2	2	1	1	2	0.051	2.705	11.24	10.608	17.070	46.5	53.6	100.1	37.540	101.551	Nov. 9
4	4	3	4	2	1	2	2	0.110	2.764	11.263	10.635	16.962	49.3	55.5	104.8	38.393	106.129	Nov. 9
5	4	3	2	2	1	2	2	0.036	2.690	11.245	10.602	17.367	46.7	53.8	100.5	37.919	102.004	Nov. 9
6	4	5	4	2	1	2	2	0.106	2.760	11.278	10.606	18.151	53	58.7	111.7	40.993	113.131	Nov. 9
7	4	3	4	2	1	2	2	0.075	2.728	11.255	10.608	17.475	49.2	55.4	104.6	38.866	106.040	Nov. 9
8	7	3	2	3	1	0	1	0.132	2.786	11.254	10.618	17.178	51	57.2	108.2	39.305	109.502	Nov. 9
9	4	5	4	2	1	2	2	0.043	2.696	11.278	10.575	18.988	52.1	58.4	110.5	41.585	112.132	Nov. 9
10	5	1	4	2	1	2	1	0.076	2.730	11.263	10.626	17.205	48.3	54.8	103.1	38.289	104.516	Nov. 9
11	7	3	2	3	1	0	1	0.150	2.804	11.255	10.624	17.043	51.7	57.4	109.1	39.354	110.355	Nov. 9
12	7	3	2	3	1	0	1	0.150	2.804	11.257	10.626	17.043	51.7	57.4	109.1	39.354	110.355	Nov. 9
13	0	3	4	3	1	2	1	0.062	2.716	11.255	10.6	17.276	47.6	54.7	102.3	38.196	103.747	Nov. 9
14	7	1	3	3	1	2	1	0.097	2.751	11.268	10.605	17.487	50.8	56	106.8	39.327	108.196	Nov. 9
15	4	3	2	2	1	1	2	0.040	2.693	11.237	10.587	17.144	46	53.5	99.5	37.491	100.979	Nov. 9
16	4	3	4	0	1	2	2	0.138	2.792	11.255	10.633	16.405	48.9	55	103.9	37.652	105.132	Nov. 9
17	4	5	4	2	1	2	2	0.090	2.744	11.265	10.582	18.014	51.5	57.8	109.3	40.366	110.754	Nov. 9
18	4	5	4	2	1	2	2	0.134	2.788	11.268	10.611	17.328	51.5	57.8	109.3	39.680	110.610	Nov. 9
19	4	3	0	3	1	0	2	0.126	2.780	11.231	10.655	15.192	43.7	51.5	95.2	34.660	96.362	Nov. 9
20	7	3	4	3	0	0	2	0.133	2.787	11.273	10.574	18.436	56	60.2	116.2	42.199	117.596	Nov. 9
21	0	6	4	2	1	2	1	0.014	2.668	11.322	10.586	19.412	51.9	58.3	110.2	41.947	111.927	Nov. 9
22	2	1	4	2	1	1	1	0.000	2.654	11.222	10.618	15.931	40.3	49	89.3	34.192	90.741	Nov. 9
23	7	3	0	3	1	0	1	0.095	2.749	11.262	10.614	17.091	49.3	54.9	104.2	38.399	105.568	Nov. 9
24	7	3	2	3	1	0	1	0.168	2.822	11.272	10.636	16.775	52	57.1	109.1	39.085	110.299	Nov. 9

Appendix I: Chord Distribution Values

Mountain Quail

0.00980389	1.0056899
0.10539222	0.97816009
0.19117652	0.87942945
0.25245097	0.91666672
0.30392153	0.90690683
0.37009805	0.86036038
0.44852944	0.78700135
0.5	0.77386086
0.55147056	0.74918389
0.63235292	0.76028526
0.71568625	0.72868787
0.79166667	0.67267269
0.86519611	0.57563809
0.91666667	0.48443185
0.95833333	0.32448237
0.99019611	0.26173541

Ring Necked Pheasant

0	1
0.05583753	1.06774206
0.12690356	1.03702667
0.18781722	0.99419353
0.25126894	0.97741935
0.31218272	0.93870962
0.38071069	0.88387078
0.44162435	0.8
0.51015232	0.74193562
0.56852791	0.74637096
0.62944156	0.72903227
0.7005076	0.72054967
0.76395945	0.68064523
0.8248731	0.61561289
0.89340107	0.50136479
0.95177666	0.37096768
0.99238581	0.18064515

Guineafowl

0.03124991	1.02361664
0.07291658	1.06151591
0.1640624	1.06378209
0.23437495	1.03485583
0.30989582	0.98333324

0.36458328	0.89239909
0.45052079	0.81535665
0.48697914	0.80843185
0.56250001	0.76282315
0.63281243	0.7701466
0.71614577	0.64597885
0.79166664	0.65309203
0.85677074	0.58493582
0.89583325	0.48717945
0.94010408	0.44385098
0.95833333	0.3811637
0.94791656	0.32063164
0.98437492	0.15433928

Bobwhite

0	1.00464977
0.07352938	0.95776417
0.14215689	0.96252251
0.2034314	0.95045034
0.29166666	0.81481475
0.35049017	0.78868328
0.41666668	0.78475535
0.48774506	0.79193468
0.56862745	0.80598459
0.69362746	0.81372789
0.76960785	0.7593746
0.82107848	0.65342266
0.86764711	0.6122251
0.91911762	0.50633241
0.95343137	0.288027
0.98284312	0.27692883

Chukar

0	1.00022379
0.02995392	0.98825119
0.08064511	0.9732746
0.15437784	0.95317222
0.22119819	0.88350451
0.31336401	0.79778462
0.40092162	0.67270905
0.47695851	0.68882175
0.55299541	0.68040581
0.63364052	0.62200104
0.72811063	0.60936551
0.80184336	0.56877568
0.88248847	0.47892392
0.94930881	0.31419929

Blue Grouse

0.06225682	1.04739904
0.09533074	1.05785112
0.13618675	1.06370495
0.18287941	1.11067186
0.2217899	1.09435261
0.26459142	1.08226866
0.30739294	1.09535898
0.34241249	1.04876036
0.38132297	1.06545429
0.42023346	1.03581237
0.45330739	1.01446257
0.48638132	1.00048591
0.52334628	0.94545429
0.56614781	0.89876022
0.60116725	0.8954785
0.63813232	0.87724823
0.67898832	0.83629988
0.7373541	0.80057486
0.76653689	0.77685943
0.79961082	0.76446283
0.82490267	0.76859498
0.84241244	0.76328213
0.86381315	0.73313786
0.89105052	0.67995192
0.91050581	0.58944268
0.91634237	0.57398017
0.9396887	0.52789229
0.95525286	0.36525956
0.96887159	0.34563159
0.97665367	0.32319952

Turkey

0.04927536	0.93245873
0.08405801	0.93926102
0.11884065	0.89824265
0.1565217	0.87188216
0.18550726	0.87706504
0.23478262	0.83503407
0.26956527	0.84240363
0.30724631	0.83219955
0.34782604	0.75672883
0.39130432	0.77125854
0.42028988	0.75765312
0.44637676	0.74640964
0.48405795	0.74620618
0.53043476	0.75898922
0.53043476	0.75898922
0.57101449	0.76822157
0.6028986	0.77492382
0.6376811	0.78008455
0.689855	0.78927039

0.72173911	0.77396419
0.75652176	0.74724387
0.7942028	0.70830395
0.81739128	0.68785982
0.84927539	0.62532712
0.88985497	0.55024755
0.96811589	0.337585

Ptarmigan

0	1
0.02427189	0.93035712
0.04126213	0.91910704
0.05339802	0.91107132
0.08737862	0.93418356
0.10922333	0.91296987
0.14077676	0.89323288
0.16747571	0.90563901
0.20388348	0.90206755
0.24271844	0.87857133
0.27184469	0.8861111
0.29611646	0.88142854
0.33009706	0.84642863
0.36165048	0.81910724
0.39077673	0.77589298
0.42718451	0.77161652
0.45631063	0.7617346
0.47815535	0.73163272
0.48786405	0.72074823
0.51213595	0.72103165
0.53640772	0.70119058
0.55825243	0.68626364
0.57766985	0.66785709
0.60922327	0.65357125
0.64320387	0.64474782
0.67233012	0.62857139
0.69174754	0.61845236
0.71601943	0.62837286
0.73786402	0.61111099
0.75485438	0.65873001
0.76699027	0.63055548
0.77912616	0.61499993
0.78883486	0.61119042
0.81310676	0.59833328
0.83252417	0.55595239
0.83737865	0.55952371
0.85679607	0.54246042
0.87864078	0.51567465
0.89320384	0.49857148
0.90776691	0.47142853
0.92475727	0.42428569
0.94417468	0.34285707

	0.95631069	0.32142865
	0.97087375	0.3021428
	0.97572811	0.28142864
Spruce Grouse		
	0.07910747	1.03694153
	0.11561863	1.0517611
	0.15618656	1.04610527
	0.19269771	1.04789509
	0.23529403	1.03240053
	0.27991885	1.02405485
	0.32860035	0.98379963
	0.3651115	0.9506404
	0.40567943	0.78465018
	0.44827586	0.72371143
	0.48073023	0.83251929
	0.51521299	0.85223364
	0.55172414	0.82130582
	0.57403644	0.82159822
	0.59229207	0.82591205
	0.62068966	0.81653297
	0.64503035	0.82226039
	0.67139955	0.82130582
	0.69776874	0.80876275
	0.72008115	0.79106518
	0.74239345	0.77920957
	0.77484782	0.74634865
	0.79918862	0.69737963
	0.83367138	0.62027482
	0.86409736	0.59877117
	0.89655172	0.57308981
	0.92292092	0.49061572
	0.94726162	0.42664554
	0.96754563	0.23523884
	0.98580116	0.27720645
Scaled Grouse		
	0.02605213	0.98200898
	0.06212426	0.98439245
	0.1002004	1.00020907
	0.13226453	1.01538471
	0.16833667	1.04147169
	0.2044088	1.01003338
	0.24649295	1.03827574
	0.28456908	0.96373327
	0.31462921	0.97212942
	0.34869735	0.94314385
	0.38476948	0.90095186
	0.4028056	0.88018885
	0.43086173	0.86148265
	0.46492986	0.87273371

0.48697389	0.87056856
0.51903802	0.88060195
0.55110215	0.86321069
0.57114227	0.85746141
0.60521041	0.79933117
0.64729455	0.82671411
0.68937869	0.86048745
0.72545093	0.84472063
0.75551095	0.83127673
0.78156308	0.79125825
0.8036072	0.78007155
0.82965933	0.73104791
0.86773547	0.6291807
0.8957916	0.61956532
0.91983962	0.53260888

California Quail

0	0.99942835
0.05910165	1.00800308
0.12765952	0.92765026
0.19385343	0.92581316
0.25295508	0.90311664
0.31914898	0.80945136
0.38297868	0.76356185
0.46099289	0.74902448
0.50118198	0.74768309
0.60756498	0.76933573
0.70921992	0.81617657
0.78014188	0.76355018
0.85106383	0.68267292
0.89834518	0.59603673
0.95508274	0.53353637
0.97872347	0.36788601
0.98817969	0.25813007

Red Tailed Hawk

0.00212324	1.00064643
0.02760087	1.00064617
0.05944802	0.99965193
0.09129516	0.99547507
0.12101917	1.03393656
0.15286632	1.03167403
0.19320601	1.06961355
0.22929943	1.04524881
0.25902343	1.05429867
0.29087058	1.06406275
0.32271762	1.08338726
0.34819536	1.10216718
0.38216564	0.97618479
0.40764337	1.00393466
0.43949052	1.01719437

0.4734608	0.96742083
0.50106157	0.95897418
0.52866244	0.96380081
0.56263272	0.88070763
0.59447987	0.86098539
0.64118896	0.85520358
0.69214444	0.75414775
0.72611472	0.7189722
0.760085	0.71153833
0.79617842	0.6559715
0.8301487	0.56958745
0.87473466	0.49321272
0.91719749	0.44444452
0.96178345	0.3451842

Goldfinch

0	0.98787873
0.03632478	1.01969713
0.07264957	1.01666682
0.10470086	1.00825388
0.13675216	1.01666665
0.1666667	1.01361113
0.19658114	1.00912289
0.2222222	0.98807005
0.25427349	0.97833335
0.28632478	0.9525
0.31837608	0.93090906
0.34829063	0.89142855
0.38247866	0.87450978
0.41452985	0.87039228
0.4444444	0.83354175
0.4722222	0.7912499
0.50213675	0.77222221
0.5277778	0.75571415
0.55982909	0.72078436
0.59188028	0.68878803
0.61752134	0.66333344
0.65384612	0.61256401
0.67948718	0.58636371
0.71153847	0.55999995
0.74358976	0.54666666
0.7735042	0.50897437
0.79487177	0.51435892
0.81837608	0.5212821
0.84615388	0.40833338
0.87179483	0.40534488
0.90170937	0.4193334
0.92735043	0.34866663
0.95299138	0.21199975

Canada Goose

0.0081968	0.99370316
0.02868854	0.96320324
0.04918039	0.92099547
0.06352461	0.87950923
0.0881148	0.85214772
0.11475417	0.8691306
0.14139343	0.86580078
0.1680328	0.87878769
0.20286886	0.87986995
0.22745906	0.86031735
0.27254099	0.86868682
0.31147541	0.86824764
0.34016395	0.87631399
0.36680332	0.79097086
0.39754103	0.78643578
0.42213123	0.78329498
0.45081966	0.78416807
0.47336068	0.78499257
0.51024592	0.74777843
0.55327868	0.71614086
0.57991805	0.70129849
0.60655742	0.69610377
0.64139348	0.63419899
0.6639345	0.61818176
0.69057377	0.58379709
0.71106561	0.54545451
0.7438525	0.52284731
0.7684427	0.46272243
0.80122959	0.43722932
0.8237705	0.40760979
0.86065574	0.36796531
0.87500006	0.35930722
0.89344263	0.3226774
0.920082	0.29437224
0.94467219	0.26334788
0.98770495	0.17604618

Black Footed Albatross

0.02390431	0.99253725
0.03984062	0.95149247
0.05976098	0.81592058
0.07968124	0.75712363
0.09561754	0.75539015
0.11952185	0.73507489
0.13545816	0.71268662
0.15139437	0.72388058
0.18525891	0.70415774
0.20916332	0.69742197
0.23306773	0.68920145
0.26294822	0.72470991
0.29282861	0.73294246

0.31274897	0.71535188
0.34661351	0.7412936
0.36653386	0.73765813
0.38645412	0.74569495
0.41235056	0.72388074
0.43227092	0.70551136
0.44820713	0.6957523
0.46812749	0.68457728
0.4920318	0.65547254
0.50996013	0.66169148
0.53386454	0.62366738
0.55776885	0.64072507
0.57968124	0.65511755
0.59760957	0.64818785
0.62151388	0.65671633
0.64940234	0.63260627
0.66533865	0.63930365
0.68525891	0.63432844
0.70318724	0.60223861
0.72709155	0.62284774
0.75697204	0.60033177
0.78087645	0.5522389
0.80677289	0.53386941
0.83266932	0.4589554
0.85458161	0.42686535
0.87848602	0.36567175
0.89840638	0.35422901
0.91633461	0.3263681
0.93625497	0.30248785
0.96015928	0.26212714
0.98007964	0.16884334

Mourning Dove

0	1
0.02044994	0.99407129
0.04703483	0.95151532
0.0756647	0.94598167
0.10429448	0.95429833
0.14519436	0.96837956
0.18813912	0.96372947
0.22903889	0.95954424
0.25971375	0.9274588
0.29652356	0.92885373
0.33742334	0.94805207
0.37014318	0.92490121
0.40286302	0.90118588
0.43762784	0.90044477
0.4683027	0.89328067
0.50920248	0.8666008
0.55828229	0.81701948
0.607362	0.80048937

0.64417181	0.75494071
0.68711657	0.7155669
0.73006144	0.65735317
0.77505118	0.63719564
0.82617587	0.53998169
0.8732107	0.45059292
0.91820045	0.34478576
0.95501026	0.27980036
0.98568511	0.19804443

Chromosome 7732100 (Day 2007)

0	1
0.07008092	1.19237236
0.1374663	1.36842119
0.20754723	1.49924812
0.2722372	1.43766084
0.35309976	1.14736867
0.4097035	1.10125337
0.47708888	1.02456163
0.5444744	0.94342123
0.61725073	0.85388458
0.6819407	0.71067258
0.75202163	0.72098258
0.81671159	0.71929837
0.88948793	0.60620745
0.95687331	0.35479092

Chromosome 6611110 (Present Study)

0	0.99182473
0.07202209	1.23907
0.15789469	1.41615945
0.24930745	1.45751957
0.34349027	1.30000019
0.44321325	0.94571615
0.53739608	0.74316547
0.60664824	0.72392088
0.66759002	0.7387591
0.75069255	0.72028079
0.81440442	0.63758977
0.8919668	0.37589924
0.95290859	0.20309904
0.9889197	0.1203654

Zimmerman Approximation

0.00309597	0.99865046
0.08049543	1.22753021
0.15789474	1.32769718
0.23839017	1.54336273
0.31578947	1.59514167
0.39938087	1.50024289
0.47058824	1.42591112

0.54798771	1.30817811
0.62848298	1.1877919
0.70278648	1.07287454
0.78328175	0.87921727
0.86068122	0.67083263
0.94117649	0.38519386
0.98452017	0.18160796

Chromosome 4143120 (High AoA Best Wing)

0	1
0.10091738	1.02091528
0.16513746	1.26797321
0.23853205	1.47712383
0.30275213	1.45632771
0.38073379	1.33613397
0.45871545	1.3284311
0.54587162	0.23529311
0.61467877	0.5816998
0.68807336	0.56209135
0.76605502	0.76470564
0.84862375	0.29411733
0.92660578	0.26797402
0.96789014	0.18300608
0.99082586	0.12490913

Feathers Retracted

0.02433635	1.05051038
0.07300887	1.17806101
0.12168139	1.27119324
0.181416	1.35337187
0.22123896	1.3720846
0.26327444	1.30531714
0.40707965	0.86366232
0.45132748	0.56250011
0.54646017	0.33954095
0.58185844	0.29969387
0.61946904	0.29810499
0.64823009	0.29154521
0.69026539	0.28423747
0.72566365	0.2839689
0.76327426	0.29417298
0.79424783	0.26479586
0.82964591	0.25720276
0.86504417	0.24744894
0.90265478	0.23214285
0.9358407	0.19642864
0.95796452	0.15153056
0.98230087	0.09948975
0.99557513	0.0673468

Appendix J: Tuft Studies

Feathered Zimmerman Approximation Wing at 11.8^0 AoA

Tufts

Voltage (volts)	V0 (volts)	Drag 1 (g)	Lscale (g)	Rscale (g)	Normal (g)	Drag (g)	Lift (g)	Cl	Cd
15.122	14.35	19.701	45	37.6	82.600	36.593	84.970	0.275	0.118
15.09	14.349	18.910	45.9	37.4	83.300	35.945	85.490	0.277	0.116
15.091	14.351	18.885	46	38.2	84.200	36.103	86.366	0.280	0.117

No Tufts

Voltage (volts)	V0 (volts)	Drag 1 (g)	Lscale (g)	Rscale (g)	Normal (g)	Drag (g)	Lift (g)	Cl	Cd
14.901	14.163	18.834	57.8	78.2	136.000	46.645	137.061	0.444	0.151
14.884	14.067	20.850	57.2	79	136.200	48.702	137.677	0.446	0.158
14.883	14.181	17.915	56.2	80	136.200	45.767	137.064	0.444	0.148

rho kg/m^3	V m/s	Area m^2
1.2035	17.912	0.0157

Appendix K: Aluminum Wing Tests

	L/D	voltage	v0	Drag	Lscale	Rscale	Lift
		(volts)	(volts)	(g)	(g)	(g)	(g)
Clean Zimmerman	3.230	8.740	7.960	55.798	87.0	93.2	180.2
	3.293	8.740	8.000	55.031	87.5	93.7	181.2
	3.340	8.740	8.035	54.017	86.8	93.6	180.4
	3.347	8.745	8.050	53.488	86.0	93.0	179.0
	3.321	8.740	8.025	54.117	86.6	93.1	179.7
Kaolin Zimmerman	3.128	8.740	7.880	57.966	88.6	92.7	181.3
	2.954	8.705	7.710	61.062	87.0	93.4	180.4
	3.072	8.710	7.810	58.795	87.3	93.3	180.6
	3.081	8.705	7.820	58.103	86.2	92.8	179.0
	3.112	8.700	7.840	57.455	86.7	92.1	178.8
Tuft Zimmerman	3.088	8.765	7.920	56.472	84.4	90.0	174.4
	3.269	8.770	8.060	52.739	84.0	88.4	172.4
	3.136	8.765	7.965	54.914	84.0	88.2	172.2
	3.111	8.760	7.940	55.509	83.2	89.5	172.7
	3.246	8.755	8.040	52.371	83.0	87.0	170.0
Low AoA Zimmerman	3.518	8.410	7.940	16.543	24.5	33.7	58.2
	3.708	8.420	7.985	15.642	24.7	33.3	58.0
	3.729	8.420	7.990	15.500	24.7	33.1	57.8
	3.699	8.420	7.985	15.626	24.6	33.2	57.8
	3.669	8.415	7.975	15.753	24.6	33.2	57.8
Clean Pheasant	2.803	8.660	7.825	49.518	62.0	76.8	138.8
	2.981	8.665	7.960	45.716	61.8	74.5	136.3
	2.847	8.670	7.890	47.247	61.0	73.5	134.5
	2.854	8.670	7.890	47.410	61.3	74.0	135.3
	2.835	8.665	7.880	47.271	60.5	73.5	134.0
Kaolin Pheasant	2.725	8.700	7.745	53.107	68.7	76.0	144.7
	2.798	8.720	7.825	51.507	68.3	75.8	144.1
	2.861	8.695	7.845	50.440	68.7	75.6	144.3
	2.798	8.700	7.800	51.814	69.0	76.0	145.0
	2.858	8.755	7.900	50.665	68.5	76.3	144.8
Tuft Pheasant	3.068	8.590	7.825	46.249	64.4	77.5	141.9
	3.218	8.590	7.920	44.130	64.3	77.7	142.0
	3.175	8.585	7.890	44.631	64.4	77.3	141.7
	3.182	8.580	7.885	44.815	64.6	78.0	142.6
	3.168	8.580	7.880	44.785	64.9	77.0	141.9
Low AoA Pheasant	3.546	8.400	7.925	16.498	21.8	36.7	58.5
	3.661	8.405	7.950	16.009	21.8	36.8	58.6
	3.743	8.400	7.960	15.628	21.9	36.6	58.5
	3.709	8.405	7.960	15.744	21.9	36.5	58.4
	3.709	8.405	7.960	15.744	21.9	36.5	58.4

Clean Best High AoA	2.833	8.625	7.815	48.885	64.0	74.5	138.5
	3.153	8.650	8.035	43.955	63.7	74.9	138.6
	2.989	8.675	7.965	46.367	64.2	74.4	138.6
	2.933	8.690	7.945	47.255	63.4	75.2	138.6
	3.002	8.700	8.000	46.031	63.0	75.2	138.2
Kaolin Best High AoA	2.831	8.705	7.885	49.425	65.5	74.4	139.9
	2.738	8.675	7.790	51.054	64.8	75.0	139.8
	2.717	8.690	7.785	51.705	65.8	74.7	140.5
	2.831	8.700	7.880	49.425	64.9	75.0	139.9
	2.866	8.680	7.890	48.438	63.9	74.9	138.8
Tuft Best High AoA	2.823	8.730	7.910	49.236	63.8	75.2	139.0
	2.905	8.795	8.020	48.462	66.5	74.3	140.8
	2.928	8.760	8.010	47.439	62.8	76.1	138.9
	2.966	8.755	8.030	46.763	63.1	75.6	138.7
	2.959	8.760	8.030	46.911	62.9	75.9	138.8
Low AoA Best High AoA	3.118	8.950	8.440	18.182	23.4	33.3	56.7
	3.262	8.945	8.465	17.380	23.1	33.6	56.7
	3.217	8.950	8.460	17.655	23.5	33.3	56.8
	3.200	8.956	8.465	17.658	23.3	33.2	56.5
	3.092	8.955	8.440	18.308	23.4	33.2	56.6